MULTIFACETED REGULATION OF NEURONAL L-TYPE Ca^{2+} CHANNELS BY THE N-TERMINAL DOMAIN: FROM CAMKII TARGETING TO NUCLEAR SIGNALING

By

Xiaohan Wang

Dissertation

Submitted to the Faculty of the

Graduate School of Vanderbilt University

in partial fulfillment of the requirements

for the degree of

DOCTOR OF PHILOSOPHY

in

Neuroscience

February 28, 2018

Nashville, Tennessee

Approved:

Roger J. Colbran, Ph.D.

Ariel Y. Deutch, Ph.D.

Brad A. Grueter, Ph.D.

David A. Jacobson, Ph.D.

Randy D. Blakely, Ph.D.

ACKNOWLEDGEMENTS

First, I would like to thank my advisor, Dr. Roger Colbran, for his tremendous support and great mentoring. You have made me a critical thinker and a better scientist and, for that, I will always be grateful. I would also like to thank the members of my committee for their guidance on my projects and on my career development throughout my graduate school. I am thankful for my former and current lab members who have been fun and inspiring to work with. I would also like to acknowledge Drs. Kevin Currie, Amy Lee, Teru Nakagawa, Kristie Rose, Qi Zhang for their generous help with my projects. I also want to thank the Vanderbilt International Scholar Program for supporting my graduate training at Vanderbilt. I am also grateful for the Vanderbilt neuroscience community that offers me this great training environment.

TABLE OF CONTENTS

Page

LIST OF FIGURES

Page

CHAPTER I

INTRODUCTION

1.1 Introduction overview

The ability to undergo sustained synaptic plasticity is one of the fundamental features of a neuron that enables an organism to learn from experience and adapt to the environment. Appropriate Ca^{2+} influx through the plasma membrane plays a key role in neuronal excitability and plasticity (Berridge, 1998). Understanding the regulation of Ca^{2+} channels is therefore critical for gaining a full appreciation neuronal physiology. Moreover, excessive Ca^{2+} influx via excitotoxicity is central to pathological processes such as ischemia.

The work in this dissertation focuses on multiple ways of regulating the neuronal L-type voltage-gated Ca^{2+} channel (LTCC). In this chapter of introduction, I will first briefly review the general background of voltage-gated Ca^{2+} channels in Section1.2. Sections 1.3 and 1.4 will then focus on different *functions* and *regulation* of L-type Ca^{2+} channel signaling pathways, respectively. I will then briefly review in Section 1.5 an important downstream Ca^{2+} effector, Ca^{2+}/calmodulin-dependent protein kinase II (CaMKII), which plays a critical role in both mediating L-type Ca^{2+} channel signaling and regulating its channel function. In Section 1.6, I will discuss in detail L-type Ca^{2+} channel-dependent, CaMKII-mediated nuclear CREB signaling. Finally, in Section 1.7, I will briefly summarize the work described in this dissertation.

1.2 An overview of voltage-gated Ca^{2+} channels

1.2.1 Ca^{2+} as a second messenger

Ca^{2+} is one of the key second messengers in neurons (Berridge, 1998). Intracellular Ca^{2+} regulates a variety of processes such as gene expression, neurotransmitter release, and synaptic plasticity (Clapham, 2007). Cells maintain a huge Ca^{2+} gradient between the cytosol (~10^{-7} M) and the extracellular space (~2 x 10^{-3} M) (Clapham, 2007). While this allows for Ca^{2+} to serve as an effective second messenger, it also poses challenges for cells to regulate Ca^{2+} entry properly, requiring both temporal and spatial confinement of Ca^{2+} entry. How cells achieve and utilize specific Ca^{2+} entry for downstream signaling pathways will be the focus of this dissertation.

1.2.2 Ligand-gated Ca^{2+} channels and voltage-gated Ca^{2+} channel

There are many different types of Ca^{2+} channels in cells. By the mode of their activation, the majority of Ca^{2+} channels can be categorized as either ligand-gated channels or voltage-gate channels (Tsien and Tsien, 1990). Additional modes of activation exist, but contribute to total Ca^{2+} influx to a lesser extent. For example, non-selective cation channels can be sensitive to temperature, such as Transient receptor potential (Trp) channels (although some Trp channels are also ligand-gated (Clapham, 2003)), and others can be sensitive to mechanical stress, such as Piezo1 and 2 (Coste et al., 2010).

The most well known ligand-gated Ca^{2+} channels include AMPA and NMDA receptors (Fig. 1.1A, (Huganir and Nicoll, 2013; Paoletti et al., 2013)). Both AMPA and NMDA receptors require glutamate binding in order to open the channel (Traynelis et al., 2010). In addition, NMDA receptors need membrane depolarization to eject a Mg^{2+} ion that

blocks the pore at resting membrane potential. Thus, activation of NMDA receptor requires both presynaptic glutamate release and postsynaptic depolarization, a feature viewed as a coincidence detector (Mayer et al., 1984; Nowak et al., 1984). Unlike NMDA receptors, AMPA receptors are permeable to Ca^{2+} only in the absence of an edited GluA2 subunit (Hollmann et al., 1991). Therefore, NMDA receptors are typically thought to be the major ligand-gated Ca^{2+} channels in neurons.

Voltage-dependent Ca^{2+} current was first recorded in cardiac Purkinje fibers 50 years ago (Reuter, 1967). Since then, multiple different Ca^{2+} currents have been identified (Catterall, 2000). Based on their physiological and pharmacological properties, voltage-gated Ca^{2+} channels can be grouped into five different types: L-, P/Q-, N-, R-, and T-type (Fig. 1.1B, (Catterall, 2000; Ertel et al., 2000)). Among these, L-type Ca^{2+} channels are activated at high membrane potential and exhibit slow inactivation when using Ba^{2+} as the charge carrier, while T-type Ca^{2+} channels are activated at lower membrane potential and exhibit faster inactivation (Nowycky et al., 1985). The voltage dependency and inactivation kinetics of P/Q-, N-, and R-type Ca^{2+} channels lie in between L- and T-type Ca^{2+} channels, and resemble more L-type than T-type channels (Nowycky et al., 1985; Randall and Tsien, 1995). Therefore, T-type Ca^{2+} channels are also referred to as low-voltage activated channels (LVA) and the rest as high-voltage activated channels (HVA) (Catterall, 2011).

1.2.3 Molecular components of voltage-gated Ca^{2+} channels

All voltage-gated Ca^{2+} channels have a pore-forming $\alpha 1$ subunit, which is the major determinant for channel physiological and pharmacological properties. High voltage-activated channels also have an intracellular β subunit, and a membrane integrated,

disulfide bond-linked α2-δ subunit (Catterall, 2000). In mammals, α1 subunits are encoded by 10 different genes that can be divided into three subfamilies: Ca_V1-Ca_V3 (Fig. 1.1B, (Ertel et al., 2000)). The four Ca_V1 genes encode L-type Ca^{2+} channels. $Ca_V2.1$, $Ca_V2.2$, and $Ca_V2.3$ genes correspond to P/Q-, N-, and R-type channels, respectively. The three Ca_V3 genes encode T-type channels. Genes within the same subfamily share higher amino acid similarity (>70%) than genes across the subfamilies (<40%), with Ca_V3 channels being the least related to the rest of the VGCCs. Thus the sequence diversity nicely correlates with the physiological and pharmacological differences mentioned above. However, the nature of other unique properties contributed by sequence diversity remains largely unexplored.

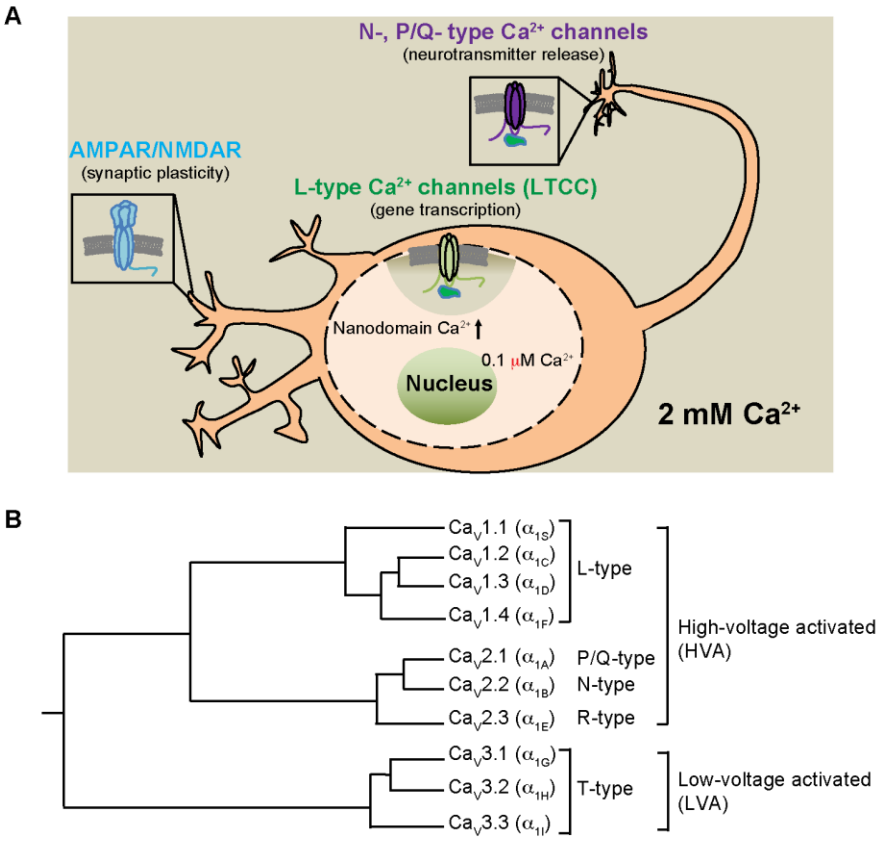

FIGURE 1.1 Ligand- and voltage-gated Ca^{2+} channels in neurons. *A*. a diagram of representative Ca^{2+} channels and their function in neurons. Neurons maintain a high Ca^{2+} gradient: ~0.1 μM intracellularly vs ~2 mM extracellularly. Ca^{2+} channels on the plasma membrane conduct Ca^{2+} influx that leads to Ca^{2+} level increase within a nanodomain or globally. *B*. Phylogeny and classification of voltage-gated Ca^{2+} channel pore-forming α1 subunits (figure adapted from (Ertel et al., 2000)). The 10 pore-forming α subunits can be divided into two big groups: high-voltage activated (HVA) and low-voltage activated (LVA) channels. L-, P/Q-, N-, and R-type Ca^{2+} channels all belong to HVA channels, and T-type Ca^{2+} channels are LVA channels. All HVA channels are composed of α1, β, and α2δ subunits, while LVA channels do not seem to contain β subunits.

Each α1 gene encodes a protein with 4 repetitive domains (I-IV), each of which contains 6 transmembrane segments (S1-S6). The channel pore is composed of S5, S6, and the extracellular loop connecting S5 and S6 from each domain. S4 serves as the voltage sensor (Wu et al., 2016; Wu et al., 2015).

All high-voltage activated channels also contain a β subunit, which binds to the intracellular linker between domains I and II (I-II linker) of α1 subunit at the α interacting domain (AID). The existence of four β genes further contributes to the diverse physiological properties of Ca^{2+} channels by modulating α1 subunit trafficking and channel kinetics (Hofmann et al., 1994). One well-known example is that although almost every β subunit accelerates channel inactivation, the β2a subunit (that has an N-terminal palmitoylation site) slows channel inactivation (He et al., 2007). In addition, different β subunits may have different subcellular localizations, further diversifying the channel properties in the spatial domain (Obermair et al., 2010).

Of the four L-type Ca^{2+} channel α1 subunits, $Ca_V1.1$ is specifically expressed in skeletal muscle, and $Ca_V1.4$ is specifically expressed in retina. $Ca_V1.2$ and $Ca_V1.3$ are more ubiquitously expressed, mainly in the brain, endocrine cells, cardiac cells, and smooth muscle (Catterall, 2000). All four β subunits are expressed in the brain, with β3 being the most abundant (Ludwig et al., 1997). This dissertation will focus on neuronal L-type Ca^{2+} channels, namely $Ca_V1.2$ and $Ca_V1.3$.

1.3 Functions of neuronal L-type Ca^{2+} channels

As discussed above, Ca^{2+} can serve as a dynamic and effective second messenger in all cell types. In muscle cells, L-type Ca^{2+} current causes muscle contraction upon membrane depolarization, a phenomenon known as excitation-contraction (E-C) coupling (Bers, 2002). In pancreatic β cells, L-type Ca^{2+} currents stimulate insulin secretion that is critical for glucose homeostasis (Braun et al., 2008). Work in this dissertation focuses on the roles of L-type Ca^{2+} channels in synaptic plasticity, regulation of gene expression, and other more specialized functions in neurons.

1.3.1 Role of LTCCs in synaptic plasticity

Long-term potentiation (LTP) is thought to be a key memory substrate in hippocampus (Morris, 2013). The most well studied form of LTP is mediated by NMDA receptors (Collingridge et al., 1983; Malenka and Nicoll, 1999; Teyler and DiScenna, 1987). In addition, an NMDA-independent component of LTP in hippocampus can be blocked by L-type Ca^{2+} channel antagonist (Grover and Teyler, 1990; Morgan and Teyler, 1999). Bilateral blockade of L-type Ca^{2+} channels, but not the NMDA receptor in the dorsal CA1 region of the hippocampus, impairs long-term memory retention in the Morris water maze test (Da Silva et al., 2013). Interestingly, infusion of CaMKII inhibitor AIP in the same region for 60 s does not affect short-term memory retention, but affects memory retention 5 days later. In addition, the effect of CaMKII inhibition can be rescued by blocking protein degradation (Da Silva et al., 2013). These data suggest that the L-type Ca^{2+} channels play a role in LTP that is required for both short-term and long-term memory formation in this particular behavioral paradigm, while CaMKII is required for

new protein synthesis that is necessary for memory consolidation. The molecular mechanisms (both known and unknown) of how L-type Ca^{2+} channels and CaMKII are involved in new protein synthesis and memory consolidation will be further discussed in Section 1.3.2 and Chapter II.

L-type Ca^{2+} channels also play an important role in endocannabinoid (eCB)-mediated short- and long-term depression in the dorsal striatum, and it is thought that these forms of synaptic plasticity are important for acquiring finer motor skills (Cui et al., 2013; Dayan and Cohen, 2011). Most striatal neurons (~95%) are GABAergic medium spiny neurons (Surmeier et al., 2007). They receive glutamatergic input from motor cortex and thalamus as well dopaminergic input from substantia nigra pars compacta (Alexander and Crutcher, 1990). The glutamate transmission is decreased upon paired stimulation of the post-synaptic and pre-synaptic cells. Pharmacological studies have shown that both the short- and long-term eCB-dependent inhibition of transmission requires postsynaptic activation of L-type Ca^{2+} channels (some also require metabotropic glutamate receptors) followed by presynaptic activation of eCB receptors (Mathur and Lovinger, 2012). Using $Ca_V1.3$ knockout mice, Surmeier's group showed that $Ca_V1.3$, but not $Ca_V1.2$, is required for eCB-mediated striatal LTD (Wang et al., 2006). Although the details are not yet completely understood, it is thought that the synthesis and/or the mobilization of the eCB require Ca^{2+} influx through the L-type Ca^{2+} channels. Since there are 10 different members of voltage-gated Ca^{2+} channels, this again highlights the importance of highly compartmentalized Ca^{2+} signaling pathways in neurons.

1.3.2 Role of LTCCs in excitation-transcription coupling

For an early phase synaptic plasticity to last for a longer period, neurons need a mechanism to signal the membrane depolarization event back to the nucleus, so that new mRNAs can be transcribed and new proteins synthesized to support long-term structural changes (Flavell and Greenberg, 2008). The process of linking membrane depolarization to nuclear gene transcription is called excitation-transcription (E-T) coupling (Deisseroth et al., 2003).

There are several pathways that can convey synaptic/somatic information to the nucleus. One pathway involves direct Ca^{2+} diffusion into the nucleus to bind to a transcriptional repressor downstream regulatory element antagonistic modulator (DREAM). Binding of Ca^{2+} causes DREAM to dissociate from a downstream regulatory element (DRE) and lift the repression of gene transcription by DREAM (Carrion et al., 1999).

The excitation signal can also be conveyed in an indirect manner. Ca^{2+} influx through L-type Ca^{2+} channels can cause calcineurin-dependent dephosphorylation of nuclear factor of activated T cells (NFAT, specifically NFATc4 in hippocampus). Dephosphorylation of NFATc4 helps to reveal multiple nuclear localization signals (NLS) to initiate active transport of NFATc4 into the nucleus, which subsequently activates transcription of genes encoding IP_3 receptor and other proteins (Graef et al., 1999).

A third pathway can employ direct Ca^{2+} diffusion and/or indirect Ca^{2+}/calmodulin active transport to the nucleus. In either case, increase of Ca^{2+}/calmodulin activates nuclear Ca^{2+}/calmodulin-dependent protein kinase kinase (CaMKK), which phosphorylates and

activates CaMKIV. Activated CaMKIV then phosphorylates transcription factor CREB at the Serine133 site to increase transcription of downstream immediate early genes such as *c-fos*, *Arc* and *Homer1a* (Bito et al., 1996; Deisseroth et al., 1996; Hardingham et al., 2001).

Among the three pathways mentioned above, L-type Ca^{2+} channels are preferentially linked to those that involve active transportation of NFATc4 or Ca^{2+}/calmodulin (Deisseroth et al., 1996; Graef et al., 1999; Wheeler et al., 2012). Wheeler and colleagues proposed that the Ca^{2+} influx through P/Q- and N-type Ca^{2+} channels is curbed by the mitochondrial buffering in superior cervical ganglion (SCG) neurons, making these channel less efficient in signaling to the nucleus. However, whether this is also the case for neurons in the central nervous system (where the neuronal morphology is very different than SCGs) remains unclear. Chapter II will present data showing an alternative mechanism for preferred nuclear signaling by L-type Ca^{2+} channels.

1.3.3 Other specialized functions of LTCC in specific brain regions

In addition to mediating synaptic plasticity and excitation-transcription coupling, L-type Ca^{2+} channels have other highly specialized functions in particular brain regions.

$Ca_V1.4$ is required for maturation of photoreceptor synaptic ribbons in the retina (Haeseleer et al., 2004; Liu et al., 2013). Consistent with this, a null mutation of $Ca_V1.4$ in humans leads to congenital stationary night blindness (Strom et al., 1998).

Throughout most of the brain regions, $Ca_V1.2$ expresses at a higher levels than $Ca_V1.3$. However, the $Ca_V1.3$ expression level is higher than $Ca_V1.2$ in cochlear inner hair cells

(Brandt et al., 2003) and in substantia nigra pars compacta (SNc) dopaminergic neurons (Takada et al., 2001). In cochlear inner hair cells, $Ca_V1.3$ is not only important for normal hair cell development, but also for activation of small conductance Ca^{2+}-activated K^+ channel (SK) for normal synaptic transmission (Brandt et al., 2003). Consistent with this, mice lacking the $Ca_V1.3$ gene have congenital deafness (Platzer et al., 2000).

In SNc dopaminergic neurons, Ca^{2+} influx through the $Ca_V1.3$ L-type Ca^{2+} channels is coupled to SK channels and together they are required for autonomous firing (Guzman et al., 2009; Putzier et al., 2009). To further highlight the importance of L-type Ca^{2+} channels in SNc dopaminergic neurons, recent work by Beckstead's group showed that aging decreases L-type Ca^{2+} current in SNc as well as pacemaker firing fidelity in SNc (Branch et al., 2014). Interestingly, this seems to correlate with increased Ca^{2+}-dependent proteolysis of L-type Ca^{2+} channels in aged rats (Michailidis et al., 2014). The impact of Ca^{2+}-dependent proteolysis on L-type Ca^{2+} channels and neurons will be further discussed in the Section 1.4.7 and Chapter V.

1.4 Regulation of neuronal L-type Ca^{2+} channels

As discussed in Sections 1.2 and 1.3, Ca^{2+} can engage many different cellular processes in neurons. One prerequisite to achieve the multi-function properties of Ca^{2+} is to have highly compartmentalized Ca^{2+} signaling pathways that are tightly regulated in the temporal domain as well. In this section, I am going to discuss the multiple ways that L-type Ca^{2+} channels can be regulated to achieve this goal.

1.4.1 L-type Ca^{2+} channel localization

Neurons are highly differentiated cells (Kandel et al., 2000). One advantage of having specialized subcellular compartments such as axon terminal, dendrites, and spines is the ability for neurons to process multiple signals locally without interfering with each other. With more than one type of voltage-gated Ca^{2+} channels in the same neuron, targeting them to the right subcellular location is critical. Neuronal L-type Ca^{2+} channels have been detected in the somas and proximal dendrites (Ahlijanian et al., 1990; Westenbroek et al., 1990). It is proposed that the L-type Ca^{2+} channel at the base of major dendrites can serve to mediate Ca^{2+} entry in response to summed excitatory inputs from distal dendrites (Westenbroek et al., 1990). In contrast, N-type Ca^{2+} channels have been found in the presynaptic nerve terminals (Robitaille et al., 1990), consistent with the functional data that N-type Ca^{2+} channels are responsible for neurotransmitter release (Catterall, 2011). It is worth noting that the precise subcellular localization of L-type Ca^{2+} channels remains disputed due to lack of reliable antibodies for staining.

1.4.2 Interaction with scaffold proteins

As discussed in Sections 1.4.1 and 1.3, Ca^{2+} channel localization is regulated and their downstream signaling pathways can be highly specialized and compartmentalized. The current view is that Ca^{2+} channels achieve these properties at least partially through interacting with specific scaffold proteins that target them to the right subcellular locations and connect with proper downstream signaling machineries. Here I am going to review the specific scaffold proteins that interact with $Ca_V1.2$ and $Ca_V1.3$, the two major neuronal L-type Ca^{2+} channel types.

AKAP15 and AKAP150, A-kinase anchoring protein 15 and 150, are members of a protein family that binds to the regulatory subunit of protein kinase A (PKA) (Michel and Scott, 2002; Scott et al., 2013). AKAP proteins have been well documented in bringing PKA to a particular substrate to enhance signaling specificity and efficiency. Several groups showed that $Ca_V1.2$ is actually one of these substrates (Gao et al., 1997; Hall et al., 2007; Oliveria et al., 2007). Catterall's group first showed that AKAP15 binds to leucine zipper site on $Ca_V1.2$ channels(Hulme et al., 2003). Hell's group showed that AKAP150 also binds to the same leucine zipper site and is critical in mediating PKA phosphorylation of $Ca_V1.2$ C-terminal domain at the Ser1928 site to facilitate the channel function (Hall et al., 2007). However, it is worth noting that genetic deletion of both AKAP15 and AKAP150 does not fully abolish the facilitation of $Ca_V1.2$ in response to isoproterenol (Jones et al., 2012), suggesting there other undiscovered scaffold proteins that are also contributing to PKA recruitment.

Sather and Dell'Acqua's groups also showed that AKAP150 could recruit the Ca^{2+}-dependent phosphatase calcineurin to the channel to negatively regulate channel function (Oliveria et al., 2007). More recently, Sather and Dell'Acqua's groups showed that AKAP150 recruitment of PKA and calcineurin enhances Ca^{2+} current while also increasing Ca^{2+}-dependent inactivation (Dittmer et al., 2014). Furthermore, AKAP-mediated co-recruitment of PKA and calcineurin helps to maintain a basal level of phosphorylation of the channel while allowing calcineurin to dephosphorylate NFATc4 for nuclear signaling (Murphy et al., 2014). It is also worth noting that $Ca_V1.3$ has not been reported to directly bind to AKAP150 because the AKAP binding domain in the C-terminus of $Ca_V1.2$ (Oliveria et al., 2007) is not conserved in $Ca_V1.3$.

Shank3, SH3 And Multiple Ankyrin Repeat Domains 3, is a multi-domain scaffold protein found in the postsynaptic density (PSD) (Naisbitt et al., 1999; Tu et al., 1999). Shank3 possesses a PDZ (postsynaptic density protein 95 (PSD95)/discs large homologue 1/zonula occludens 1) domain. In addition, Shank3 has a DUF535 domain (protein domain of unknown function 535) at the very N-terminus, an ANK (ankyrin repeat) domain, an SH3 domain (SRC homologue 3 domain superfamily), a proline-rich region, and a SAM (sterile alpha motif) domain (Monteiro and Feng, 2017). Shank proteins can undergo multimerization through the SAM domain, making it an even larger scaffold complex (Naisbitt et al., 1999). Bezprozvanny's group showed that Shank3 directly interacts with the unique PDZ binding domain (that contains ITTL (Ile-Thr-Thr-Leu)) at the very C-terminus of $Ca_V1.3$ (Zhang et al., 2005a). It is proposed that the proline-rich region of Shank3 can recruit Homer1 (Tu et al., 1999), which in turn tethers metabotropic glutamate receptor (mGluRs) to the proximity of $Ca_V1.3$ (Stanika et al., 2015). This seems to coincide well with the fact that L-type Ca^{2+} channel and mGluRs are often synergistic in downstream signaling pathways, such as endocannabinoids synthesis and mobilization (please see Section 1.3.1). In addition, Shank3 strongly interacts with GKAP (also known as SAPAP). In fact, Shank proteins were first identified through a yeast two-hybrid assay using GKAP as bait (Naisbitt et al., 1999). GKAP is a PSD95 interacting protein. In this regard, the Shank3/GKAP interaction could bring $Ca_V1.3$ L-type Ca^{2+} channel to the NMDA receptor/PSD95 complex as well.

Erbin, like Shank3, is also a PDZ domain containing scaffold protein. In a screen for PDZ-containing proteins that bind to the ITTL region in the $Ca_V1.3$ C-terminus, Lee's group identified Erbin as a binding candidate. They found that Erbin specifically

interacts with $Ca_V1.3$ but not $Ca_V1.2$, and the $Ca_V1.3$/Erbin interaction can enhance the voltage-dependent facilitation of $Ca_V1.3$ (Calin-Jageman et al., 2007). Interestingly, the effect of Erbin on $Ca_V1.3$ is β subunit-dependent, as Erbin shows effect when β1b is the auxiliary subunit but not β4.

Densin, also known as Densin-180 or LRRC7 (Leucine Rich Repeat Containing 7), is found to be enriched in the PSD of neurons. It contains 16 leucine-rich repeats in the N-terminus and a PDZ domain in the C-terminus. Through its multiple domains, densin can recruit CaMKII (Jiao et al., 2011; Robison et al., 2005; Strack et al., 2000b), MAGUIN (Ohtakara et al., 2002), β-catenin (Heikkila et al., 2007), and δ-catenin (Izawa et al., 2002). Lee's group found that densin interacts with $Ca_V1.3$ through the very C-terminus ITTL PDZ binding domain (Jenkins et al., 2010). This is proposed as one mechanism to recruit CaMKII to $Ca_V1.3$ for Ca^{2+}-dependent facilitation of Ca^{2+} entry via the channel. More recently, Lee's group found that densin also interacts with $Ca_V1.2$ (but not $Ca_V1.3$) through the N-terminal domain, and this interaction seems to be required for $Ca_V1.2$ surface trafficking in a CaMKII-independent manner (Wang et al., 2017).

In addition to scaffolding proteins that interact with the pore-forming α1 subunit discussed above, neuronal L-type Ca^{2+} channels interact with many proteins through the intracellular β subunits (for a thorough review please refer to (Buraei and Yang, 2010)). These include kinases (such as CaMKII, MAP kinases), ryanodine receptors, and presynaptic proteins (such as synaptotagmin I and RIM1). However, since β

subunits also associate with Ca_V2 P/Q, N and R type Ca^{2+} channels, how many of these interactions specifically contribute to L-type Ca^{2+} channel regulation remains unclear.

Are there other interacting proteins that could determine L-type Ca^{2+} channel specificity? Chapter II will directly answer this question by using an unbiased proteomics screen to search for $Ca_V1.3$ and $Ca_V1.2$ interaction proteins. I will also present data characterizing CaMKII as one of these interaction proteins and its role in selectively linking L-type Ca^{2+} channels to nuclear signaling.

1.4.3 L-type Ca^{2+} Channel clustering

Both specific localization and interaction are ways to achieve spatial regulation of the Ca^{2+} signaling. A third way to achieve this goal is to cluster the Ca^{2+} channels together to amplify the Ca^{2+} signaling locally. It has been shown that C-terminal domains of $Ca_V1.2$ can dimerize through Ca^{2+}/calmodulin bridging (Fallon et al., 2009). Santana's group then showed that $Ca_V1.2$ C-terminal domains can form clusters in cardiomyocytes and the clustered $Ca_V1.2$ channels undergo coupled gating (Dixon et al., 2012). Artificially fusing the channels together yields larger Ca^{2+} currents. Using super resolution microscopy, Santana's group estimated that that the size of cluster is about 8 channels per cluster (Dixon et al., 2015). In addition, they showed that clustering also exists among $Ca_V1.3$ channels in neurons, although they only observed clustering among $Ca_V1.3_S$ channels (the short splice isoform of the channel), but not among the $Ca_V1.3_L$ channels (Moreno et al., 2016). Like $Ca_V1.2$ channels, the size of the $Ca_V1.3$ cluster is also about 8 channels per cluster. However, one issue remains unsolved in this model: if there is only one Ca^{2+}/calmodulin binding site in the $Ca_V1.2$ C-terminal domain, the resulting cluster size should be two instead of eight.

In addition to Ca^{2+}/calmodulin, Shapiro's lab recently showed that the scaffold protein AKAP150 (for more details, please see Section 1.4.2) plays an important role in clustering $Ca_V1.2$ Ca^{2+} channels as well as M-type K^+ channels, TRPV1 channels, and G-protein coupled receptors (Zhang et al., 2016). Like Santana's group, they used super resolution microscopy to show that $Ca_V1.2$ and TRPV1 channels exist in the same macromolecular complex with AKAP150 in wild-type sensory neurons but not in AKAP150 knockout neurons. As discussed in Section 1.4.2, AKAP150 does not seem to interact with $Ca_V1.3$. Also, $Ca_V1.2$/AKAP interaction does not seem to be Ca^{2+}-dependent. Whether there are other Ca^{2+}-dependent clustering mechanisms remains unknown. Chapter III will present data showing one potential mechanism to cluster $Ca_V1.3$ channels in a Ca^{2+}-dependent way that involves CaMKII interaction with the channel.

1.4.4 Regulation of L-type Ca^{2+} channels by Ca^{2+}-binding proteins

The kinetics of Ca^{2+} influx via L-type Ca^{2+} channels is also tightly regulated. For example, Ca^{2+} influx does not typically persist with the same amplitude for an extended time. In other words, the channel has a set of mechanisms to inactivate itself to limit Ca^{2+} influx. On the other hand, neurons (and other cell types as well, such as cardiomyocytes) also have mechanisms that allow for increased Ca^{2+} influx when necessary. The next three sections will focus on the regulation of Ca^{2+} channel kinetics. This section will first briefly review the channel regulation by Ca^{2+}-binding proteins, which is not the main focus of this dissertation, and is reviewed in details elsewhere (Ben-Johny and Yue, 2014; Budde et al., 2002).

It is now well established that Ca^{2+} influx through the channel can inactivate the channel, a phenomenon called Ca^{2+}-dependent inactivation (CDI) (Budde et al., 2002; Yue et al., 1990). By using a Ca^{2+} binding deficient mutant of calmodulin, several groups showed that the Ca^{2+} sensitivity of the Ca^{2+} channel is mediated by the ubiquitous Ca^{2+}-binding protein calmodulin (Peterson et al., 1999; Zuhlke et al., 1999). Furthermore, they showed that calmodulin binding to the IQ-like motif in the C-terminus of L-type Ca^{2+} channels is critical for the CDI. Mutating the IQ domain to prevent CDI revealed a form of Ca^{2+}-dependent facilitation (CDF), which also depends on Ca^{2+}/calmodulin (Zuhlke et al., 1999). In addition, Yue's group later identified another Ca^{2+}/calmodulin binding site in the N-terminal domain, which is only present in L-type Ca^{2+} channels (Dick et al., 2008; Tadross et al., 2008). Unlike the C-terminal IQ-like motif, the calmodulin binding site in the N-terminal domain confers channel sensitivity to Ca^{2+} influx within a localized nanodomain. It is now proposed that the two lobes of calmodulin bind to N-terminus and C-terminus of the Ca^{2+} channel, respectively, bringing the two intracellular domains and regulating the channel function (Johny et al., 2013).

Another class of Ca^{2+}-binding proteins that has also been shown to regulate the channel function is Ca^{2+}-binding proteins (CaBPs, (Haeseleer et al., 2000)). Lee's lab first showed that CaBP1 facilitates $Ca_V1.2$ channel function by antagonizing calmodulin function (Zhou et al., 2004). They later found that CaBP1 binds to the membrane proximal part of the $Ca_V1.2$ N-terminus (Oz et al., 2011; Zhou et al., 2005). Interestingly, deleting the membrane distal part of $Ca_V1.2$ N-terminus also inhibited CaBP1 effect, suggesting $Ca_V1.2$ N-terminus has separate modules for CaBP1 binding and

functioning, and that N-terminus may have some intra-molecular interactions to regulate the channel function. This idea is further supported by a study from Yue's group showing that rather than directly competing with calmodulin, CaBP4 eliminates calmodulin inactivation of $Ca_V1.3$ through an allosteric mechanism involving the N-terminal domain of the channel (Yang et al., 2014). Taken together, these data showed that Ca^{2+} binding proteins regulate L-type Ca^{2+} channel kinetics (either inactivation or facilitation) through interacting with both the N-terminal domain and the C-terminal domain, and that within the N-terminal domain, there might be intramolecular or allosteric regulation between different binding sites.

1.4.5 Regulation of L-type Ca^{2+} channels by phosphorylation

Phosphorylation also plays an important role in regulating the channel function. The first kinase that was shown to phosphorylate and regulate L-type Ca^{2+} channels is cAMP-dependent protein kinase A (PKA). It was first found that stimulation of β-adrenergic receptor enhances Ca^{2+} influx in skeletal muscle cells (Reuter and Scholz, 1977). Later, it was shown that Ca^{2+} influx enhancement is due to facilitation of L-type Ca^{2+} currents by increased level of intracellular cyclic AMP (cAMP) and subsequent activation of PKA (Schmid et al., 1985; Sculptoreanu et al., 1993a; Sculptoreanu et al., 1993b). Initial protein microsequencing and peptide mapping from Catterall's lab showed that PKA preferentially phosphorylates $Ca_V1.2$ at Ser1928 in the distal C-terminus (De Jongh et al., 1996). More recently, another PKA phosphorylation site, Ser1700 in the proximal part of C-terminus, has been identified (Fuller et al., 2010). The two sites seem to have different roles in regulating $Ca_V1.2$ function. Phosphorylation of Ser1700 is shown to be required for PKA-mediated $Ca_V1.2$ facilitation in cardiac myocytes (Fuller et al., 2010).

On the other hand, phosphorylation of Ser1928 is required for $Ca_V1.2$ facilitation specifically mediated by β2-adrenergic receptor, but not β1-adrenergic receptor, in neurons (Qian et al., 2017).

Comparing to $Ca_V1.2$, we know much less about PKA phosphorylation of $Ca_V1.3$. Tavalin's group showed that the catalytic subunit of PKA specifically enhances the Ca^{2+} current of $Ca_V1.3_L$ (the long C-tail splice variant), but not the $Ca_V1.3_S$ (the short variant) (Liang and Tavalin, 2007). Furthermore, PKA's regulation of $Ca_V1.3$ depends on the identity of the β subunit that is coexpressed. A sustained current enhancement is observed when β2a is coexpressed, while a transient current enhancement is seen when β3 is coexpressed.

PKA can also phosphorylate the Ca^{2+} channel β2 subunit at Ser478 and Ser479. The facilitation effect of these two phosphoryaltion sites can be revealed in tsA-201 expressing $Ca_V1.2$ Δ1905 channels, which lack the dominant phosphorylation site of Ser1928 in cardiac myocytes (Bunemann et al., 1999).

In addition to PKA, protein kinase C (PKC) can regulate $Ca_V1.2$ L-type Ca^{2+} channels through phosphorylation. Activation of PKC causes a transient increase (at 5 s) followed by a sustained decrease of $Ca_V1.2$ channels in cardiac myocytes (up to 20 minutes (Lacerda et al., 1988)). Interestingly, the sustained repression of $Ca_V1.2$ channels by PKC is not seen in $Ca_V1.2$ isoforms cloned from the brain (Stea et al., 1995). It was later found that PKC represses the channel function by phosphorylating the cardiac isoform of $Ca_V1.2$ at Thr27 and Thr31, which are absent from the brain isoform (McHugh et al.,

2000). Therefore, the N-terminal domain of $Ca_V1.2$ represents a tissue-specific site for PKC regulation.

More recently, it was shown that cGMP-dependent protein kinase (PKG) could also phosphorylate L-type Ca^{2+} channels and regulate channel function (Sandoval et al., 2017). In this case, activated PKG represses $Ca_V1.3$ function through phosphorylating Ser793 and Ser860 within the II-III linker of the channel.

Ca^{2+} ions coming through the Ca^{2+} channel can bind to ubiquitous Ca^{2+} sensor calmodulin. Ca^{2+}/calmodulin can then bind to the regulatory domain of Ca^{2+}/calmodulin-dependent protein kinase II (CaMKII) to disinhibit the catalytic domain, which phosphorylates the Ca^{2+} channel itself, forming a feedback loop. The function and regulation of CaMKII will be further discussed in Section 1.5. Here I am gong to focus on CaMKII phosphorylation of the L-type Ca^{2+} channels. CaMKII can phosphorylate both β2 subunit (Thr498) and the $Ca_V1.2$ α1 subunit (Ser1512/Ser1570) (Grueter et al., 2008; Koval et al., 2010; Lee et al., 2006). In either case, CaMKII phosphorylation facilitates the channel function by increasing the current density. It is also proposed that CaMKII can phosphorylate Ser1486 of $Ca_V1.3$ at the C-terminal domain (Gao et al., 2006). Mutation of Ser1486 to alanine prevents the leftward shift of the current-voltage curve caused by CaMKII. However, whether Ser1486 is a bona fide CaMKII phosphorylation site has not be directly tested yet. In Chapter III, I will present data showing that Ser1486 is not a CaMKII phosphorylation site. I will also show data that identity novel CaMKII phosphorylation sites of $Ca_V1.3$.

1.4.6 Regulation of L-type Ca^{2+} channels by G proteins

It is well established that G proteins regulate voltage-gated Ca^{2+} channels (Catterall, 2000). In addition to elevated second messenger such as cAMP and subsequent PKA phosphorylation, G proteins regulate the channel function through direct interaction (Buraei and Yang, 2010; Herlitze et al., 1996; Ikeda, 1996). $G\beta\gamma$ can bind to I-II linker of the α subunit, potentially through competing with the β subunit (Buraei and Yang, 2010). However, most of the work has been focused on presynaptic P/Q- or N-type Ca^{2+} channels (Ca_V2 channels).

A study from Surmeier's group suggested some interesting potential mechanisms through which GPCRs could regulate L-type Ca^{2+} channels (Olson et al., 2005). In this study, they observed that activation of D_2 dopaminergic receptor and M_1 muscarinic receptor selectively suppresses $Ca_V1.3$, but not $Ca_V1.2$ or $Ca_V2.1/2.2$, Ca^{2+} channel currents in striatal medium spiny neurons. They further showed that this repression requires the C-terminal $Ca_V1.3$ PDZ binding domain (which interacts with Shank3) and the interaction between Shank3 and Homer. This study serves as a nice starting point showing that multiple scaffold proteins are required for selective GPCR regulation of L-type Ca^{2+} channels. However, whether a second messenger or direct protein-protein interaction is required for this regulation still remains to be tested.

1.4.7 Alternative splicing, RNA-editing, and Proteolysis

Both α and β subunits undergo alternative splicing, which contributes significantly to the channel diversity (Buraei and Yang, 2010; McHugh et al., 2000; Xu and Lipscombe, 2001). For $Ca_V1.3$, there are at least three alternative splicing sites: exon 11 that

encodes extra 20 amino acids within the I-II linker; exon 32 that encodes extra 15 amino acids within IVS3-IVS4; and exon 42 and 42a which are mutually exclusive within the C-terminal domain (Xu and Lipscombe, 2001). Alternative splicing of exon 42 and 42a leads to a long ($Ca_V1.3_L$) and a short C-terminal domain ($Ca_V1.3_S$), respectively. $Ca_V1.3_L$ contains a C-terminal modulator (CTM) that is absent in $Ca_V1.3_S$. CTM is involved in an intramolecular interaction within the C-terminal domain and can block calmodulin from accessing the Pre-IQ motif, leading to different gating properties between $Ca_V1.3_L$ and $Ca_V1.3_S$ (Singh et al., 2008). $Ca_V1.3_S$ also lacks the PDZ binding in the C-tail of $Ca_V1.3_L$ that is important of recruiting Shank3, Erbin, and Densin (see Section 1.4.2 for more details). The PDZ domain in $Ca_V1.3_L$ has been shown to promote membrane expression of the channel in cultured neurons (Stanika et al., 2016). In addition, overexpression of $Ca_V1.3_S$ leads to abnormal dendritic spine elongation (Stanika et al., 2016). Together, these studies highlight the importance of alternative splicing of $Ca_V1.3$ in regulating channel function and neuron morphology.

In addition to alternative splicing, the mRNA of $Ca_V1.3$ was recently shown to undergo RNA editing at the IQ domain. Adenosine deaminases acting on RNA (ADARs) can convert Adenosine to Inosine (A-to-I editing) through hydrolytic deamination (Keegan et al., 2001). Interestingly, the ATA codon that encodes the isoleucine in the IQ domain in $Ca_V1.3$ can be converted to ATI by ADAR2 (Huang et al., 2012). The ATI acts as ATG during translation, which gives rise to methionine instead of isoleucine. The overall outcome is that IQ-to-MQ editing slows down the Ca^{2+}-dependent inactivation of the channel, resulting in weaker Ca^{2+}-dependent inactivation and more Ca^{2+} influx.

Finally, certain proteases can cleave L-type Ca^{2+} channel α1 subunits at specific positions. This further contributes to the complexity of the channel regulation. The Ca^{2+}-dependent protease calpain can cleave $Ca_V1.2$ at the C-terminal domain upon Ca^{2+} influx through NMDA receptors (De Jongh et al., 1994; Hell et al., 1996). The cleaved C-terminal fragment turns out to be a nuclear protein and regulates transcription (Gomez-Ospina et al., 2006). Recently, another proteolysis site within the $Ca_V1.2$ II-II linker has been proposed (Michailidis et al., 2014). The cleavage of this site is also mediated by calpain and is more prominent in aged rats. After the cleavage, although the two parts of the channel remain associated and still conduct Ca^{2+} influx, the current density is lower than the intact channel. Comparing to $Ca_V1.2$, the proteolysis of $Ca_V1.3$ is much less understood. In Chapter V, I will present data showing that the N-terminal domain of $Ca_V1.3$ can also undergo Ca^{2+}-dependent proteolysis, and the product of the cleavage is a nuclear protein that regulates neuronal transcription and morphology.

1.5 CaMKII as an important Ca^{2+} effector

Upon Ca^{2+} influx through the Ca^{2+} channels, Ca^{2+} binds calmodulin that activates specific downstream effectors. One such effector is Ca^{2+}/calmodulin-dependent protein kinase II (CaMKII). Chapters II and III will present data showing how CaMKII interaction with L-type Ca^{2+} channels regulates channel function. This section will briefly review different CaMKII subunits and their diverse functions in neurons.

1.5.1 CaMKII structure and the Ca^{2+} regulation

CaMKII is a multifunctional serine/threonine protein kinase that plays key roles in a variety of different processes such as development, cardiac function, and learning and memory (Colbran and Brown, 2004; Hudmon and Schulman, 2002). It comprises as much as 1% of total protein in the forebrain and up to 2% of total protein in hippocampus (Erondu and Kennedy, 1985). A CaMKII holoenzyme is a dodecamer that contains two rings of six subunits. Each subunit has a catalytic domain, an auto-inhibition regulatory domain, a linker region with varying size, and an association domain. In mammalian genomes, CaMKII subunits are encoded by four different genes: *CAMK2A, B, C, D* (Hudmon and Schulman, 2002). Subunits encoded by different CaMKII genes are highly conserved within the catalytic domain and regulatory domain but are more diverse in the linker region and association domain.

CaMKII activity is tightly regulated by the cytosolic Ca^{2+} level. Fig. 1.2 shows the structure of a human CaMKII from the top-view and side-view. At the resting state when cytosolic Ca^{2+} level is low, CaMKII catalytic domain binds to the regulatory domain so that the kinase activity is auto-inhibited. When the cytosolic Ca^{2+} level is elevated, Ca^{2+}/calmodulin binds to the regulatory domain and releases the catalytic domain from being inhibited, activating the subunit. When two adjacent CaMKII subunits bind Ca^{2+}/calmodulin, one subunit phosphorylates the regulatory domain of the other subunit (Thr286 for CaMKIIα, Thr287 for CaMKII$\beta/\gamma/\delta$ (Hanson et al., 1994)). Thus, the phosphorylated regulatory domain can no longer block the catalytic domain and the subunit retains Ca^{2+}-independent (or autonomous) activity even after cytosolic Ca^{2+} levels retreats. The extent of phosphorylation of CaMKII subunits depends on Ca^{2+}

spike frequency. Therefore CaMKII has long been postulated as a molecular substrate for memory and frequency decoder for neuronal activity (Lisman et al., 2012). This is consistent with the observation that mice with a mutant CaMKII that cannot undergo autophosphorylation exhibit impaired learning during Morris water maze (Giese et al., 1998). However, recent data from experiments with better temporal resolution revealed that CaMKII activity is required during the induction phase, but not the maintenance phase of LTP (Murakoshi et al., 2017).

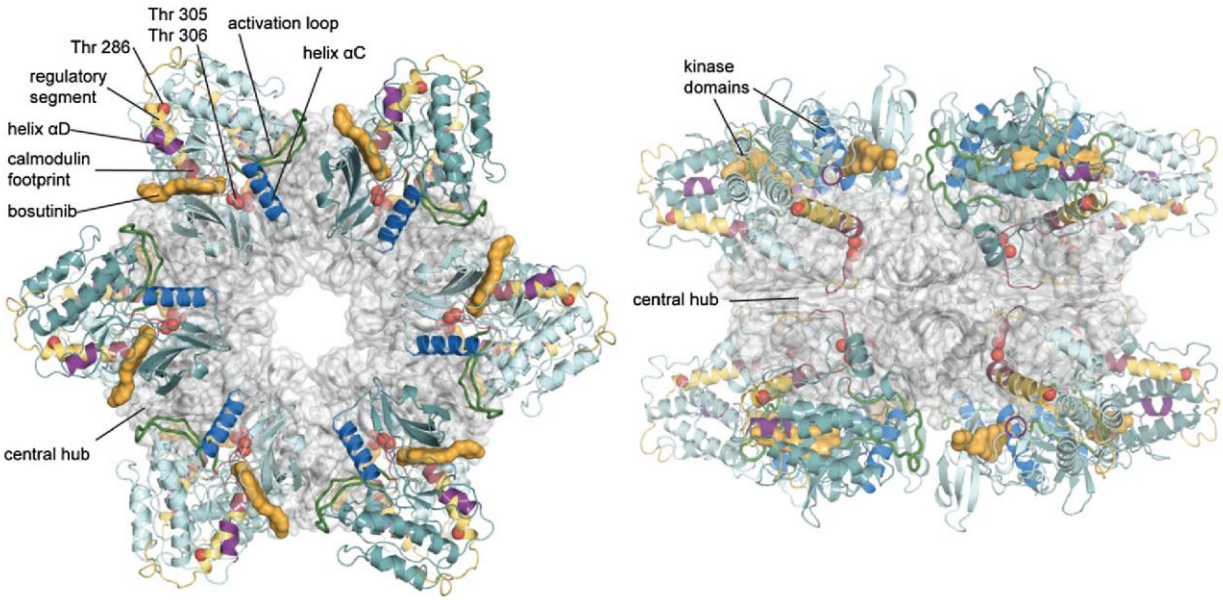

FIGURE 1.2 Structure of an inactivated CaMKII holoenzyme (Figure from (Chao et al., 2011)). Top view (left) and side view (right) of crystalized human CaMKIIα. CaMKII is a dodecameric protein, composed of two stacked rings, each of which has 6 subunits. Under low Ca^{2+} condition, the catalytic domain binds the regulatory domain, preventing it from accessing substrates. Upon Ca^{2+} influx, Ca^{2+}/calmodulin bind to the regulatory domain, disinhibiting the catalytic domain. When two adjacent CaMKII subunits are Ca^{2+}/calmodulin-bound, one subunit can phosphorylate the Thr286 site of the other in a trans-subunit, intra-holoenzyme way. Thr286 phosphorylation prevents re-binding of the catalytic domain, rendering the subunit constitutively active.

1.5.2 Functions of CaMKII as a protein kinase

As a kinase, all four CaMKII subunits can phosphorylate multiple substrates including ion channels and scaffold proteins in a similar way. CaMKII phosphorylation and its effects on neuronal physiology have been extensively studied over the past three decades. Section 1.4.5 has discussed CaMKII phosphorylation of L-type Ca^{2+} channels. Here I am going to review just a few other CaMKII substrates that are relevant to this work. For a full list of CaMKII substrates and their roles in neuronal physiology, please refer to a recent review (Shonesy et al., 2014).

Perhaps one the best-known CaMKII substrates is the GluA1 subunit of the AMPA receptor (Barria et al., 1997a; Barria et al., 1997b; Roche et al., 1996). It was found that LTP enhances phosphorylation of the GluA1 Ser831 site in a CaMKII dependent manner (Barria et al., 1997b), and Ser831 phosphorylation increases the unitary conductance of the AMPAR receptor (Benke et al., 1998). This fits well with the indispensible role of CaMKII in LTP induction mentioned in Section 1.5.1. However, recent works have challenged this “receptor-centric model” of LTP (Herring and Nicoll, 2016). First, neurons with AMPA receptor that lacks the Ser831-containing C-tail exhibit normal LTP (Granger et al., 2013). Second, more sophisticated biochemical analysis of the mouse hippocampus showed that during LTP, less than 1% of the GluA1 subunits are phosphorylated at the Ser831 site (Hosokawa et al., 2015) (however, this finding was recently challenged by other labs, see (Diering et al., 2016)). Therefore, phosphorylation of GluA1 at Ser831 does not seem to be the sole reason that CaMKII is required for LTP. Recently, Herring and Nicoll summarized alternative models (PSD-centric and vesicle-centric models) for CaMKII involvement in AMPAR/NMDAR-

mediated LTP induction (Herring and Nicoll, 2016). However, it is worth noticing that a recent study shows that mice with S831A mutation lack extinction of cocaine conditioned place preference, suggesting Ser831 does play a role in some forms of synaptic plasticity (Burgdorf et al., 2017).

CaMKII can also phosphorylate the GluN2B subunit of NMDA receptors at the C-tail (Omkumar et al., 1996; Strack et al., 2000a). Phosphorylation of GluN2B Ser1303 by CaMKII promotes the dissociation of pre-formed complexes of CaMKII and GluN2B (Strack et al., 2000a). More recently, it was shown that the effect of Ser1303 phosphorylation on channel kinetics depends on intracellular Cl^- concentration (Tavalin and Colbran, 2017). When the intracellular Cl^- is high, Ser1303 phosphorylation by CaMKII enhances GluN2B desensitization; when the intracellular Cl^- is low, Ser1303 phosphorylation decreases GluN2B desensitization. This result is especially intriguing given that the intracellular Cl^- concentration is developmentally regulated and renders GABA receptor different effects on membrane potential (Ben-Ari, 2002; Rivera et al., 1999).

In addition to glutamate receptors, CaMKII can also phosphorylate other key signaling molecules that are involved in synaptic plasticity. CaMKII is shown to phosphorylate the Ser142 site of the CREB transcription factor, preventing it from dimerization and from binding to CREB-binding protein (Wu and McMurray, 2001). More recently, CaMKII is reported to phosphorylate diacylglycerol lipase-α (DAGLα), a key enzyme that produces the endocannabinoid 2-arachidonoylglycerol (2-AG) (Shonesy et al., 2013).

Phosphorylation of DAGLα reduces its enzyme activity and reduces 2-AG-mediated depolarization-induced suppression excitation (DSE) in striatal medium spiny neurons.

1.5.3 Functions of CaMKII as a scaffold protein

In addition to its kinase activity, CaMKII also plays important roles through direct protein-protein interaction. Many CaMKII associated proteins (CaMKAPs) have been identified during the past several decades. Common themes begin to emerge as more and more CaMKAPs were identified. Here I am going to briefly discuss some of the CaMKAPs and group them in different classes based on binding properties.

Upon Ca^{2+}/calmodulin binding, the catalytic domain is released from the regulatory domain, rendering it accessible to multiple CaMKAPs. NMDA receptor GluN2B subunit, voltage-gated Ca^{2+} channel β1/2 subunits are representative CaMKAPs in this class (Abiria and Colbran, 2010; Bayer et al., 2001; Grueter et al., 2008; Strack and Colbran, 1998; Strack et al., 2000a). Interestingly, the CaMKII binding motifs of these CaMKAPs resemble the regulatory domain of CaMKII. Interaction between activated CaMKII and GluN2B subunit is shown to be important to recruit CaMKII to PSD as well as for LTP (Barria and Malinow, 2005). Consistent with this, mice carrying two mutations that impair CaMKII binding show deficits in memory consolidation (Halt et al., 2012).

Activated CaMKII can also interact with a CaMKII inhibitor protein CaMKIIN, as well as the densin-IN domain (Chang et al., 1998; Jiao et al., 2011). Neither the peptide of CaMKIIN (N-tide) nor the densin-IN domain shares sequence similarity with GluN2B or Ca^{2+} channel β subunits. Thus these two proteins seem to represent another class of CaMKAPs that inhibit the kinase activity in a substrate-dependent manner.

A third class of CaMKAPs interacts with CaMKII when it is in inactive form. The best example of this class is F-actin. Inactive CaMKIIβ associates with actin, and is released from actin upon Ca^{2+}/calmodulin binding (Shen and Meyer, 1999). It is now proposed that in addition to dynamically regulating CaMKII distribution, CaMKIIβ binding to F-actin also prevents access of actin from actin remodeling protein, therefore stabilizing the cytoskeleton (Kim et al., 2015).

Recently, more CaMKAPs have been identified, although the nature of the interaction for many of them has not been well characterized. For example, CaMKII is shown to bind to and phosphorylate proteasomes and serve as scaffold protein to recruit proteasomes to spines (Bingol et al., 2010). In this work, Sheng and colleagues showed that autophosphorylated CaMKII is a postsynaptic scaffold protein for the proteasome, yet it is unclear whether autophosphorylation is required for proteasome binding or for postsynaptic shuttling of the CaMKII/proteasome complex. Recent studies from Wang's lab showed that CaMKII can interact with metabotropic glutamate receptor 1 and 5 (mGlu1 and mGlu5) (Jin et al., 2013a; Jin et al., 2013b). Surprisingly, Ca^{2+}/calmodulin enhances CaMKII binding to mGlu1 but inhibits CaMKII binding to mGlu5. Lastly, a recent proteomics study from Colbran's group identified 138 novel CaMKAPs from mouse forebrain that are mostly enriched in the synaptic fractions (Baucum et al., 2015). More work needs to be done to characterize these interactions and understand how they are compared to existing CaMKAPs.

1.5.4 Other CaMKII autophosphorylation sites

In addition to the Thr286 site, CaMKII can autophosphorylate other sites under different conditions. One such site(s) is Thr305/Thr306 that lies in the middle of the Ca^{2+}/calmodulin binding domain (Colbran and Soderling, 1990; Hanson and Schulman, 1992). In the basal state or after Ca^{2+}/calmodulin dissociates from the Thr286 phosphorylated subunit, Thr305/Thr306 can undergo autophosphorylation that prevents Ca^{2+}/calmodulin from rebinding (Mukherji and Soderling, 1994). Thr305/Thr306 autophosphorylation seems to negatively regulate CaMKII association with the PSD. In cultured neurons, changing Thr305/Thr306 to alanines greatly slowed down the dissociation of CaMKII from the synapses (Shen et al., 2000). In a mouse model where Thr305 was mutated to aspartic acid to mimic autophosphorylation, both hippocampal LTP and learning are greatly impaired (Elgersma et al., 2002).

A recent study systematically analyzed other CaMKII autophosphorylation sites using a proteomics approach (Baucum et al., 2015). Multiple novel phosphorylation sites (Ser78, Thr261, Ser275, Ser315, Thr320/Thr321, Ser331, and Thr378) have been discovered in addition to Thr286 and Thr305/Thr306. By comparison with mice in which Thr286 was mutated to alanine, phosphorylation of Ser275, Ser315, Thr320/Thr321 was shown to depend on Thr286 autophosphorylation. The physiological significance of Ser331 autophosphorylation has been further demonstrated in a recent study from Torregrossa's group where they showed that Ser331 autophosphorylation is reversibly regulated in cocaine-associated memory reconsolidation and extinction, and that mimicking Ser331 phosphorylation inhibits kinase activity (Rich et al., 2016).

1.6 LTCC-mediated nuclear CREB signaling

I have briefly reviewed three major pathways in neuronal excitation-transcription coupling in Section 1.3.2. Here I am going to focus on the pathway mediated by the transcriptional factor CREB and the underlying mechanisms.

1.6.1 Transcriptional factor CREB and memory formation

CREB (cAMP responsive element binding protein) is a member of a transcriptional factor family that share similar structures and functions (Silva et al., 1998). The transcriptional activity of CREB is critically regulated by the phosphorylation of Ser133 in the kinase inducible domain. As its name suggests, increased level of cytosolic cAMP can lead to CREB activation. This is achieved through dis-inhibition of the catalytic subunit of Protein Kinase A (PKA) and its subsequent nuclear translocation and phosphorylation of CREB Ser133 site (Bacskai et al., 1993). Phosphorylation of CREB Ser133 then recruits CREB-binding protein (CBP), a key regulator of RNA polymerase II-mediated transcription (Chrivia et al., 1993; Kalkhoven, 2004). In addition to PKA, CREB can also be phosphorylated by other kinases, including CaMKII (see Section 1.5.2), CaMKIV, PKC, and casein kinases (Gonzalez et al., 1989; Wu and McMurray, 2001). I am going to focus here and later in Chapter II on the pathway that involves phosphorylation of CREB Ser133 by CaMKIV.

It has been well established that new protein synthesis is required for long-term memory formation (Davis and Squire, 1984; Flexner et al., 1963). The role of CREB in memory was first shown by Kandel's group (Dash et al., 1990). They injected the cAMP-responsive element (CRE, the DNA fragment that CREB binds to) to the nucleus of

Aplysia sensory neurons to block CREB binding. They found that disruption of CREB binding to its DNA targets selectively blocked serotonin-induced long-term facilitation but not short term facilitation. The importance of CREB in memory retention was further demonstrated in mammals by Silva's lab, where they found that CREB mutant mice showed normal short-term memory but were deficient in long-term memory in cued or contextual conditioning and Morris water maze text (Bourtchuladze et al., 1994)).

1.6.2 Mechanism of L-type Ca^{2+} channel-mediated CREB phosphorylation

L-type Ca^{2+} channels activation can induce global increases of neuronal Ca^{2+} concentrations. However, at least under some conditions, the initiation of L-type Ca^{2+} channels signaling to trigger nuclear CREB phosphorylation appears to require increased Ca^{2+} concentrations only within a nanodomain in the immediate vicinity of the channel. In this paradigm, Ca^{2+} binds to the ubiquitous Ca^{2+} sensor, calmodulin, within the L-type Ca^{2+} channels nanodomain, and Ca^{2+}/calmodulin then translocates to the nucleus to activate CaMKK (Ca^{2+}/calmodulin-dependent protein kinase kinase). CaMKK then phosphorylates a nuclear localized kinase CaMKIV, which in turn phosphorylate CREB at Ser133 (Deisseroth et al., 1998; Ma et al., 2013).

Using this stimulation paradigm, CaMKII is specifically recruited to L-type Ca^{2+} channels (Li et al., 2016; Wheeler et al., 2008). In fact, recent studies indicate that this form of excitation-transcription coupling requires precisely coordinated recruitment and activation of two CaMKII holoenzymes within the L-type Ca^{2+} channel nanodomain (Li et al., 2016; Ma et al., 2014). It was proposed that CaMKIIγ serves as a nuclear shuttle for Ca^{2+}/calmodulin, which activates nuclear CaMKIV. In this model, CaMKIIγ achieves the

shuttle function through several steps: 1) Ca^{2+} influx through L-type Ca^{2+} channels recruits CaMKIIα/β and CaMKIIγ to the vicinity of the channel; 2) phosphorylation at Thr287 of CaMKIIγ (presumably by CaMKIIα/β) traps calmodulin; 3) dephosphorylation of Ser334 exposes the unique nuclear localization signal of CaMKIIγ by a Ca^{2+}-dependent phosphatase calcineurin; 4) CaMKIIγ then shuttles to the nuclear and delivers calmodulin that is needed for CaMKK, CaMKIV, and CREB activation.

Chapter II will focus on the first step of this process. CaMKII has been reported to directly interact with multiple proteins within LTCC complexes, including the pore-forming $\alpha1$ ($Ca_V1.2$ or $Ca_V1.3$) subunits, auxiliary $\beta1$ or $\beta2$ subunits, and associated scaffolding proteins such as densin (Abiria and Colbran, 2010; Grueter et al., 2008; Hudmon et al., 2005; Jenkins et al., 2010; Simms et al., 2014). CaMKII interactions with $\beta2$ and densin play a role in modulating Ca^{2+}-dependent facilitation of $Ca_V1.2$ and $Ca_V1.3$ LTCCs, respectively (Grueter et al., 2008; Jenkins et al., 2010; Koval et al., 2010). However, the roles, if any, of these interactions in E-T coupling are unclear. Chapter II will present data showing that activated CaMKII directly interacts with the N-terminal domain of neuronal L-type Ca^{2+} channels, and that this helps to CaMKII to initiate downstream nuclear signaling.

1.6.3 L-type Ca^{2+} channel-mediated E-T coupling in disease and behavior

Mutations of L-type Ca^{2+} channels have been linked to multiple neurological and psychological diseases. For example, mutations of $Ca_V1.3$ are associated with Autism Spectrum Disorder (ASD) (De Rubeis et al., 2014; Pinggera et al., 2014; Pinggera and Striessnig, 2016). In addition, a mutation of $Ca_V1.2$ (G402S) that causes autistic

symptoms in Timothy syndrome disrupts L-type Ca^{2+} channel-mediate excitation transcription coupling (Li et al., 2016). A *de novo* mutation of CaMKIIα (E183V) found in an ASD patient was shown to disrupt CaMKII interactions with Ca^{2+} channel β subunit, which may serve as one of the docking sites in L-type Ca^{2+} channel-mediated E-T coupling (Stephenson et al., 2017).

A study from Rajadhyaksha's group showed that $Ca_V1.3$, but not $Ca_V1.2$, specifically mediates CREB Ser133 phosphorylation in naïve mice that were challenged with acute amphetamine or cocaine in the nucleus accumbens (Giordano et al., 2010).

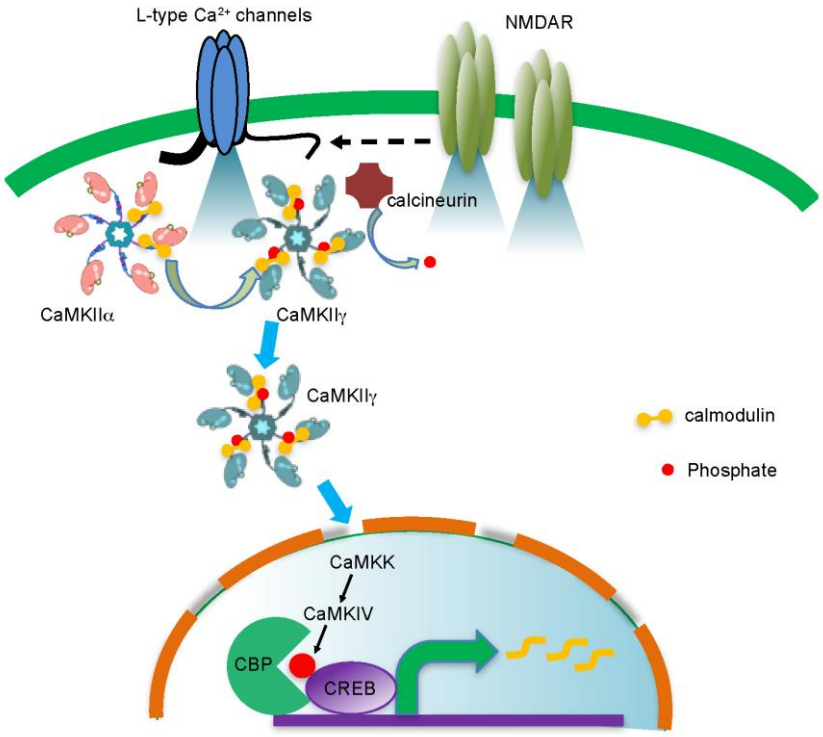

FIGURE 1.3 L-type Ca^{2+} channel-mediated excitation-transcription coupling. Ca^{2+} influx through L-type Ca^{2+} channels recruits CaMKIIα and CaMKIIγ to the vicinity of the channel. It is suggested that CaMKIIα can phosphorylate CaMKIIγ Thr287 in a trans-holoenzyme manner. Thr287 phosphorylation enhances calmodulin binding by ~1000 fold, a phenomenon known as “calmodulin trapping”. In the meantime, Ca^{2+}-dependent phosphatase calcineurin dephosphorylates CaMKIIγ at the Ser334 site, exposing a functional nuclear localization signal that is masked by Ser334 phosphorylation. CaMKIIγ then translocates to the nucleus with trapped calmodulin. In the nucleus, calmodulin activates Ca^{2+}/calmodulin-dependent kinase kinase (CaMKK), which phosphorylates and activates CaMKIV. CaMKIV in turn phosphorylates Ser133 of the CREB transcription factor, which recruits CREB-binding protein (CPB) and initiates transcription of downstream genes. More recently, it was found that the voltage-induced conformational change of the channel is also required for E-T coupling, and that NMDA receptors somehow are functional linked to L-type Ca^{2+} channels.

1.7 An overview of work reported in this dissertation

In the following chapters, I describe multiple forms of L-type Ca^{2+} channel regulation, all of which depend on a critical region of the intracellular N-terminal domain of the α subunit that contains the tri-basic residues RKR (referred to the RKR motif hereafter).

Chapter II presents data showing activated CaMKII can directly interact with L-type Ca^{2+} channel α subunit through the RKR motif within the N-terminal domain. This interaction is critical in targeting CaMKII to the L-type Ca^{2+} channel, and is required for L-type Ca^{2+} channel mediated excitation-transcription coupling.

Chapter III presents data on other potential physiological significances of the CaMKII/L-type Ca^{2+} channel interaction. First, this interaction helps to cluster the Ca^{2+} channels *in vitro* in a Ca^{2+} dependent manner. Second, this interaction recruits CaMKII to the vicinity of the channel to facilitate CaMKII phosphorylation of the channel.

Chapter IV describes a novel interaction between the L-type Ca^{2+} channel $\alpha 1$ subunit and the β subunits. In addition to the canonical interaction between the $\alpha 1$ subunit I-II linker and the β subunit, we found that the β subunit can also interact with the $\alpha 1$ subunit through the RKR motif in the N-terminal domain. This novel NTD/β subunit interaction seems to regulate the Ca^{2+}-dependent inactivation (CDI) of the channel.

Chapter V presents data showing that the N-terminal domain of $Ca_V1.3$ L-type Ca^{2+} channels can undergo proteolysis. The RKR motif in the N-terminal domain serves as a functional nuclear localization signal and is critical in translocating the N-terminal

domain to the nucleus. The N-terminal domain of the $Ca_V1.3$ L-type Ca^{2+} channel is predicted to be a DNA binding protein, and overexpression of the N-terminal domain in cultured neurons changed both the transcription and the cell morphology of neurons.

Taken together, data described in this thesis show important roles of the L-type Ca^{2+} channel N-terminal domain in regulating channel functions and downstream signaling pathways.

CHAPTER II

CAMKII INTERACTS WITH $Ca_V1.3$ L-TYPE Ca^{2+} CHANNEL N-TERMINAL DOMAIN TO MEDIATE ITS NUCLEAR SIGNALING

Summary

Neuronal excitation can induce new mRNA transcription, a phenomenon called excitation–transcription (E-T) coupling. Among several pathways implicated in E-T coupling, activation of voltage-gated L-type Ca^{2+} channels (LTCCs) in the plasma membrane can initiate a signaling pathway that ultimately increases nuclear CREB phosphorylation and, in most cases, expression of immediate early genes. Initiation of this long-range pathway has been shown to require recruitment of Ca^{2+}-sensitive enzymes to a nanodomain in the immediate vicinity of the LTCC by an unknown mechanism. In this chapter, I show that activated Ca^{2+}/calmodulin-dependent protein kinase II (CaMKII) strongly interacts with a novel binding motif in the N-terminal domain of Ca_V1 LTCC $\alpha1$ subunits that is not conserved in Ca_V2 or Ca_V3 voltage-gated Ca^{2+} channel subunits. Mutations in the $Ca_V1.3$ $\alpha1$ subunit N-terminal domain or in the CaMKII catalytic domain that largely prevent the *in vitro* interaction also disrupt CaMKII association with intact LTCC complexes isolated by immunoprecipitation. Furthermore, these same mutations interfere with E-T coupling in cultured hippocampal neurons. Taken together, data shown here define a novel molecular interaction with the neuronal

LTCC that is required for the initiation of a long-range signal to the nucleus that is critical for learning and memory.

2.1 Experimental procedures

Animals

Wild-type C57/B6J mice were purchased from Jackson Laboratory, ME. Timed pregnant Sprague Dawley rats were purchased from Charles River Laboratories, MA. Embryonic day 18.5 pregnant rats were euthanized in a CO_2 chamber before embryos were removed from the uterus. All animal experiments were approved by the Vanderbilt University Institutional Animal Care and Use Committee and were carried out following the US National Institutes of Health Guide for the Care and Use of Laboratory Animals.

GST pulldown from mouse forebrain for mass spectrometry

Three month-old male mice were decapitated without anesthetization and forebrains were homogenized in a low ionic strength lysis buffer (2 mM Tris-HCl, pH 7.5, 2 mM EDTA, 2 mM EGTA, 1 mM DTT, 1 µM Microcystin-LR with protease inhibitors) (Baucum et al., 2010). After 30 min incubation at 4°C, lysates were cleared by low speed centrifugation (500 x *g*). A final concentration of 150 mM NaCl and 1% Triton X-100 was added to the supernatant and the protein concentration was adjusted to ~1mg/ml. A total of 5 mg of GST protein was used for GST pulldown followed by Mass Spectrometry.

DNA constructs

Rat $Ca_V1.3$ complete coding sequence (Genbank accession number AF370010) was a gift from Dr. Diane Lipscombe, Brown University, Providence, RI. The intracellular domains contain: NTD, M1-K126; I-II, G407-V543; II-III, D773-H906; III-IV, G1169-S1225; CTD, M1469-L2164. Rabbit $Ca_V1.2$ cDNA (a gift from Dr. William Thiel, Genbank accession number X15539) was used to amplify a fragment encoding the $Ca_V1.2$ CTD (D1507-L2171). DNAs encoding all other $Ca_V1.2$ intracellular domains were amplified from a rat $Ca_V1.2$ cDNA construct (a gift from Dr. Gerald W. Zamponi, University of Calgary, Canada, Genbank accession number: NM_012517): NTD, M1-K124; I-II, S405-N524; II-III, Q754-I901; III-IV, V1167-Y1220. DNAs encoding the $Ca_V2.2$ NTD (M1-P95) and $Ca_V3.2$ NTD (M1-D140) were amplified from a bovine cDNA construct (a gift from Dr. Aaron Fox, University of Chicago, Chicago, IL) and a human cDNA construct (a gift from Dr. Edward Perez-Reyes, University of Virginia, Charlottesville, VA, Addgene plasmid ID 45809) respectively. DNAs encoding rat $Ca_V1.3$ NTD fragments M69-L93, Q94-S110, and L111-K126 were also amplified. DNAs encoding previously defined minimal CaMKII-binding domains in the $Ca_V1.2$ CTD (G1639 to K1660; (Hudmon et al., 2005)) and the rat Ca^{2+} channel β2a subunit (H485 to E505; (Grueter et al., 2008)) were also generated. All cDNAs were inserted into pGEX-4T1 using traditional ligation or sequence and ligation independent cloning (SLIC; (Li and Elledge, 2007)).

A plasmid encoding $Ca_V1.3$ with an N-terminal HA-tag (pCGNH-$Ca_V1.3$, for co-immunoprecipitation) was made by inserting rat $Ca_V1.3$ cDNA into pCGN vector (a gift from Dr. Winship Herr, Université de Lausanne, Switzerland, Addgene plasmid ID

53308). $Ca_V1.3$ chimeric constructs were made in the following way: pCGNH-$Ca_V1.3$ was used as a template to delete the N-terminal domain of $Ca_V1.3$, leaving the BamHI site intact (pCGNH-$Ca_V1.3$-ΔNTD); cDNAs encoding the $Ca_V2.2$ and $Ca_V3.2$ NTDs were then inserted into the BamHI site using SLIC. Plasmid encoding $Ca_V1.3$ with an extracellular HA-tag was generated by first removing the sequence encoding the N-terminal HA in pCGNH-$Ca_V1.3$, and then inserting the sequence encoding an HA tag flanked by flexible linkers on both ends between Q693 and K694 (pCGN0-$Ca_V1.3$-sHA). The inserted amino acid sequence is: TRH**YPYDVPDYA**VTFDEMQ, where the HA sequence is in bold (Altier et al., 2002). The nimodipine-resistant $Ca_V1.3$ was then generated by mutagenesis of pCGN0-$Ca_V1.3$-sHA to generate a T1033Y mutant (Dolmetsch et al., 2001; He et al., 1997). The region encoding M69-L93 was deleted from pCGN0-$Ca_V1.3$-sHA plasmid to remove the CaMKII binding domain. Site-directed mutagenesis, epitope insertions and all deletions were done following the one-step mutagenesis protocol described by Liu et al (Liu and Naismith, 2008).

CaMKII shRNA constructs for pCREB staining were expressed with GFP using a pLL3.7 plasmid (a gift from Luk Van Parijs lab, Massachusetts Institute of Technology, Cambridge, Massachusetts) that was modified to replace the CMV promoter with a 0.4kb fragment of the mouse CaMKIIα promoter (designated as pLLCK) that is primarily active only in excitatory neurons (Dittgen et al., 2004). The shRNA sequences were designed following Ma et al (Ma et al., 2014). The shRNA-targeted sequence in the mouse CaMKIIα cDNA contains two mismatches from the corresponding rat sequence, rendering it resistant to the shRNA. Knockdown and shRNA-resistance were confirmed by western blot and immunostaining. All constructs were confirmed by DNA sequencing.

Recombinant mouse CaMKIIα and GST-tagged protein purification

Expression and purification of recombinant mouse CaMKIIα has been described previously (McNeill and Colbran, 1995). pGEX-4T1 plasmids were transformed into BL21(DE3) bacteria cells to express GST-tagged proteins. Cells were grown in LB media at 37°C to reach OD~0.6. IPTG (0.2 mM) was then added to induce the protein expression at room temperature for 2 hours. We found that the $Ca_V1.2$ and $Ca_V1.3$ full-length C-terminal domain fragments do not express well in BL21(DE3) cells. We identified several rare codons in the cDNAs encoding both CTDs, and found that their expression was substantially improved in Rosetta 2(DE3) BL21 cells engineered to contain rare tRNAs (EMD Millipore Cat. #71400). Expressed proteins were purified using Pierce Glutathione Agarose beads (Cat. #16101) following manufacturer's instructions. Eluted proteins were then dialyzed in 10 mM HEPES pH 7.5, 25 μM PMSF, 62.5 μM Benzamidine, 62.5 μM EDTA, 0.1% TritonX-100 overnight with one buffer change.

CaMKII autophosphorylation and GST pulldown

Purified mouse CaMKIIα was incubated with 50 mM HEPES, pH 7.5, 10 mM $Mg(CH_3COO)_2$, 0.5 mM $CaCl_2$, 2.5 μM calmodulin, 40 μM ATP on ice for 90 s before addition of EDTA (20 mM final) to terminate phosphorylation by chelation of Mg^{2+} and Ca^{2+}. The reaction was then diluted 10-fold using 1X GST pulldown buffer (50 mM Tris-HCl pH 7.5; 150 mM NaCl; 1% (v/v) Triton X-100). A final protein concentration of 125 nM was used for both CaMKIIα and GST-tagged proteins. An aliquot (5%) of each incubation was saved as input followed by addition of 5 μl pre-washed Glutathione Magnetic Beads (Pierce, Cat. #88821, 25% v/v). After incubating at 4°C for 1 h, beads

were separated magnetically and washed three times with GST pulldown buffer. GST protein complexes were eluted by incubation with 40 μl of 20 mM glutathione (pH 8.0) in GST pulldown buffer at 4˚C for 10 min.

Cell culture, transfection and co-immunoprecipitation

Mouse CaMKIIα pcDNA was co-transfected with pcDNA empty vector (control) or pCGNH-Cav1.3, β3 and α2-δ subunits. A total of 10 μg DNA were transfected into one 6-cm dish of HEK293T cells. Amounts of DNA transfected were: CaMKIIα, 2 μg; pCGNH-Cav1.3 (WT, mutant or chimeras), 4 μg, pcDNA-β3, 2 μg; pcDNA-α2δ, 2 μg. After 48 hours of transfection, cells were lysed in 50 mM Tris-HCl, 150 mM NaCl, 1 mM EDTA, 1 mM EGTA, 1 mM DTT, 1% NP-40 (v/v), 1 mM Microcystin-LR and protease inhibitor cocktails. Cell lysates were cleared by low speed centrifugation (500 x *g*), and supernatant was used for subsequent co-immunoprecipitation. Where indicated, lysates were supplemented with 2 mM $CaCl_2$, 2 mM $MgCl_2$, 1 mM ATP and 1 μM calmodulin (final concentrations) to activate CaMKII prior to immunoprecipitation. Cell lysates were incubated at 4˚C for 1 hour with rabbit anti-HA (Santa Cruz, Cat. #sc805, 1:500) and 10 μl prewashed Dynabeads Protein A (Thermo Fisher Scientific, Cat. #10001D, 25% v/v). The beads were isolated magnetically and washed three times using lysis buffer before eluting proteins using 1X Laemmli sample buffer.

Fluorescent plate-binding assay

Fluorescent plate-binding assay has been previously described (Stephenson et al., 2017). Briefly, GST fusion proteins (200 pmol in 0.1 ml plate binding buffer (PBB): 50 mM Tris-HCl pH 7.5, 200 mM NaCl, 0.1 mM EDTA, 5 mM 2-mercaptoethanol, 0.1%

(v/v) Tween-20, 5 mg/ml bovine serum albumin) were added to the wells of glutathione-coated 96 well plates (Thermo Fisher Scientific, Cat. #15340). After incubation overnight at 4°C, the wells were washed with PBB, before adding lysates of transfected HEK293FT cells (100 µl) containing ~150 nM mApple-CaMKIIα WT or mutant proteins and supplemented with 2.5 mM $CaCl_2$, 1 µM calmodulin, 10 mM $MgCl_2$, and 400 µM ADP. After an additional 2-h incubation at 4°C, wells were washed in wash buffer (50 mM Tris-HCl pH 7.5, 150 mM NaCl, 0.5% (v/v) Triton X-100, and 2.4 mM $CaCl_2$) 2 times and bound mApple-CaMKIIα was detected using a fluorescent plate reader at 592 nm.

Electrophysiology

HEK293T cells in 35 mm dishes were transfected with 2 µg $Ca_V1.3$ WT or Δ69-93 pcDNAs together with 1 µg β3, 1 µg α2δ and 0.05 µg EGFP pcDNAs. Cells were split into new dishes 36 hours after transfection, and whole cell Ca^{2+} currents were recorded at room temperature 48 hours after transfection. Data were collected through Axopatch 200B amplifier and pCLAMP10 software (Molecular Devices, CA). Pipette resistance was 4-6 MΩ when loaded with the intracellular solution and immersed in the extracellular solution. Series resistance and membrane capacitance were compensated up to 80%. The intracellular solution contained (in mM): 132 CsCl, 10 Tetraethylammonium chloride (TEA-Cl), 10 EGTA, 1 $MgCl_2$, 3 Mg-ATP, 5 HEPES, pH 7.3 adjusted by CsOH. The external solution contained (in mM): 112 NaCl, 20 TEA-Cl, 10 $CaCl_2$, 5 CsCl, 1 $MgCl_2$, 10 HEPES, 5 glucose, pH 7.3 adjusted by NaOH. The osmolarity is 300 mOsm for the intracellular solution, and 305 mOsm for the extracellular solution. For current-voltage protocols, the membrane voltage was

depolarized in 50-ms steps from -70 mV to various voltages in 10 sec intervals. A P/4 protocol was used for leak subtraction.

Primary hippocampal neuron cultures and pCREB assay

Dissociated rat E18 hippocampal neurons were prepared as previously described (Sala et al., 2003), and transfected after 6-8 days *in vitro* (DIV). A total of 1 μg of DNA was transfected into each well of a 12-well plate using Lipofectamine 2000 with a DNA:lipid ratio of 1:1. For the pharmacological knock-in experiment, 0.6 μg of pCGN0-Ca_V1.3-sHA T1033Y, 0.2 μg pcDNA-β3, and 0.2 μg pcDNA-α2δ were transfected. For shRNA experiments, 0.4 μg pLLCK-ratCaMKIIα shRNA, 0.4 μg pLLCK-ratCaMKIIβ shRNA, and 0.2 μg pcDNA msCaMKIIα were transfected. Transfection complexes were incubated with neurons for 3 hours before switching back to conditioned medium. After an additional 72-h, neurons were pre-incubated with 5K Tyrode's solution (150 mM NaCl, 5 mM KCl, 2 mM $CaCl_2$, 2 mM $MgCl_2$, 10 mM glucose and 10 mM HEPES pH 7.5 (~313 mOsm)) with 1 μM TTX, 10 μM APV and 50 μM NBQX to suppress intrinsic neuronal activity by blocking sodium channels, NMDA receptors and AMPA receptors, respectively. Neurons were then treated with either 5K Tyrode's or 40K Tyrode's solution (adjusted to 40 mM KCl and 115 mM NaCl) containing TTX, APV and NBQX for 90-s. For nimodipine-treatment, neurons were incubated in 5K Tyrode's solution containing 10 μM nimodipine (plus TTX, APV and NBQX) for about 2-min before switching to 40K Tyrode's solution plus 10 μM nimodipine, TTX, APV and NBQX. Neurons were fixed using ice-cold 4% paraformaldehyde-4% sucrose in 0.1 M Phosphate Buffer pH 7.4 for 8 minutes, washed three times with PBS, permeabilized with PBS+0.2% Triton X-100, and then incubated with block solution for one hour (1X

PBS, 0.1% Triton X-100 (v/v), 2.5% BSA (w/v), 5% Normal Donkey Serum (w/v), 1% glycerol (v/v)). Neurons were then incubated overnight with primary antibodies: rabbit anti-pCREB (1:1000, Cell Signaling, Cat. #9198), and either mouse anti-HA (1:1000, Biolegend Cat. #901502) for pharmacological knock-in experiment or mouse anti-CaMKIIα (1:2000, Thermo Fisher Scientific, Cat# MA1-048) for shRNA experiments. The next morning, neurons were washed three times in PBS+0.2% Triton X-100 and incubated with 2nd antibody for one hour. Secondary antibodies (from Thermo Fisher Scientific) were diluted 1:1000 in block solution: donkey anti-Rabbit Alexa Fluor 647 (Cat# A-31573) and donkey anti-Mouse Alexa Fluor 546 (Cat# A-10036). After washing three times in PBS, neurons were mounted on slides using Prolong Gold Antifade Mountant with DAPI (Thermo Fisher Scientific Cat# P36931).

Neuronal pCREB imaging and quantification

Images were collected using an Olympus FV-1000 inverted confocal microscope with a 40x/1.30 Plan-Neofluar oil lens. The binocular lens was used to identify transfected neurons based on the Alexa 546 signal from the HA staining or EGFP from the shRNA construct. The DAPI channel was then used to focus on the z plane that yielded the highest DAPI signal (one that presumably runs across the nuclei) for image acquisition. Images were then collected in all the channels and MetaMorph Microscope Automation and Image Analysis Software (Molecular Devices) was used to quantify the pCREB signal. Briefly, nuclei were identified by thresholding the DAPI channel to create and select the nuclear regions of interest (ROIs). The ROIs were then transferred to other channels to measure the average pCREB intensity.

The relative pCREB intensity was computed as ($pCREB^{x}$-$pCREB^{\underline{5K}}$)/($pCREB^{\underline{40K}}$-$pCREB^{\underline{5K}}$), where $pCREB^{x}$ is the pCREB signal being calculated, and $pCREB^{\underline{5K}}$ and $pCREB^{\underline{40K}}$ are the average signals of the 5K and 40K conditions in that batch of cultured neurons, respectively. Data shown were collected from images of the indicated total number of neurons from 3~4 independent cultures.

Neuronal Ca^{2+} imaging

Dissociated rat hippocampal neurons cultured in coated 29 mm glass bottom dishes (Cellvis, Cat# D29-10-1.5-N) were transfected with a total of 2 μg DNA/dish after 8 DIV. All neurons (nontransfected for Fig. 7A, transfected with shRNA vectors for Fig. 8A) were imaged on DIV 13-14. Because GFP fluorescent interferes with Fura-2 imaging, CaMKII shRNA constructs lacking the CaMKII promoter and GFP were cotransfected with an mApple expression construct to label transfected cells. Cells were incubated in the culture medium (Neural Basal Medium with 2% B27, 0.25% Glutamax, and 1% Penicillin-Streptomycin) supplemented with 2 μM Fura-2 acetoxymethyl ester (Thermo Fisher Scientific, Cat# F1221) for 20 minutes at 37°C. Cells were then washed twice with 5K Tyrode's solution and incubated for 15 minutes at 37°C in 5K Tyrode's solution with TTX, APV and NBQX (as above). For nimodipine-treated groups, this solution was replaced with 5K Tyrode's solution containing 10 μM nimodipine (in addition to TTX, APV and NBQX) ~5 min before imaging. Fura-2 fluorescence images were collected using a Nikon Eclipse TE2000-U microscope equipped with an Epi-fluorescence Illuminator (Sutter Instrument Company) and an HQ2 CCD camera (PhotoMetrics Inc.). Baseline Ca^{2+} was recorded for 30 s in 5K Tyrode's solution before replacing by 40K Tyrode's solution. Cell somas were selected as regions of interest using Nikon

Elements software; transfected neurons were selected based on mApple fluorescence. The ratios of emitted fluorescence (505 nm) intensities at excitation wavelengths of 340 and 380 nm (F340/F380) were measured every 5 s, and the response of individual cells at each time point was quantified as the change in fluorescence ratio above baseline (ΔF= (340/380 value)/(baseline 340/380 value)). The peak change in fluorescence ratio was used to compare responses between cells in each group (ΔF = (maximum 340/380 value)/ (baseline 340/380 value)) and outlier cells were excluded based on a ROUT outliers test (Q = 1%). The numbers of excluded outliers were: Fig. 7A, 31 of 246 cells from 40+NIM group; Fig 8A, 1 of 18 cells from the control group (mApple only) and 1 of 24 cells from the CaMKIIα/β shRNA group.

2.2 Results

2.2.1 A proteomics approach to identify L-type Ca^{2+} channel complexes

CaMKII has been suggested to interact with the pore-forming α1 subunits of Ca_V1.2 and Ca_V1.3 (Hudmon et al., 2005; Jenkins et al., 2010; Simms et al., 2014), although it is unclear which LTCC domains mediate this interaction. To address this question, we first expressed and purified a family of GST-fusion proteins containing each of the intracellular domains from the Ca_V1.2 and Ca_V1.3 α1 subunits. After incubating each protein with mouse forebrain extracts (Fig. 2.1A, B), the resulting complexes were isolated using glutathione agarose, eluted using 20 mM glutathione and resolved by SDS-PAGE for LC-MS/MS analysis.

Consistent with previous findings (Pragnell et al., 1994), Ca^{2+} channel β auxiliary subunits were specifically detected in complexes isolated using the linker domains that connect transmembrane domains I and II of both $Ca_V1.2$ and $Ca_V1.3$ (Fig. 2.1C1). However, based on the number of spectral counts, the most abundant proteins detected in any of these complexes were the four CaMKII isoforms, which were specifically detected in $Ca_V1.3$ and $Ca_V1.2$ NTD complexes with an ~5:1 ratio of spectral counts (Fig. 2.1C2). These data show that brain CaMKII isoforms can directly or indirectly associate with the N-terminal domain of $Ca_V1.3$ and $Ca_V1.2$.

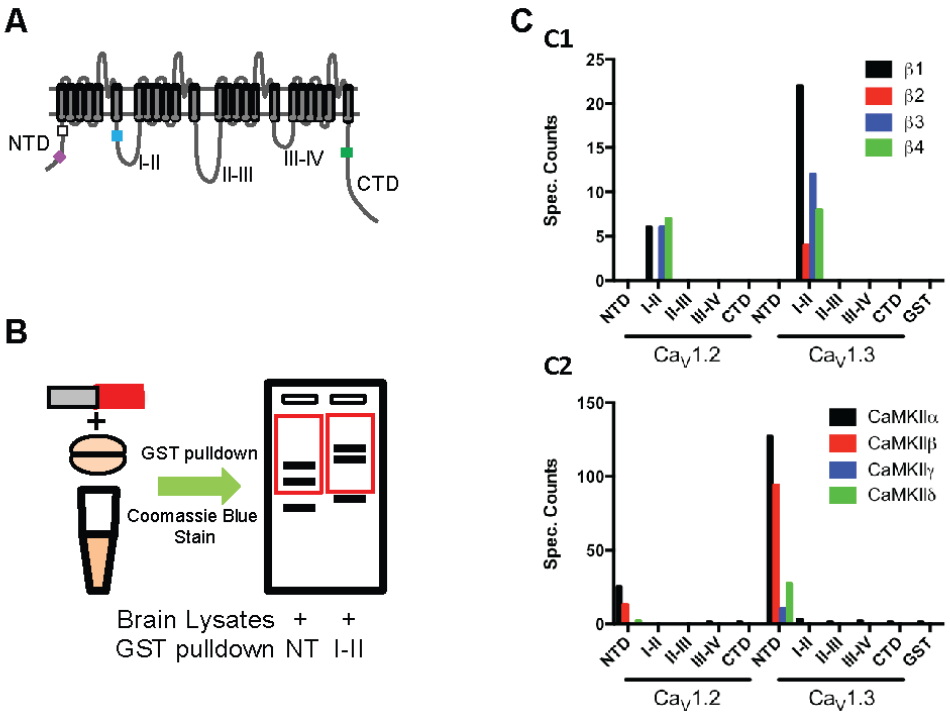

FIGURE 2.1 Proteomics detection of a specific CaMKII interaction with LTCC N terminal domains. *A*, domain structure of L-type Ca^{2+} channels. Rectangular boxes in the intracellular domains indicate approximate positions of previously reported calmodulin- (NSCaTE) (purple box) and CaMKII- (white box) binding domains in the NTD, the α subunit interaction domain (AID, for β subunit interaction) in the I/II linker (blue box), and overlapping calmodulin- and CaMKII-binding sites in the CTD (green box). *B*. a flow chart of the proteomics analysis of neuronal L-type Ca^{2+} channel macrocomplexes. Purified GST-tagged $Ca_V1.2$ and $Ca_V1.3$ intracellular domains were incubated individually with mouse forebrain lysates. Proteins that bound to the GST fusion proteins were submitted for proteomics analysis (see Methods). *C*. Total spectral counts for β auxiliary subunits (C1) and CaMKII proteins (C2) detected in complexes with each LTCC intracellular domain.

2.2.2 Activated CaMKII directly binds to $Ca_V1.3$ NTD

To determine whether CaMKII directly interacts with $Ca_V1.3$ N-terminal domain, GST-fusion proteins containing each intracellular domain of the $Ca_V1.3$ $\alpha1$ subunit were incubated with purified mouse CaMKIIα. Since direct interactions of CaMKII with several neuronal proteins are differentially modulated by CaMKII activation (Jiao et al., 2011; Jin et al., 2013a; Strack et al., 2000a), we tested for direct binding following pre-incubation of CaMKIIα to induce different conformations. There was no consistently detectable binding of inactive CaMKII to any of the intracellular domains above the level of GST control, but the $Ca_V1.3$ NTD directly and specifically interacts with activated CaMKII conformations induced by pre-autophosphorylation at Thr286 (Fig. 2.2A), or by the binding of Ca^{2+}/calmodulin and ADP (Fig. 2.2B). The fact that binding of Ca^{2+}/calmodulin and ADP to CaMKII is sufficient to induce interaction with the NTD shows that Thr286 phosphorylation is not necessary for binding; rather, an open, activated conformation of CaMKII is required. Thus, these data show that activated CaMKII directly interacts with the NTD of $Ca_V1.3$ with very high selectivity.

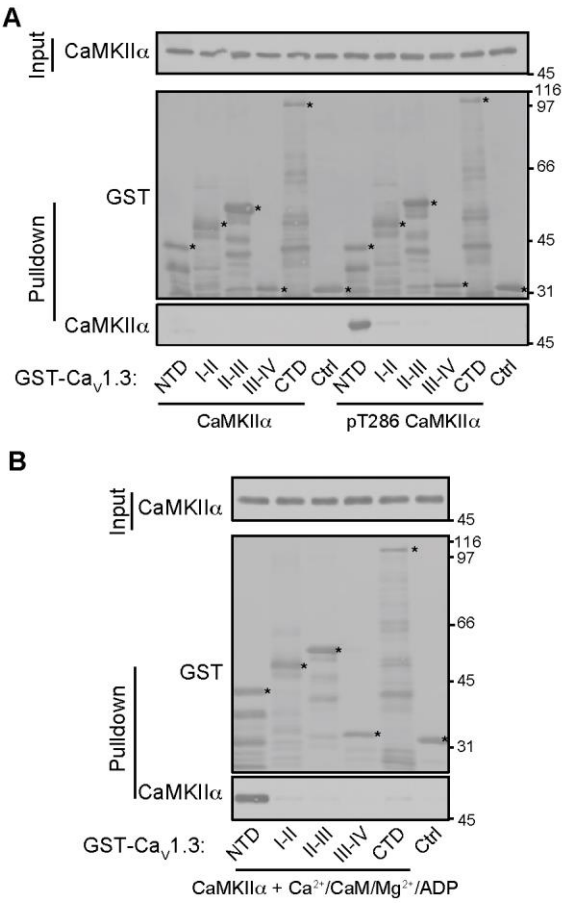

FIGURE 2.2 Activated CaMKII specifically binds to the LTCC NTD. *A.* Glutathione-agarose co-sedimentation assays show that there is no reliably detectable interaction of inactive (non-autophosphorylated) conformations of CaMKIIα with any of the Ca$_V$1.3 intracellular domains, but that activated (pre-autophosphorylated, pT286) CaMKIIα specifically binds to the NTD. *C*. Activation of CaMKIIα by binding of Ca^{2+}/calmodulin and Mg-ADP is sufficient for interaction with the Ca$_V$1.3 NTD. Despite extensive efforts to further optimize the experimental conditions, some of these proteins were partially degraded; however, full-length proteins were readily detected (indicated by asterisks). The immunoblots shown are representative of three independent experiments.

2.2.3 CaMKII/NTD interaction is L-type channel specific

In order to further investigate the specificity of this novel CaMKII interaction, we compared the amino acid sequences of NTDs from all 10 human VGCC α1 subunits. The NTDs are quite divergent in the initial membrane-distal sections but become more conserved in the membrane-proximal region (Fig. 2.3A). A similar conservation pattern holds true for mouse and rat VGCCs. To test binding specificity, we expressed and purified GST-tagged NTDs from $Ca_V1.2$, $Ca_V2.2$ and $Ca_V3.2$. As noted above, pre-activated purified CaMKII robustly interacts with the $Ca_V1.3$ NTD, and there was a slightly weaker interaction with the $Ca_V1.2$ NTD. However, interaction of pre-activated CaMKII with the $Ca_V2.2$ and $Ca_V3.2$ NTDs was barely detected above the GST negative control (Fig. 2.3B, C). These data show that activated CaMKII selectively interacts with NTDs of the LTCCs.

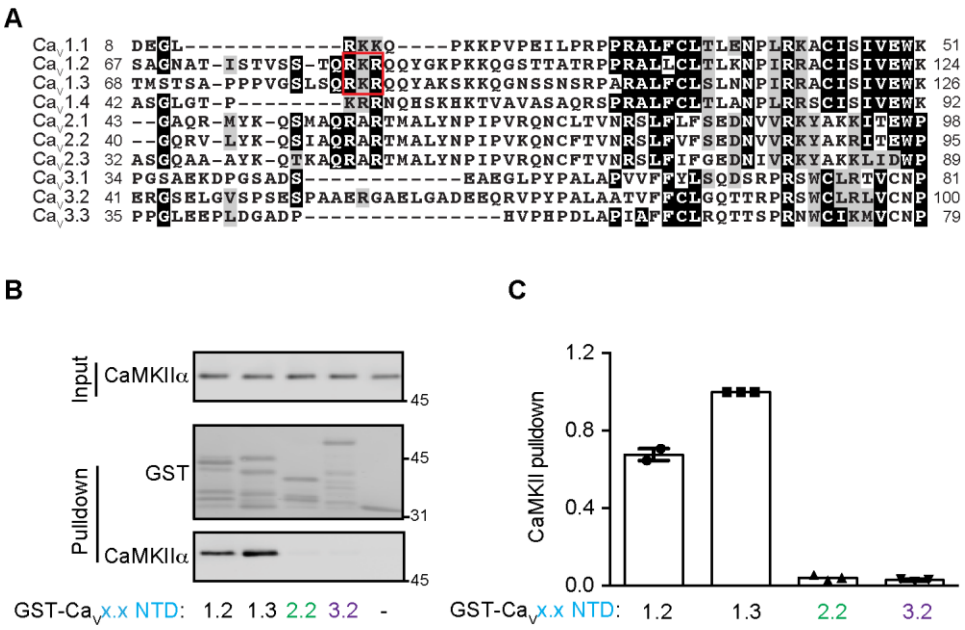

FIGURE 2.3 CaMKII specifically binds to LTCC NTDs. *A*. Alignment of membrane proximal regions of the NTDs from all human VGCCs. Ca^{2+} channel NTDs are more conserved in membrane-proximal regions but become more divergent in the distal regions. *B*. Representative glutathione-agarose co-sedimentation assay comparing the binding of activated CaMKII to GST-NTDs from Ca_V1, Ca_V2 and Ca_V3 Ca^{2+} channels. *C*. Quantitation of 2-3 independent experiments similar to those shown in B. The $Ca_V1.3$ NTD shows the strongest binding to CaMKIIα, followed by $Ca_V1.2$, while interactions with $Ca_V2.2$ and $Ca_V3.2$ are barely detected. All values were normalized to $Ca_V1.3$ NTD pulldown.

2.2.4 Molecular determinants for CaV1.3 NTD interaction with CaMKII

Previous studies indicate that the $Ca_V1.2$ and $Ca_V1.3$ NTDs contain conserved binding sites for calmodulin (residues S52-K64 in $Ca_V1.3$), termed NSCaTE (Dick et al., 2008; Tadross et al., 2008), and for CaMKII (K110-W123 in $Ca_V1.2$) (Simms et al., 2014). To investigate the potential roles of these domains in the CaMKII binding detected here, we mapped the site of direct CaMKII interaction in the $Ca_V1.3$ NTD (Fig. 2.4A). There was no detectable interaction between pre-activated CaMKII and the membrane distal fragment (NT-A: amino acids 1-68) containing the NSCaTE domain (Fig. 2.4B), but the membrane proximal fragment (NT-B: amino acids 69-126) robustly interacts with pre-activated CaMKII. Further dissection of NT-B revealed that pre-activated CaMKII interacts with a GST-tagged fragment containing residues 69-93 (NT-B1), but not with two fragments containing more membrane proximal residues 94-110 or 111-126 (NT-B2 and NT-B3, Fig. 2.4C).

The amino acid sequence of $Ca_V1.3$ residues 69-93 shares little identifiable similarity with known CaMKII-binding domains in other proteins (Bayer et al., 2001; Grueter et al., 2008; Strack et al., 2000a). However, we identified three basic amino acids in $Ca_V1.3$ (Arg^{83}-Lys^{84}-Arg^{85}) that are largely conserved in NTDs of $Ca_V1.2$ and other LTCC $\alpha1$ subunits, but not in the NTDs of $Ca_V2.2$ or $Ca_V3.2$ (which do not bind CaMKII), or of other $\alpha1$ subunits (Fig. 2.3A). Replacement of this RKR motif with three alanines in the $Ca_V1.3$ NTD almost completely abrogated binding of pre-activated CaMKII (Fig. 2.4D). These data identify three amino acids in the $Ca_V1.3$ NTD that are required for strong and direct *in vitro* interactions with pre-activated CaMKII.

Comparison of the NTD sequences of Ca_V1 and Ca_V2 channels revealed that only one residue in the $Ca_V1.3$ RKR motif was not conserved in Ca_V2 channels (Fig. 2.3A). To test the importance of the each of the amino acids in CaMKII interaction, we created single and double alanine mutation of the $R^{83}KR^{85}$ and performed GST pulldown assay. As shown in Fig. 2.4E and F, mutation of any one of the three amino acids is sufficient to disrupt the interaction between CaMKII and $Ca_V1.3$ N-terminal domain. Substitution of Lys^{84} or Arg^{85} with an alanine has a consistently stronger effect than substitution of Arg^{83}, suggesting Lys^{84} and Arg^{85} are more critical in mediating CaMKII/$Ca_V1.3$ NTD interaction.

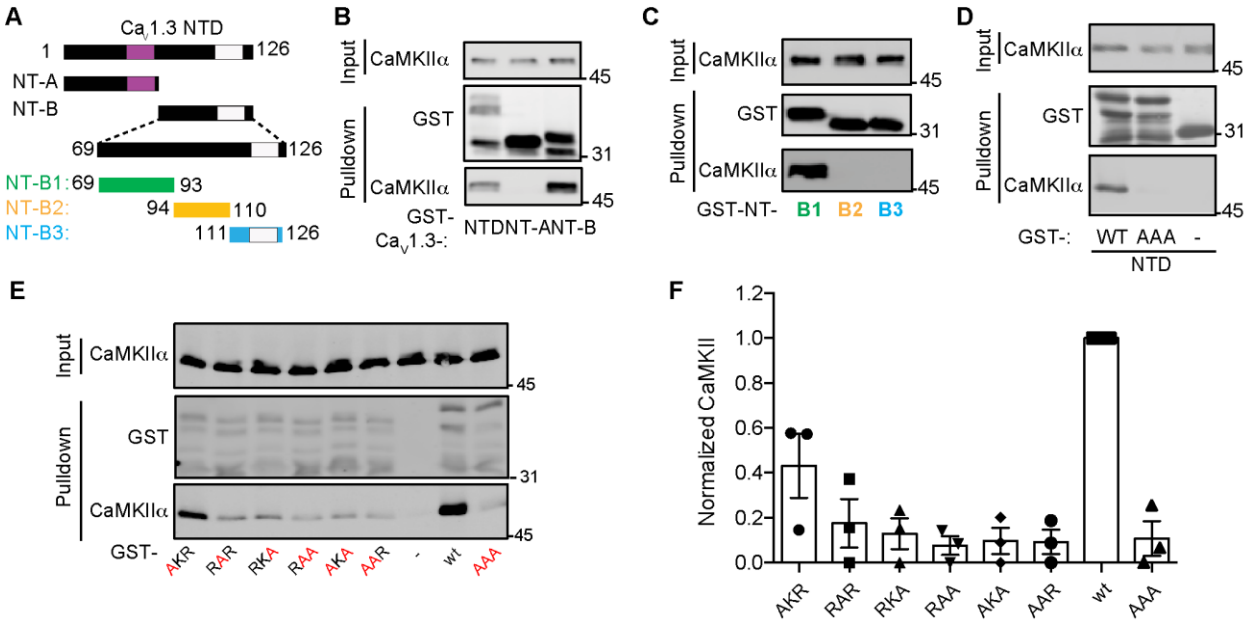

FIGURE 2.4 Characterization of the Cav1.3 NTD CaMKII binding domain. *A*. Truncations used to map the CaMKII interaction site in the Cav1.3 NTD. Purple and white rectangles indicate approximate positions of previously-defined NSCaTE calmodulin-binding and CaMKII-binding domains, respectively (see legend to Fig. 1 and main text). *B*. Glutathione-agarose co-sedimentation assay comparing binding of activated CaMKIIα to the full-length Cav1.3 NTD, the membrane-distal part (NT-A) and the membrane-proximal part (NT-B). *C*. Analysis of further NTD truncations reveals that the NT-B1 region (residues 68-93) is sufficient for binding of activated CaMKIIα. *D*. Mutation of amino acids $R^{83}KR^{85}$ to AAA within the full-length Cav1.3 NTD blocks Cav1.3-CaMKIIα interaction. *E*. and *F*. Further analysis and quantification of the effects of single or double mutation of the three basic amino acids $R^{83}KR^{85}$ on CaMKII binding. These immunoblots are representative of at least three independent replicates. Experiments in panels E and F were performed by Brynna Paulukaitis.

Preferential interactions of pre-activated CaMKII with several other CaMKII-associated proteins (CaMKAPs) are mediated by the catalytic domain. Therefore, to identify CaMKIIα residues critical for binding to the $Ca_V1.3$ NTD, we screened previously characterized as well as novel CaMKII mutations in the catalytic domain (Fig. 2.5A) using a fluorescence-based 96-well plate binding assay (see Methods). An I205K mutation, previously shown to disrupt binding to GluN2B and the densin-IN domain (Bayer et al., 2001; Bayer et al., 2006; Jiao et al., 2011), also reduced binding to the $Ca_V1.3$ NTD by ~80% (Fig. 2.5B). We identified two additional CaMKII mutations (V102E and E109K) that also significantly interfere with binding to the $Ca_V1.3$ NTD (Fig. 2.5B), whereas another mutation (Y210E) had no significant impact. Strikingly, the CaMKIIα-V102E mutation had no significant effect on binding to the β2a subunit of VGCCs, the densin-IN or -CTD domains (Fig 2.5C) or to GluN2B (not shown). In combination, these data suggest that the mechanism underlying binding of activated conformations of CaMKII to the $Ca_V1.3$ NTD is partially distinct from the mechanisms for binding to other known CaMKAPs.

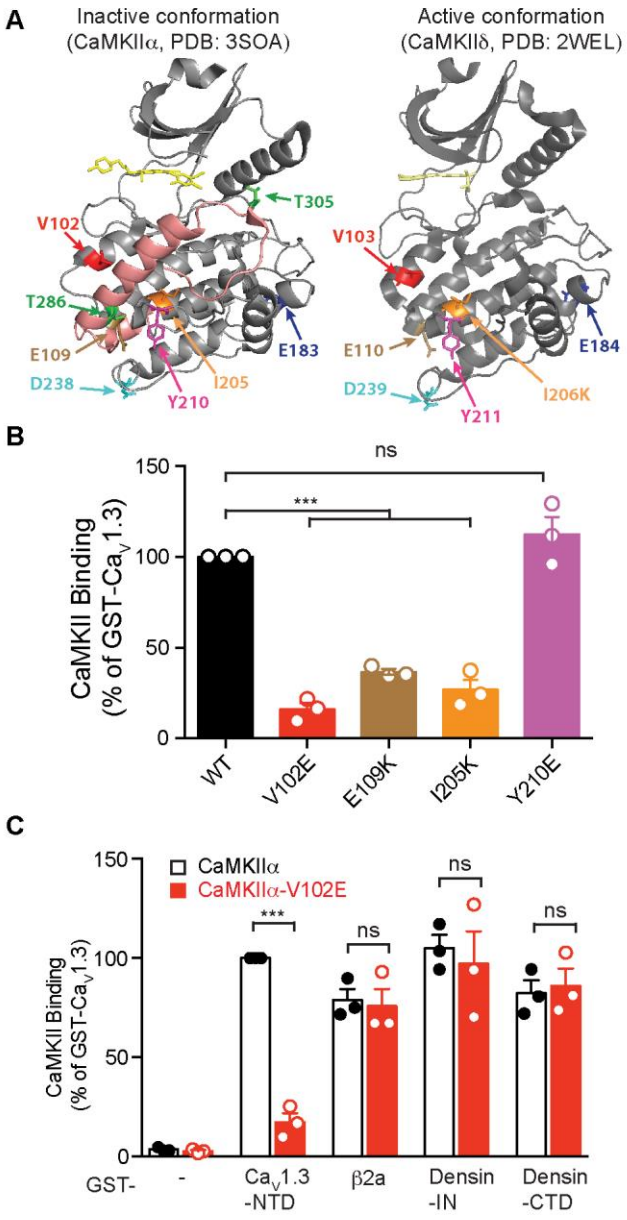

FIGURE 2.5 Identification of a CaMKII mutation that specifically disrupts binding to the Cav1.3 NTD. *A*. CaMKII structures. Left, a single CaMKIIα subunit in an inactive (autoinhibited) conformation with an inhibitor (Bosutinib, yellow) bound in the nucleotide binding site (PDB:3SOA, (Chao et al., 2011)). Right, a single CaMKIIδ subunit in an activated conformation (displaced regulatory domain) with a bound inhibitor (SU6656, yellow) (PDB:2WEL (Rellos et al., 2010)). The catalytic and regulatory domains are

shown in grey and pink, respectively. For clarity of presentation, C-terminal holoenzyme association domains are not shown and the displaced regulatory domain with bound Ca^{2+}/calmodulin is not shown in PDB:2WEL. T286 and T305 (green) are two regulatory autophosphorylation sites. Mutation of I205/6 (orange) to Lys disrupts CaMKII interaction with GluN2B and Densin-IN (Bayer et al., 2001; Jiao et al., 2011), whereas mutation of D238/9 (cyan) to Arg disrupts GluN2B binding but spares interactions with Densin-IN (Jiao et al., 2011). A naturally occurring *de novo* E183 (purple) to Val mutation in CaMKIIα is linked to autism spectrum disorder and disrupts CaMKII interaction with multiple CaMKAPs *(Iossifov et al., 2014; Stephenson et al., 2017). B.* A 96-well glutathione plate assay to screen activated mApple-tagged CaMKIIα mutants for interactions with GST-tagged $Ca_V1.3$ NTD. *C*. Binding of activated mApple-tagged WT and V102E-CaMKIIα to multiple GST-CaMKAP proteins in the 96-well plate assay. A V102E mutation selectively disrupts CaMKIIα binding to the $Ca_V1.3$ NTD: V102/3 is highlighted in red in Panel A. Data from three independent experiments were analyzed by one-way ANOVA (for panel *B*) and two-way ANOVA followed by Sidak's multiple comparison test (for panel *C*), respectively. ***, $p<0.001$; ns, not significant ($p>0.05$). Experiments in panels B and C were performed by Christian Marks and Tyler Perfitt.

2.2.5 The $Ca_V1.3$ NTD is important for CaMKII association with LTCC complexes

In order to begin to address the importance of the $Ca_V1.3$ NTD in CaMKII targeting to LTCC complexes, we first directly compared CaMKII binding to GST fusion proteins containing the $Ca_V1.3$ NT-B1 fragment or previously defined minimal CaMKII-binding domains in the VGCC $\beta2$ subunit (residues 485-505) (Grueter et al., 2008) and a $Ca_V1.2$ CTD fragment (residues 1639-1660) that is fully conserved in $Ca_V1.3$ (Hudmon et al., 2005). Although we did not detect CaMKII binding to the full length $Ca_V1.3$ CTD (Fig. 2.2B,C), we rationalized that the full-length CTD may adopt a conformation that prevents CaMKII interaction with this previously defined domain, perhaps due to binding of a C-terminal modulatory domain to the calmodulin-binding IQ domain (Singh et al., 2008). Similar levels of pre-activated CaMKII bound to the $Ca_V1.3$ NT-B1 and $\beta2$-(485-505) fragments, but we could not detect an interaction with the $Ca_V1.3$ CTD-(1639-1660) fragment under these conditions (Fig 2.6A). Nevertheless, these data indicate that CaMKII can directly interact with multiple components of native LTCC complexes.

The most abundant VGCC auxiliary β subunit in the brain appears to be $\beta3$ (Ludwig et al., 1997). Therefore, we investigated whether the NTD is important for CaMKII targeting to $Ca_V1.3$ LTCC complexes containing the $\beta3$ subunit. CaMKIIα, $\beta3$ and the $\alpha2\delta$ subunit were co-expressed in HEK293T cells with the HA-tagged WT $Ca_V1.3$ $\alpha1$ subunit, or with chimeric $\alpha1$ subunits in which the $Ca_V1.3$ NTD was replaced with NTDs from either $Ca_V2.2$ or $Ca_V3.2$ NTD (Fig. 2.6B). Antibodies to the HA-tag were then used to immunoprecipitate $\alpha1$ subunits from aliquots of the same cell lysate in the presence of EDTA, or following addition of excess Ca^{2+}/CaM and Mg^{2+}-ATP to activate CaMKIIα (see Methods). Immunoblotting revealed that the HA-immune complexes isolated in the

presence of Ca^{2+}/calmodulin/Mg^{2+}-ATP contained significantly more HA-$Ca_V1.3$ $\alpha1$ subunit and CaMKIIα, relative to immune complexes isolated in parallel in the presence of excess EDTA. Similar data were obtained from two independent sets of experiments (Figs. 2.6C, D). Combining the quantitative analysis of these two data sets revealed that Ca^{2+}/CaM/Mg^{2+}-ATP increased the levels of HA-$Ca_V1.3$ and CaMKIIα by 2.5±0.3-fold and 12.8±2.6 fold, respectively (mean±S.E.M., n=7; $p<0.01$ for both, one-sample *t* test compared to a theoretical value of 1.00 indicating no change). Therefore, addition of Ca^{2+}/calmodulin/Mg^{2+} /ATP significantly increases the ratio of CaMKII to HA-$Ca_V1.3$ in the immune complexes by 6.7±2.3-fold (n=7; $p<0.001$).

In order to explore the mechanism underlying these changes, we first found that addition of Ca^{2+}/calmodulin/Mg^{2+}/ATP failed to increase the levels of immunoprecipitated HA-$Ca_V1.3$ in the absence of co-expressed CaMKIIα (data not shown). Moreover, replacement of the entire $Ca_V1.3$ NTD with corresponding NTDs from $Ca_V2.2$ or $Ca_V3.2$ (Fig. 2.6B) abrogated Ca^{2+}/calmodulin/Mg^{2+}/ATP-induced increases in the levels of both HA-tagged channels and CaMKIIα in the HA-immune complexes, as well as in the CaMKIIα/HA-$Ca_V1.3$-chimera ratio (Fig. 2.6C). Similarly, significant Ca^{2+}/calmodulin /Mg^{2+}/ATP-induced increases in levels of CaMKII and HA-$Ca_V1.3$ and in the CaMKII to HA-$Ca_V1.3$ ratio in the HA-immune complexes were prevented by deletion of residues 69-93 or mutation of $R^{83}KR^{85}$ to AAA within the $Ca_V1.3$ NTD (Fig. 2.6D). Finally, CaMKIIα-V102E mutation also prevented Ca^{2+}/calmodulin/Mg^{2+}/ ATP-induced increases in levels of HA-$Ca_V1.3$ and CaMKIIα, and in the CaMKIIα/HA-$Ca_V1.3$ ratio, in HA-immune complexes (Fig. 2.6D). Since all of the

molecular changes tested here disrupt the CaMKII-NTD interaction *in vitro*, these data collectively indicate that CaMKIIα interaction with the NTD is required for activity-dependent association of CaMKIIα with intact HA-Ca$_V$1.3 complexes, as well as for a more modest increase in the immunoprecipitation of HA-Ca$_V$1.3.

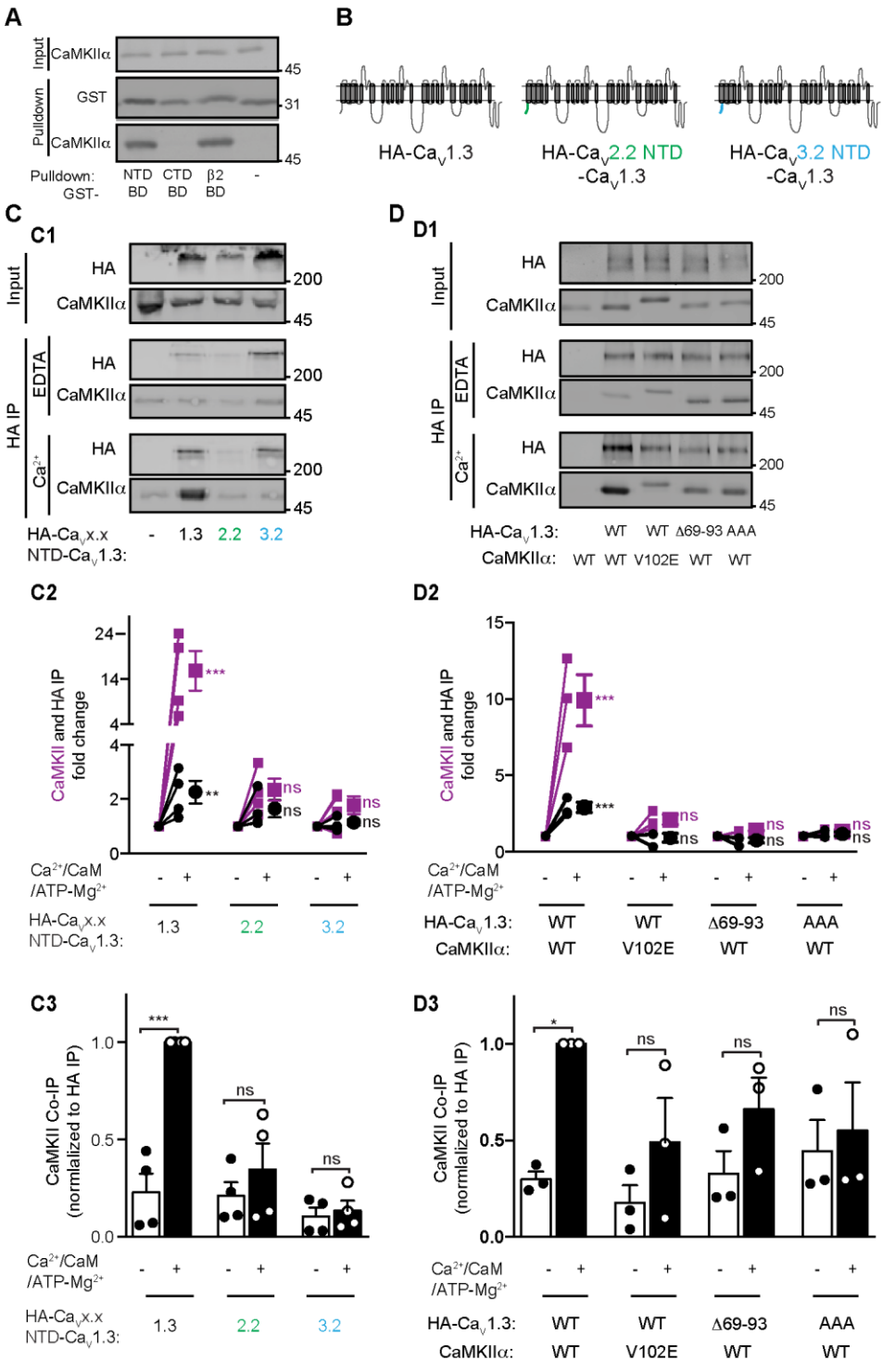

FIGURE 2.6 The NTD is important for CaMKII association with LTCC complexes. *A*. Pre-activated CaMKIIα robustly interacts with the minimal CaMKII-binding sites from the CaV1.3 NTD and the β2 auxiliary subunit, but not with a previously reported minimal

CaMKII-binding site in the $Ca_V1.2$ CTD that is identical in $Ca_V1.3$. *B*. A schematic diagram showing the structure of chimeric $Ca_Vx.x$ NTD-$Ca_V1.3$ channels in which the $Ca_V1.3$ NTD was substituted by NTDs from $Ca_V2.2$ or $Ca_V3.2$. *C.* Equal aliquots of lysates from cells expressing CaMKIIα with WT or NTD chimeric HA-tagged $Ca_V1.3$s were immunoprecipitated using anti-HA antibodies without (EDTA) or with the addition of excess Ca^{2+}/calmodulin/Mg^{2+}-ATP. *C2* plots levels of immunoprecipitated HA-$Ca_V1.3$ proteins (black) and CaMKII (purple) in the presence of Ca^{2+}/calmodulin/Mg^{2+}/ATP normalized to levels isolated in the presence of EDTA in each experiment. *C3* compares levels of immunoprecipitated CaMKIIα normalized to immunoprecipitated HA proteins in the presence of EDTA and Ca^{2+}/calmodulin/Mg^{2+}-ATP. *D*. Similar analysis of the co-immunoprecipitation of WT or V102E-CaMKIIα with WT, Δ69-93 or RKR-AAA HA-$Ca_V1.3$ in the presence of EDTA or Ca^{2+}/calmodulin/Mg^{2+}/ATP. Levels of immunoprecipitated HA-$Ca_V1.3$ and CaMKIIα are compared in *D2*, and normalized CaMKIIα/HA-$Ca_V1.3$ ratios are shown in *D3*. Data are from 3-4 independent experiments, and analyzed by two-way ANOVA followed by Sidak's multiple comparison test. *, $p<0.05$; ***, $p<0.001$; ns, not significant ($p>0.05$).

2.2.6 The $Ca_V1.3$ NTD Δ69-93 deletion does not affect Ca^{2+} influx

In order to assess the impact of the NTD CaMKII-binding site on LTCC activity, we compared Ca^{2+} influx via WT and Δ69-93 $Ca_V1.3$ LTCCs containing β3 and α2δ subunits in HEK293T cells. Whole cell currents were elicited by step depolarizations from the holding voltage of -70 mV to a series of test voltages, which were held for 50 ms (Fig. 2.7A). Analysis of the current-voltage relationships indicated that deletion of amino acids 69-93 had no significant effect on voltage-dependent activation (WT: $V_{1/2}$ = -11.4± 3.2 mV, k = 5.3±2.8 mV, n = 13; Δ69-93: $V_{1/2}$ = -9.2±5.2 mV, k = 8.8±4.7 mV, n = 15; p>0.05 for both, two-tailed unpaired student *t* test) or on the maximal current density (10.9±2.6 pA/pF for WT vs 8.6±2.5 pA/pF for Δ69-93, p = 0.49, two-tailed unpaired student *t* test, Fig. 2.7A-C). Furthermore, there was no difference in residual current measured 30 ms after depolarization to 0 mV, indicating that fast inactivation kinetics also were unaffected (Fig. 2.7D). These data suggest that the deletion of NTD residues 69-93 has no significant effect on the properties of $Ca_V1.3$/β3/α2δ LTCCs.

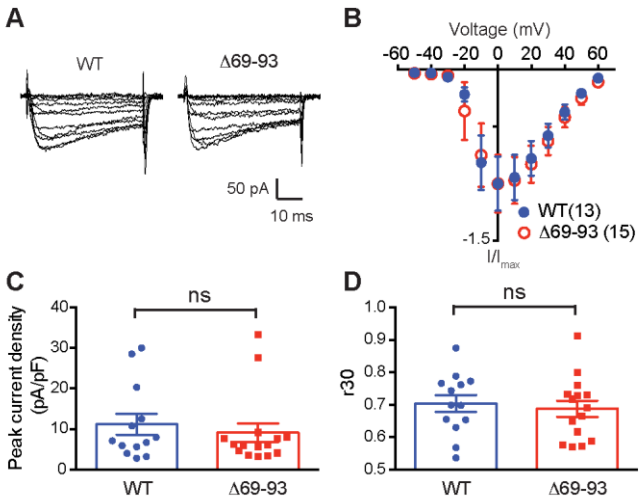

FIGURE 2.7 Deletion of residues 69-93 from the $Ca_V1.3$ NTD does not affect Ca^{2+} influx via $Ca_V1.3$ LTCCs. *A*. Representative Ca^{2+} currents elicited by step depolarizations (50 ms) to various voltages for $Ca_V1.3$-WT (left) and $Ca_V1.3$-Δ69-93 LTCCs. Scale bars: 10 ms (horizontal) and 50 pA (vertical), respectively. *B*. No significant difference in current-voltage (I-V) relationships for $Ca_V1.3$-WT and $Ca_V1.3$-Δ69-93 LTCCs (P>0.05, two-way ANOVA followed by Sidak's multiple comparison test). *C*. No significant difference in peak current densities of $Ca_V1.3$-WT and $Ca_V1.3$-Δ69-93 LTCCs. *D*. No significant difference in fast inactivation of $Ca_V1.3$-WT and $Ca_V1.3$-Δ69-93 LTCCs, based on the fraction of residual current measured 30 ms after depolarization from -70 mV to 0 mV. Data were collected from 5 independent transfections, n=13 for WT and n=15 for Δ69-93. Data were analyzed by two-tailed unpaired student *t* test; ns, not significant (p>0.05).

2.2.7 $Ca_V1.3$ NTD is required for LTCC-and CaMKII-mediated nuclear signaling

We then tested whether the NTD-CaMKII interaction is important for LTCC-mediated downstream signaling to increase Ser133 phosphorylation of the CREB transcription factor in primary cultures of hippocampal neurons. We first established a stimulation paradigm to induce LTCC-dependent increases of Ca^{2+} concentrations based on imaging neuronal Ca^{2+} with Fura2. Neurons were pre-incubated in 5 mM K^+ Tyrode's solution containing APV and CNQX to block the activation of NMDA- and AMPA-type glutamate receptors, and with tetrodotoxin (TTX) to inhibit voltage-dependent sodium channels. Neuronal depolarization by replacing the solution with 40 mM K^+ Tyrode's solution in the presence of APV, CNQX and TTX induced a significant increase in intracellular (somatic) Ca^{2+}, which is reduced by ~80% in the presence of 10 μM nimodipine, a highly selective LTCC antagonist (Fig. 2.8A). In parallel, we showed that depolarization with 40 mM KCl in the presence of APV, CNQX and TTX for 90 seconds induces a robust increase of nuclear staining using a phospho-Ser133 specific CREB antibody (pCREB staining) that can be completely blocked by 10 μM nimodipine (Fig. 2.8B, C), consistent with previous findings (Wheeler et al., 2008; Wheeler et al., 2012; Zhang et al., 2006). We then used a pharmacological knock-in approach (Dolmetsch et al., 2001) to compare the E-T coupling efficiency of wild-type $Ca_V1.3$ with $Ca_V1.3$-Δ69-93, which compromises CaMKII-binding. We expressed an HA-tagged nimodipine-resistant $Ca_V1.3$ mutant (T1033Y, designated as $Ca_V1.3^{DHPR}$) to allow for activation of exogenous channels while using nimodipine to block all endogenous LTCCs. The expression of $Ca_V1.3^{DHPR}$ almost completely rescued the increase of pCREB staining in the presence of nimodipine (transfected neurons were identified by staining for the HA-

epitope), but this rescue of pCREB signaling was disrupted by the deletion of NTD residues 69-93 from $Ca_V1.3^{DHPR}$, which prevents CaMKII binding (Fig. 2.8C).

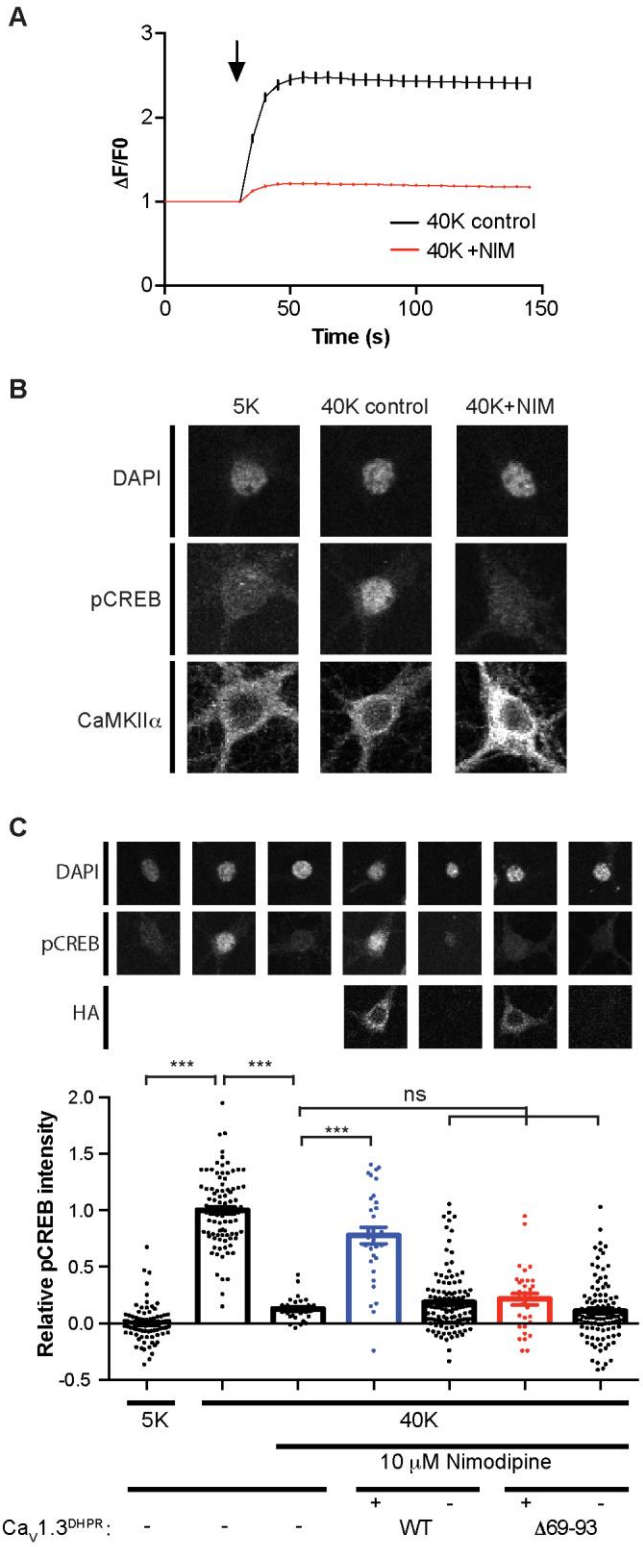
A
ΔF/F0
Time (s)
40K control
40K +NIM
B
5K
40K control
40K+NIM
DAPI
pCREB
CaMKIIα
C
DAPI
pCREB
HA
Relative pCREB intensity
***
***
ns
***
5K
40K
10 μM Nimodipine
Ca$_V$1.3^{DHPR}:
WT
Δ69-93

FIGURE 2.8 Role of the LTCC NTD in high K^+-induced CREB Ser133 phosphorylation. *A*. Ca^{2+} imaging showing that nimodipine largely prevents the high K^+-induced increase of somatic Ca^{2+}. Neurons were incubated with Tyrode's solution containing 5 mM KCl (5K) for 30 seconds and switched to Tyrode's solution containing 40 mM KCl (black arrow) for 2 minutes in the absence (40K control, n=193) or presence (40K+NIM, n=215) of 10 μM nimodipine. The black arrow indicates the buffer switch and data were plotted as mean±S.E.M. A total of 5 dishes from two independent cultures were analyzed per group. *B*. Depolarization of cultured hippocampal neurons induced LTCC-dependent Ser133 phosphorylation of CREB. Columns from left to right: neurons were incubated with 5K Tyrode's solution and then switched to 5K, 40K control, or 40K+NIM Tyrode's solution, respectively, for 90 seconds. Neurons were then fixed and stained for DAPI, CREB Ser133 phosphorylation (pCREB) and CaMKIIα. Incubation with 40 mM KCl induced an increase of pCREB that was blocked by the LTCC antagonist nimodipine. *C*. Deletion of the CaMKII-binding domain in the $Ca_V1.3$ NTD disrupts nuclear signaling. Expression of a nimodipine-resistant $Ca_V1.3$-T1033Y mutant rescues the nimodipine blockade of pCREB induction by 40mM KCl. However, deletion of the CaMKII binding domain (Δ69-93) prevents the rescue of pCREB signaling by $Ca_V1.3$-T1033Y. Each data point represents analysis of a single cell collected from 3~4 independent neuronal cultures/transfections. Pooled data were analyzed by one-way ANOVA followed by Tukey's multiple comparison test. ***, $p<0.001$; ns, not significant ($p>0.05$). All confocal images show a 40 μm x 40 μm area. Ca^{2+} imaging in panel A was performed by Christian Marks.

To complement these initial studies of E-T coupling, we examined the impact of the CaMKIIα-V102E mutation using an shRNA knockdown and rescue strategy that has been used previously to demonstrate a key role for CaMKIIα/β (Wheeler et al., 2008). We first verified that the knockdown CaMKIIα and CaMKIIβ expression by shRNA transfection had no significant effect on LTCC-dependent somatic Ca^{2+} responses to stimulation with 40 mM K^+ Tyrode's solution. Moreover, the re-expression of shRNA-resistant wild-type CaMKIIα (WT CaMKIIα^R) or CaMKIIα^R-V102E also did not alter the amplitude or kinetics Ca^{2+} responses (Fig. 2.9A). However, CaMKIIα/β knockdown significantly attenuated the increase of pCREB staining induced by 40 mM KCl, and the effect of this knockdown was largely rescued by re-expression of CaMKIIα^R-WT but not by CaMKIIα^R-K42R (a kinase dead mutant). Notably, CaMKIIα^R-V102E, which cannot bind to the Ca_V1.3 NTD but retains full kinase activity (data not shown), was also unable to rescue the pCREB staining (Fig. 2.9B). Taken together, data obtained by expressing nimodipine-resistant channels and using CaMKII knockdown/rescue approaches suggest that the NTD-CaMKII interaction is essential for LTCC-mediated E-T coupling.

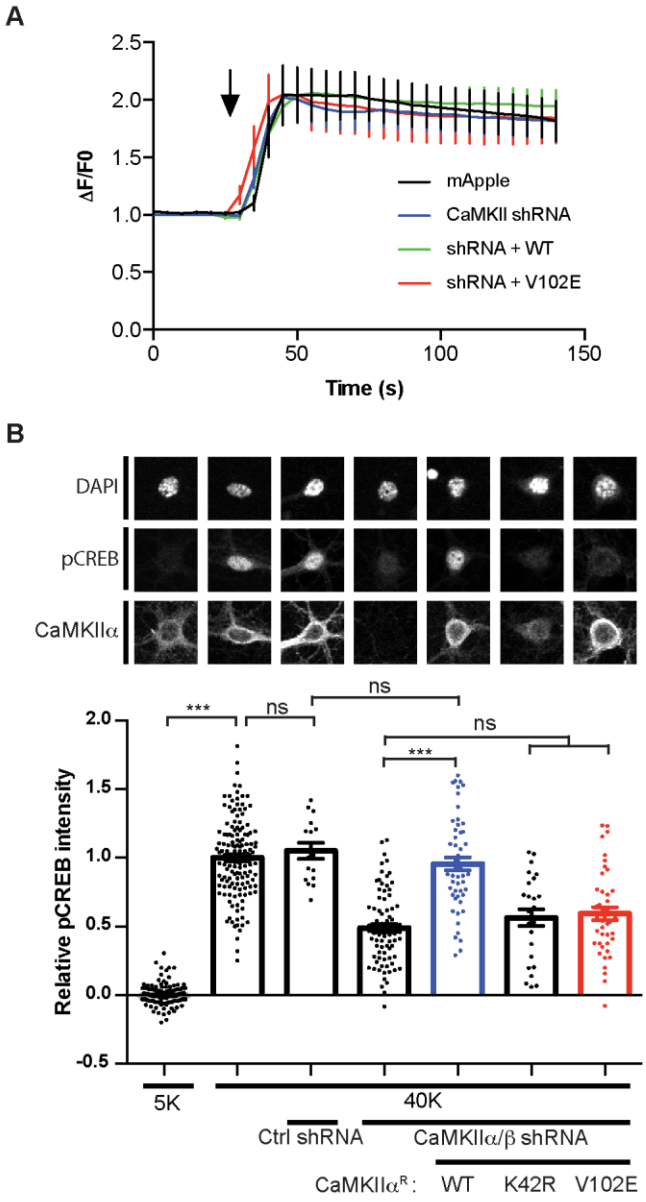

FIGURE 2.9 CaMKII-binding to the $Ca_V1.3$ NTD is required for high K^+-induced CREB Ser133 phosphorylation. *A.* CaMKIIα/β knockdown or re-expression/rescue has no effect on high K^+-induced increases of somatic Ca^{2+}. Cultured hippocampal neurons were transfected with mApple only (n=17), mApple with CaMKIIα/β shRNA (n=23), mApple/CaMKIIα/β shRNA with shRNA-resistant $CaMKII\alpha^R$-WT (n=26) or $CaMKII\alpha^R$-V102E cDNA (n=17), respectively. Transfected neurons were then monitored for Ca^{2+} influx in response to 40 mM K^+-induced depolarization (black arrow, see Fig. 7A). *B*.

The CaMKIIα-V102E mutant does not support nuclear signaling. Expression of CaMKIIα/CaMKIIβ shRNAs significantly reduces nuclear CREB phosphorylation following 40 mM KCl treatment. This reduction in CREB phosphorylation is rescued by co-expression of shRNA-resistant CaMKIIα^R-WT, but not CaMKIIα^R-K42R (kinase dead) or CaMKIIα^R-V102E (deficient in $Ca_V1.3$ NTD binding). Each data point represents analysis of a single cell collected from 3~4 independent neuronal cultures/transfections. Pooled data were analyzed by one-way ANOVA followed by Tukey's multiple comparison test. ***, $p<0.001$; ns, not significant ($p>0.05$). All confocal images show a 40 μm x 40 μm area. Ca^{2+} imaging in panel A was performed by Christian Marks.

2.2.8 Recruitment of CaMKII to $Ca_V1.3$ channels may mediate E-T coupling through enhancing trans-holoenzyme phosphorylation

Why is it important to recruit CaMKII to the vicinity of L-type Ca^{2+} channels for E-T coupling? One possibility is that CaMKIIα, CaMKIIγ, and calcineurin all need to be in the nanodomain of the channel so that CaMKIIα can efficiently phosphorylate CaMKIIγ at Thr287 to trap calmodulin, and that calcineurin can dephosphorylate CaMKIIγ at S334 to expose the functional nuclear localization signal. It is known that trans-holoenzyme phosphorylation has low efficiency. However, it is possible that by providing anchoring points for CaMKIIα and CaMKIIγ, $Ca_V1.3$ L-type Ca^{2+} channels facilitates the trans-holoenzyme phosphorylation.

To test this, we utilized the rapamycin-mediated FKBP/FRB dimerization to bring CaMKIIα and CaMKIIγ to the vicinity of each other, and asked whether this enhances trans-holoenzyme phosphorylation. We expressed CaMKIIα and CaMKIIγ holoenzymes in two separate dishes: one was transfected with FRB-CaMKIIα and CaMKIIα cDNAs (1:5 ratio), and the other was transfected with DNAs encoding HA-FKBP-CaMKIIγ-K43R and HA-CaMKIIγ-K43R (kinase dead mutant, 1:5 ratio). By expressing FRB- and FKBP-tagged CaMKIIs at lower stoichiometry ratio, we were hoping to reduce possible protein aggregations among the enzymes. We then lysed the cells and mixed the two lysates together with Ca^{2+}/calmodulin/Mg-ATP on ice for 5 minutes in the absence or presence of 5 nM rapamycin. Since the CaMKIIγ has the K43R mutation (kinase dead), all phosphorylations that occur to CaMKIIγ should be from the trans-holoenzyme phosphorylation by CaMKIIα. As shown in Fig. 2.10, rapamycin causes significant shift

of both HA-FKBP-CaMKIIγ-K43R and HA-CaMKIIγ-K43R, suggesting simultaneous recruitment of CaMKIIα and CaMKIIγ to the L-type Ca^{2+} could enhance trans-holoenzyme phosphorylation of CaMKIIγ by CaMKIIα.

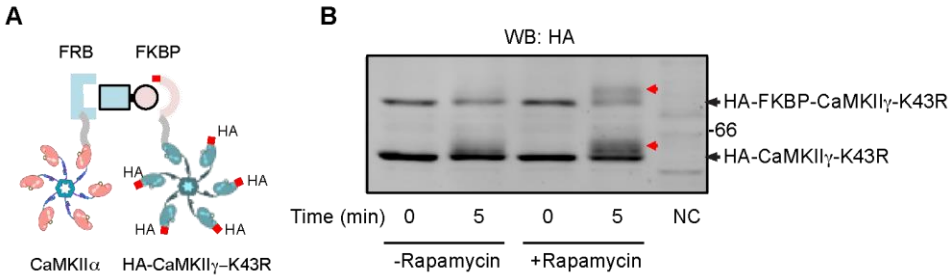

FIGURE 2.10 Introducing proximity between CaMKIIα and CaMKIIγ-K43R enhances trans-holoenzyme phosphorylation. *A.* a schematic diagram of the experiment design. HEK293T cell lysates co-expressing FRB-CaMKIIα and CaMKIIα (1:5 ratio) were mixed with lysates co-expressing HA-FKBP-CaMKIIγ-K43R and HA-CaMKIIγ-K43R (1:5 ratio) in the presence or absence of 5 nM rapamycin on ice for 5 minutes. Ca^{2+}/calmodulin/Mg-ATP were added to the mixture to allow for phosphorylation to occur. Rapamycin causes rapid chemically-induced dimerization (CID) between FKBP and FRB, bring the tagged proteins in proximity. *B.* an immunoblot showing the effect of adding Rapamycin on HA-tagged CaMKIIγ electromobility in a SDS-PAGE gel. Note that adding rapamycin induces significant reduction in the mobility of both the FKBP-tagged and non-tagged CaMKIIγ. NC, non-transfection control. Representative data were shown from two independent experiments.

2.3 Discussion

Ca^{2+} influx into neurons via ligand- and voltage-gated Ca^{2+}channels plays a key role in a variety of processes including synaptic plasticity and long-term memory formation. The molecular mechanisms that underlie the specificity and efficiency of signaling downstream of the different channels is critical to understanding their biological roles. Our data identify a novel CaMKII binding site in the NTD of LTCCs that is important for the coupling of LTCCs to a nuclear response. The specificity of this interaction for Ca_V1 LTCCs over Ca_V2 and Ca_V3 VGCCs presumably contributes to their preferential role in E-T coupling (Wheeler et al., 2012).

We systematically compared CaMKII binding to all intracellular domains of the $Ca_V1.3$ $\alpha1$ subunit, expressed as GST fusion proteins. We detected a highly specific interaction of activated CaMKII with the $Ca_V1.3$ NTD, and showed that this interaction was conserved with $Ca_V1.2$ NTDs, but not NTDs from $Ca_V2.2$ or $Ca_V3.2$ VGCCs. These data were somewhat surprising because it was previously reported that CaMKII binding to the CTD is important for Ca^{2+}-dependent facilitation (Hudmon et al., 2005), whereas we failed to detect CaMKII binding to the full length $Ca_V1.3$ CTD, or to the previously defined minimal CTD CaMKII binding domain that is 100% conserved between $Ca_V1.2$ and $Ca_V1.3$. Another prior study relied on co-immunoprecipitations from cell lysates to detect a putative CaMKII-binding site in the membrane-proximal region of the $Ca_V1.2$ NTD (residues 117-120) that is conserved in $Ca_V1.3$, and found that mutation of this motif disrupted membrane trafficking yet enhanced Ca^{2+} influx (Simms et al., 2014). However, this study provided no evidence for a direct interaction of CaMKII with this

domain (e.g., with purified proteins). Moreover, neither of these prior studies established that the domains identified are important for CaMKII association with intact LTCC complexes. Reasons for the discrepancies between the present studies and these prior studies are unclear, but it is possible that the conditions used here favor detection of more specific, high-affinity, direct interactions.

2.3.1 Comparison of NTD with previously identified CaMKII binding domains

Like several other CaMKAPs, the LTCC NTD preferentially interacts with activated CaMKII. However, the molecular bases for these interactions appear to be distinct. CaMKII-binding domains in the NMDA receptor GluN2B subunit and β1/β2 subunits of VGCCs share sequence similarity with the CaMKII autoregulatory domain, including the presence of a (auto)phosphorylation site (Grueter et al., 2008). However, these domains share no sequence similarity with the internal CaMKII-binding domain in densin, which resembles CaMKIIN, a naturally occurring CaMKII inhibitor protein (Jiao et al., 2011). Moreover, neither of these classes of CaMKII-binding domain shares noticeable sequence similarity with CaMKII-binding domains in the $Ca_V1.3$ and $Ca_V1.2$ NTDs identified here. Furthermore, we identified a V102E mutation in the CaMKIIα catalytic domain that substantially reduced interactions with the $Ca_V1.3$ NTD, without significantly affecting interactions with the β1/β2 subunits, densin or GluN2B. In contrast, an I205K mutation in the CaMKIIα catalytic domain (I206K in CaMKIIβ, γ, and δ) previously shown to interfere with binding to GluN2B (Bayer et al., 2001) and densin (Jiao et al., 2011), also disrupts CaMKII-binding to β1/β2 subunits and the $Ca_V1.3$ NTD (Fig. 4B). Taken together, despite some overlap in the CaMKII residues required for binding, these data

suggest that the newly identified $Ca_V1.3$ NTD CaMKII-binding domain represents a new class of CaMKAP.

2.3.2 Roles of the NTD and other CaMKAPs in LTCC complexes

It is well-established that CaMKII associates with LTCCs in cardiomyocytes and neurons, as revealed by co-immunoprecipitation and/or by co-localization (Abiria and Colbran, 2010; Hudmon et al., 2005; Wheeler et al., 2012), but the molecular basis for this interaction is unclear. In one series of studies, CaMKII was shown to bind directly to β1 and β2 LTCC auxiliary subunits, but not to β3 or β4 (Grueter et al., 2008), and co-immunoprecipitated from brain extracts with β1 subunits, but not β4 subunits (Abiria and Colbran, 2010). Moreover, mutation of the CaMKII-binding domain in the β2 subunit reduces CaMKII co-immunoprecipitation with $Ca_V1.2$ channels in heterologous cells (Abiria and Colbran, 2010), as well as Ca^{2+}-dependent facilitation of $Ca_V1.2$ (Koval et al., 2010). In contrast, another CaMKAP, the synaptic scaffolding protein densin, forms ternary complexes with CaMKII and $Ca_V1.3$ LTCCs in brain and is necessary for CaMKII- and Ca^{2+}-dependent facilitation of $Ca_V1.3$ (Jenkins et al., 2010). Here, we found that the α1 subunit NTD is important for CaMKII association with intact $Ca_V1.3$ LTCC complexes by co-immunoprecipitation of activated CaMKII with HA-tagged $Ca_V1.3$ LTCCs. Co-immunoprecipitation of CaMKII was substantially reduced by replacement of the $Ca_V1.3$ NTD with NTDs from $Ca_V2.2$ or $Ca_V3.2$, which do not significantly bind CaMKII *in vitro*. Similarly, co-immunoprecipitation was substantially reduced by either deletion of residues 69-93 or mutation of $R^{83}KR^{85}$ to AAA in the $Ca_V1.3$ NTD, or by the CaMKIIα-V102E mutation. Thus, the present findings demonstrate the importance of a direct CaMKII interaction with a novel CaMKII-binding

domain in $Ca_V1.3$ $\alpha1$ subunit NTD, significantly extending our understanding of biochemical mechanisms involved in LTCC signaling.

It is important to note that our heterologous cell studies were conducted using HA-tagged $Ca_V1.3$ and the $\beta3$ auxiliary subunit, which does not directly interact with CaMKII (Grueter et al., 2008). $\beta3$ is thought to be the most abundant in brain (Ludwig et al., 1997), but the other three β subunits also are expressed in neurons. It seems likely that the association of β subunit variants with VGCC $\alpha1$ subunits is determined in part by their relative expression levels. However, the $\alpha1$ subunit I-II linker domains may also exhibit selectivity for the β subunits in cells, consistent with data showing that overexpressed β subunit variants are differentially localized in cultured hippocampal neurons (Obermair et al., 2010). Nevertheless, we posit that neurons contain multiple subpopulations of $Ca_V1.3$ LTCC complexes associated with different β subunit variants. $Ca_V1.3$ LTCCs containing $\beta3$ or $\beta4$ may rely only on the NTD for CaMKII association, whereas those containing $\beta1$ or $\beta2$ have a second interaction site. Indeed, even though this novel CaMKII-binding domain is highly conserved, $Ca_V1.2$ NTD binding to CaMKII is somewhat weaker than $Ca_V1.3$ NTD (Fig. 2C), and we previously reported that CaMKII association with $Ca_V1.2$ channel complexes depends in part on interaction with $\beta2$ subunits (Abiria and Colbran, 2010).

Neuronal Ca^{2+} channels are often part of larger complexes containing other proteins. For example, a canonical PDZ domain-binding motif at the C-terminus of the long splice variant of the $Ca_V1.3$ $\alpha1$ subunit interacts with PDZ domains in synaptic scaffolding proteins like densin or Shank3 (Jenkins et al., 2010; Zhang et al., 2005a). CaMKII

interactions with such scaffolding proteins may represent an additional mechanism for targeting CaMKII to certain subpopulations of neuronal $Ca_V1.3$ LTCCs (in addition to $\alpha1$ subunit NTDs and $\beta1/2$ subunits). Indeed, the key role for densin in targeting CaMKII to promote Ca^{2+}-dependent facilitation of $Ca_V1.3$ LTCCs was noted above (Jenkins et al., 2010). Taken together, these observations indicate that there are several distinct "flavors" of neuronal $Ca_V1.3$ LTCCs complexes with different protein compositions that may associate with CaMKII in different ways, perhaps conferring distinct roles for CaMKII in regulating LTCCs and/or downstream signaling.

2.3.3 Role of CaMKII binding to the $Ca_V1.3$ NTD in E-T coupling

As noted above, the precise regulation of CREB phosphorylation at Ser133 is critical for the regulation of gene expression during normal learning and memory consolidation. Although Ser133 phosphorylation may not be sufficient for gene expression under all conditions (Hardingham et al., 1999), it is frequently used as a readout for E-T coupling to CREB, as in the current studies. It is well established that CREB phosphorylation at Ser133 is increased following the selective activation of several different receptors and ion channels, which engage diverse signal transduction pathways (e.g., cyclic AMP, Ca^{2+}, MAP kinases). Moreover, distinct Ca^{2+}-dependent pathways can be engaged to increase Ser133 phosphorylation, depending on the specific channel that generates the Ca^{2+} signal. Among the known mechanisms, selective LTCC activation is sufficient for immediate early gene expression *in vivo* (Hetzenauer et al., 2006), and for CREB Ser133 phosphorylation in cultured neurons (Bading et al., 1993; Wheeler et al., 2012). The stimulation of CREB phosphorylation can be driven by increased nuclear Ca^{2+} concentrations, which can be induced using some stimulation paradigms (e.g., NMDA

receptor activation) (Hardingham et al., 2001). However, the initiation of E-T coupling to CREB by moderate LTCC activation seems to be independent of increases in nuclear Ca^{2+}, and only requires increased Ca^{2+} concentrations in the immediate vicinity of the channel itself (Deisseroth et al., 1996; Wheeler et al., 2012). Stronger, more prolonged, stimulation paradigms may overcome this requirement for Ca^{2+} signaling within the LTCC nanodomain by recruiting additional mechanisms. This may be evident in superior cervical ganglion (SCG) neurons (Wheeler et al., 2012), where the global increase of Ca^{2+} in response to modest stimulation (40 mM KCl) involves similar contributions from Ca_V1 and Ca_V2 channels, but the resulting increase of CREB phosphorylation at Ser133 is preferentially coupled to Ca_V1 LTCCs, correlating with the co-localization of CaMKII with Ca_V1, but not Ca_V2, channels under these conditions. Ca_V2 channel-dependent increases of global Ca^{2+} in SCG neurons are shaped by mitochondria and the endoplasmic reticulum, but more robust stimulation induces Ca_V2-dependent increases of CREB phosphorylation by a mechanism that is only partially dependent on CaMKII (Wheeler et al., 2012). Sufficiently robust increases in global Ca^{2+} may result in increases of nuclear Ca^{2+} that may contribute to the stimulation of CREB phosphorylation (Hardingham et al., 2001).

In this study, we focused on an E-T coupling paradigm that has been shown to depend on signaling within the LTCC nanodomain (Deisseroth et al., 1996; Wheeler et al., 2008). We found that mutations in the $Ca_V1.3$ NTD that disrupt CaMKII binding *in vitro* interfere with E-T coupling in cultured neurons. Similarly, mutation of the CaMKII catalytic domain to selectively disrupt binding to the NTD interferes with E-T coupling. Notably, although CaMKIIα/β knockdown significantly interfered with LTCC-dependent

E-T coupling, there was no significant effect on the Ca^{2+} signal detected in the soma. Thus, the data presented herein show that a novel and unique CaMKII binding site in the N-terminal domain of $Ca_V1.3$ LTCCs plays an important role in the initiation of E-T coupling, apparently by initiating a local mechanism within the LTCC nanodomain, rather than modulating the global Ca^{2+} signal.

Our current data do not preclude additional roles for CaMKII binding to other components of LTCC complexes (see above) in E-T coupling. This may be particularly germane in light of a recent study indicating that Ca^{2+} influx drives activation and Thr286/7 autophosphorylation of a CaMKIIα or CaMKIIβ holoenzyme within the LTCC nanodomain which in turn trans-autophosphorylates a CaMKIIγ holoenzyme at Thr287, trapping bound calmodulin to be shuttled to the nucleus (Ma et al., 2014). Given the inefficiency of trans-holoenzyme autophosphorylation in solution (Hanson et al., 1994), it is tempting to speculate that this process is facilitated by simultaneous targeting of these two CaMKII holoenzymes within the LTCC nanodomain. Our data indicate that a CaMKIIα/β holoenzyme may be docked to the NTD, and it is possible that a CaMKIIγ holoenzyme interacts with other components of the larger LTCC complex. The FKBP/FRB study illustrates the proof of concept for this model (Fig. 2.10). Interestingly, CREB phosphorylation was reported to be preferentially coupled to $Ca_V1.3$ over $Ca_V1.2$ LTCCs. Thus, selective members of the $Ca_V1.3$ channel complex such as Shank3 may play an important role in E-T coupling (Zhang et al., 2005a). Moreover, Shank3 was identified as an abundant component of synaptic CaMKII complexes in a recent proteomics study (Baucum et al., 2015). Multiple CaMKII docking sites in the LTCC complex also may be linked to the voltage-dependent conformational changes that

appear to be required to initiate E-T coupling (Li et al., 2016). These conformational changes may be required to facilitate CaMKII docking and appropriately position these holoenzymes relative to other proteins within the nanodomain. Additional studies are clearly required to explore these ideas and provide further insight into the molecular mechanisms underlying the initiation of E-T coupling.

2.4 Future directions

Data we presented here indicate the RKR motif within the $Ca_V1.3$ N-terminal domain is required for CaMKII recruitment when $\beta3$ and $\alpha2\delta$ is co-expressed. Previous studies have shown that unlike $\beta1/\beta2$, $\beta3$ does not interact with activated CaMKII (Grueter et al., 2008). Therefore the $Ca_V1.3/\beta3/\alpha2\delta$ combination seems to be composed of one major CaMKII binding site. Since both $\beta1$ and $\beta2$ are also expressed in the brain (although likely not as dominant as $\beta3$), it will be interesting to test whether the $Ca_V1.3/\beta1$(or $\beta2$)$/\alpha2\delta$ combination has multiple binding sites and whether the RKR motif is still required for CaMKII recruitment.

We have shown in Fig. 2.10 that bringing CaMKIIα and CaMKIIγ together in the same complex facilitates trans-holoenzyme phosphorylation that is required for calmodulin trapping in E-T coupling. It is known that an intact C-terminal domain and Shank3 are also required for $Ca_V1.3$ mediated E-T coupling. What is the role of Shank3 in mediating E-T coupling? A recent study identified Shank3 as a potential CaMKAP through a proteomics screen (Baucum et al., 2015), and recent data from our lab have shown that

CaMKII directly binds to Shank3 (Perfitt et al., 2017). Thus it is possible that the C-terminal domain anchored Shank3 may represent another anchoring point for CaMKII holoenzymes. Further experiments will be needed to characterize the binding preference among different CaMKII holoenzymes and different Ca^{2+} channel anchoring sites.

Finally, it will be very important to move on to *in vivo* studies and ask the question how does disruption of CaMKII/RKR motif interaction affect activity-dependent gene transcription and learning and memory.

CHAPTER III

ROLE OF CAMKII/Ca_V1.3 RKR MOTIF INTERACTION IN CHANNEL CLUSTERING AND PHOSPHORYLATION

Summary

Chapter II has characterized a novel interaction between CaMKII and the Ca_V1.3 L-type Ca^{2+} channel N-terminal domain RKR motif and its role in L-type Ca^{2+} channel-mediated excitation-transcription coupling. In this chapter, I am going to present data describing other important roles of CaMKII/Ca_V1.3 RKR motif interaction. First, CaMKII holoenzymes, but not monomeric CaMKII subunits, can cluster multiple Ca_V1.3 L-type Ca^{2+} channels in a Ca^{2+}-dependent manner. This channel clustering effect depends on the interaction between CaMKII and the Ca_V1.3 RKR motif in the NTD, because deletion of the RKR motif within Ca_V1.3 or mutating CaMKII to a Ca_V1.3-binding deficient form abolishes the channel clustering. Second, through LC-MS/MS and site-directed mutagenesis, we identified three groups of CaMKII phosphorylation sites within the N-terminal, I-II linker, and II-III linker domains. Interestingly, efficient phosphorylation of the N-terminal domain by CaMKII requires intact interaction between CaMKII and the RKR motif, pointing to another important role of the CaMKII/RKR interaction in channel regulation.

3.1 Experimental procedures

DNA constructs

Rat $Ca_V1.3$ complete coding sequences (Genbank accession number: AF370010 for $Ca_V1.3_L$, and AF370009 for $Ca_V1.3_S$) were generous gifts from Dr. Diane Lipscombe, Brown University, Providence, RI. The intracellular domains contain: NTD, M1-K126; I-II, G407-V543; II-III, D773-H906; III-IV, G1169-S1225; CTD_L, M1469-L2164; CTD_S, M1460-L1643 (from AF370009). Rat β1b and β2a complete coding sequences (accession numbers X61394 and M80545, respectively) were generous gifts from Dr. Edward Perez-Reyes, University of Virginia. All cDNAs were inserted into pGEX-4T1 using traditional ligation or sequence and ligation independent cloning (SLIC; (Li and Elledge, 2007)).

A plasmid encoding $Ca_V1.3$ with an N-terminal HA-tag (pCGNH-$Ca_V1.3$, for co-immunoprecipitation) was made by inserting rat $Ca_V1.3$ cDNA into the pCGN vector (a gift from Dr. Winship Herr, Université de Lausanne, Switzerland, Addgene plasmid ID 53308). To generate Flag-$Ca_V1.3$, the DNA sequence encoding HA in the pCGN vector was first deleted to yield pCGN0 by mutagenesis. A double-stranded DNA oligo linker that encodes FLAG (Forward: CT AGC **GAC TAC AAA GAC GAT GAC GAC AAG** TCT AGA GGC G; Reverse: GA TCC GCC TCT AGA **CTT GTC GTC ATC GTC TTT GTA GTC** G, the Flag sequence is in bold) was then inserted into pCGN0 to yield pCGNF. The cDNA sequence of $Ca_V1.3$ was then inserted into pCGNF between the XbaI and BamHI sites using SLIC cloning. To make pcDNA-msCaMKII-ΔAD (association domain deleted), the DNA sequence encoding E341 to H478 was deleted

from the pcDNA-msCaMKII construct. To make $Ca_V1.3$ without CaMKII binding domain, the region encoding M69-L93 was deleted from pCGNH-$Ca_V1.3$ plasmid. Site-directed mutagenesis and all deletions were done following the one-step mutagenesis protocol described by Liu et al (Liu and Naismith, 2008). All constructs were confirmed by DNA sequencing.

Cell culture and transfection for co-immunoprecipitation

HEK293T cells were purchased from ATCC (Cat. # CRL-3216) and maintained in DMEM (Cat. #11995065) with 10% fatal bovine serum (Cat. #16140071), 1x Glutamax (Cat. # 35050061) and 100 U/mL Penicillin-Streptomycin (Cat. # 15140122). All media and supplements were purchased form Thermo Fisher Scientific. pCGNH-$Ca_V1.3$ and/or pCGNF-$Ca_V1.3$ were co-transfected with $\beta3$ and $\alpha2\text{-}\delta$ subunits, and mouse CaMKIIα pcDNA or pcDNA empty vector. For Fig. 3.1A, a total of 5 μg DNA were transfected into one 6-cm dish of HEK293T cells. Amounts of DNA transfected were: pCGNH-$Ca_V1.3$ (WT, mutant or chimeras), 2 μg, pcDNA-$\beta3$, 1 μg; pcDNA-$\alpha2\delta$, 1 μg; CaMKIIα WT or truncation, 1 μg. For Fig. 3.1B and Fig.3.2, a total of 7 μg DNA were transfected into one 6-cm dish of HEK293T cells. Amounts of DNA transfected were: pCGNH-$Ca_V1.3$ (WT or truncation), 1.5 μg, pCGNF-$Ca_V1.3$, 1.5 μg; pcDNA-$\beta3$ and pcDNA-$\alpha2\delta$, 0.75 μg each for one-channel conditions and 1.5 μg each for two-channel conditions; CaMKIIα, 1 μg. All conditions were brought to the same amount of total DNA by empty pcDNA vector.

Co-immunoprecipitation and western blot

After 48 hours of transfection, cells were lysed in 50 mM Tris-HCl, 150 mM NaCl, 1 mM EDTA, 1 mM EGTA, 1 mM DTT, 1% NP-40 (v/v), 1 mM Microcystin-LR and protease inhibitor cocktails. Cell lysates were cleared by low speed centrifugation (500 x *g*), and supernatant was used for subsequent co-immunoprecipitation. Where indicated, lysates were supplemented with 2 mM $CaCl_2$, 2 mM $MgCl_2$, 1 mM ATP and 1 μM calmodulin (final concentrations) to activate CaMKII prior to immunoprecipitation. Cell lysates were incubated at 4°C for 1 hour with rabbit anti-HA (Santa Cruz, Cat. #sc805, 1:500 or Cell Signaling, Cat. #C29F4) and 10 μl prewashed Dynabeads Protein A (Thermo Fisher Scientific, Cat. #10001D, 25% v/v). The beads were isolated magnetically and washed three times using lysis buffer before eluting proteins using 1X Laemmli sample buffer. Samples were heated at 70 °C for 3 minutes and resolved on a SDS-PAGE gel followed by transfer with constant current (1 Amp) for 1.5 hours at 4 °C. The primary antibodies used were: mouse anti-HA (1:2000, Biolegend Cat. #901502), mouse anti-CaMKIIα (1:2000, Thermo Fisher Scientific, Cat. #MA1-048), mouse anti-FLAG (1:1000, MilliporeSigma, Cat. # F3165).

Recombinant mouse CaMKIIα and GST-tagged protein purification

Expression and purification of recombinant mouse CaMKIIα has been described previously (McNeill and Colbran, 1995). pGEX-4T1 plasmids were transformed into BL21(DE3) bacteria cells to express GST-tagged proteins. Cells were grown in LB media at 37°C to reach OD~0.6. IPTG (0.2 mM) was then added to induce the protein expression at room temperature for 2 hours. We found that the $Ca_V1.2$ and $Ca_V1.3$ full-length C-terminal domain fragments do not express well in BL21(DE3) cells. We

identified several rare codons in the cDNAs encoding both CTDs, and found that their expression was substantially improved in Rosetta 2(DE3) BL21 cells engineered to contain rare tRNAs (EMD Millipore Cat. #71400). Expressed proteins were purified using Pierce Glutathione Agarose beads (Cat. #16101) following manufacturer's instructions. Eluted proteins were then dialyzed in 10 mM HEPES pH 7.5, 25 μM PMSF, 62.5 μM Benzamidine, 62.5 μM EDTA, 0.1% TritonX-100 overnight with one buffer change.

In vitro CaMKII phosphorylation assay

For CaMKII phosphorylation with ^{32}P incorporation, purified GST-tagged $Ca_V1.3$ intracellular domains (2 μg) were incubated with 10 nM purified mouse CaMKIIα in 50 mM HEPES, pH 7.5, 10 mM magnesium acetate, 0.5 mM $CaCl_2$, 2 μM calmodulin, 1 mg/mL bovine serum albumin, 1 mM DTT, and 0.4 mM [γ-^{32}P]ATP (~500 cpm/pmol) at 30 ^oC for 10 minutes before being stopped by 1x Laemmli buffer. Samples were then resolved on a SDS-PAGE gel and transferred to a nitrocellulose membrane followed by autoradiography.

CaMKII phosphorylation for mass spectrometry was performed the same way as above except that nonradioactive ATP was used. Samples were resolved on a SDS-PAGE gel and stained with Colloidal Blue (Thermo Fisher Scientific, Cat. #LC6025) for three hours and washed with deionized water overnight. The band that corresponds to full-length proteins was then excised for mass spectrometry analysis at the proteomics core lab of Vanderbilt Mass Spectrometry Research Center.

3.2 Results

3.2.1 CaMKII clusters $Ca_V1.3$ L-type Ca^{2+} channels in a Ca^{2+}-dependent way

In Section 2.2.4, we noted that the amount of HA-tagged wild-type $Ca_V1.3$ precipitated by the HA antibody was increased upon adding Ca^{2+}/calmodulin/Mg^{2+}-ATP when wild-type CaMKII is also present (Fig. 2.6). There are at least two interpretations for this observation. First, it is possible that CaMKII binding to the N-terminal domain causes conformational changes that make the HA-epitope more available to the antibody. Second, it is also possible that the HA-antibody is not exhausting all the HA-tagged $Ca_V1.3$ channels in the reaction, and CaMKII as a dodecamer can help to cluster and precipitate extra HA-tagged $Ca_V1.3$ channels that otherwise will not be precipitated.

To distinguish the two interpretations, we first repeated the co-immunoprecipitation experiment with a truncated CaMKII that lacks the association domain. CaMKII without the association domain exists as a monomer instead of dodecamer. As suggested in Fig. 2.5, the $Ca_V1.3$ binding domain seems to reside within the catalytic domain. Deleting the association domain should not interfere the interaction between CaMKII and the $Ca_V1.3$ N-terminal domain. Therefore, the putative allosteric effect from CaMKII binding, if any, should be retained. On the other hand, lacking the association domain prevents CaMKII from oligomerization. If the increased HA-$Ca_V1.3$ is due to clustering by the CaMKII holoenzyme, the increased HA-$Ca_V1.3$ in the IP should disappear upon deleting the association domain. Fig. 3.1A shows the comparison of HA-$Ca_V1.3$ coimmunoprecipitation with wild-type CaMKIIα or CaMKIIα without the association domain (CaMKIIα-ΔAD). As previously seen in Fig. 2.6, the amount of CaMKIIα that

coimmunoprecipitates with HA-$Ca_V1.3$ increases upon adding Ca^{2+}/calmodulin/Mg^{2+}-ATP. We also saw increased co-IP of CaMKII-ΔAD upon adding Ca^{2+}/calmodulin/Mg^{2+}-ATP, suggesting that the $Ca_V1.3$ binding domain within CaMKII is retained in CaMKIIα-ΔAD, and the Ca^{2+}-dependent CaMKII/ $Ca_V1.3$ interaction persists. However, the increase of HA-$Ca_V1.3$ in the immunoprecipitates upon adding Ca^{2+}/calmodulin/Mg^{2+}-ATP is only seen with wild-type CaMKIIα, but not with CaMKIIα-ΔAD. This suggests that the increased HA-$Ca_V1.3$ in the immunoprecipitates is not caused by potential CaMKII-mediated allosteric changes, but by CaMKII holoenzyme clustering.

To directly test the clustering of HA-$Ca_V1.3$ channels by CaMKII, we constructed expression vectors to coexpress a Flag-tagged $Ca_V1.3$ with HA-$Ca_V1.3$ with or without CaMKII. We then performed coimmunoprecipitation using anti-HA antibody in the presence or absence of Ca^{2+}/calmodulin/Mg^{2+}-ATP. As shown in Fig. 3.1B, in the absence of Ca^{2+}/calmodulin/Mg^{2+}-ATP and CaMKII, there is little basal level of interaction between HA-$Ca_V1.3$ and Flag-$Ca_V1.3$. Upon adding Ca^{2+}/calmodulin/Mg^{2+}-ATP, there is a stronger interaction between HA- and Flag-tagged $Ca_V1.3$ channels when CaMKII is co-expressed. Similar to what we saw in Fig. 2.6, the CaMKII effect is not seen when there is no Ca^{2+}/calmodulin/Mg^{2+}-ATP in the reaction. These data suggest that CaMKII is able to cluster at least two $Ca_V1.3$ channels in a Ca^{2+}-dependent manner.

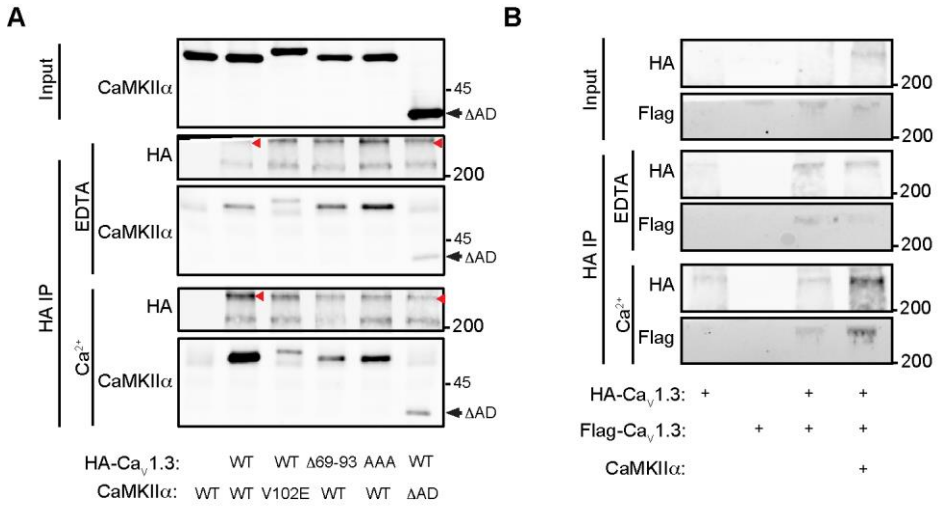

FIGURE 3.1 CaMKII holoenzyme clusters $Ca_V1.3$ L-type Ca^{2+} channels in a Ca^{2+}-dependent manner. *A*. Deletion of CaMKII association domain (ΔAD) prevents the Ca^{2+}-dependent increase of HA-$Ca_V1.3$ in the HA immunoprecipitates. Equal aliquots of lysates from cells expressing CaMKIIα (wild-type or mutation/truncation) with HA-tagged $Ca_V1.3$s (wild-type or truncation) were immunoprecipitated using anti-HA antibodies without (EDTA) or with the addition of excess Ca^{2+}/calmodulin/Mg^{2+}-ATP. Both wild-type and ΔAD CaMKII co-immunoprecipitate with HA-$Ca_V1.3$ in a Ca^{2+}-dependent way. However, the increase of HA-$Ca_V1.3$ in the wild-type condition when adding Ca^{2+}/calmodulin/Mg^{2+}-ATP is not observed in the CaMKIIα-ΔAD condition. *B*. Coexpression of CaMKIIα increases FLAG-$Ca_V1.3$ coimmunoprecipitation with HA-$Ca_V1.3$ in a Ca^{2+}-dependent manner. FLAG-$Ca_V1.3$ coimmunoprecipitates with HA-$Ca_V1.3$ weakly. However, this coimmunoprecipitation is increased when CaMKIIα is coexpressed. Representative blots are shown from two independent experiments.

3.2.2 The CaMKII/RKR motif interaction is required for channel clustering

To test whether the channel clustering effect by CaMKII depends on the interaction between CaMKII and the RKR motif in the N-terminal domain, we repeated the co-immunoprecipitation with either HA-$Ca_V1.3$ that lacks the RKR motif (HA-$Ca_V1.3$-Δ69-93) or the CaMKII mutant that does not bind to the RKR motif (CaMKII V102E). As shown in Fig. 3.2, we were able to confirm the effects of Δ69-93 and V102E on CaMKII coimmunoprecipitation when there is Ca^{2+}/calmodulin/Mg^{2+}-ATP present. Furthermore, we observed that both HA-$Ca_V1.3$-Δ69-93 and CaMKII V102E abolished the enhanced coimmunoprecipitation of Flag-tagged $Ca_V1.3$ channels when CaMKII and Ca^{2+}/calmodulin/Mg^{2+}-ATP are present. This suggests that the Ca^{2+}-dependent channel clustering effect by CaMKII depends on the interaction between CaMKII and the RKR motif in the N-terminal domain.

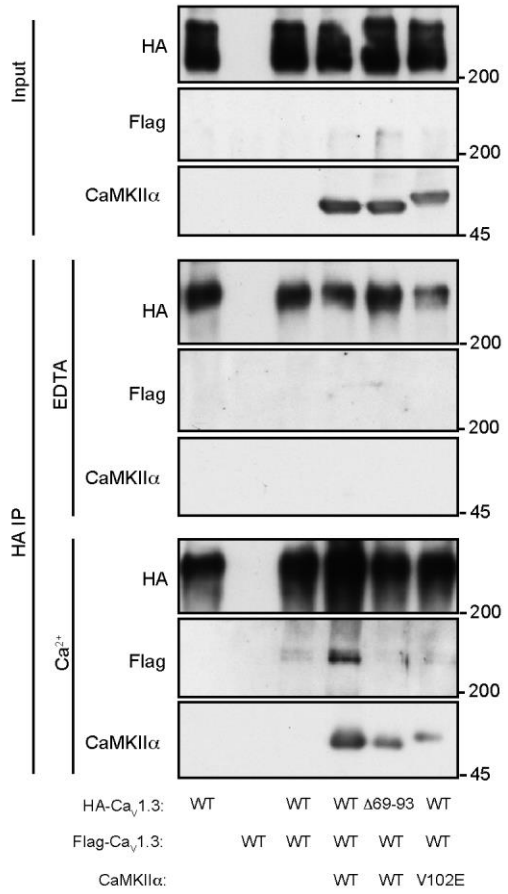

FIGURE 3.2 The interaction between CaMKII and Ca$_V$1.3 NTD RKR motif is required for channel clustering by CaMKII. HA-Ca$_V$1.3 and Flag-Ca$_V$1.3 were coexpressed in the absence of presence of CaMKII. Equal aliquots from the same lysates were immunoprecipitated using anti-HA antibodies without (EDTA) or with the addition of excess Ca^{2+}/calmodulin/Mg^{2+}-ATP. Consistent with Fig. 2.6, adding Ca^{2+}/calmodulin/Mg^{2+}-ATP increases CaMKII coimmunoprecipitation with HA-Ca$_V$1.3. This increase of CaMKII is compromised when the NTD RKR motif is deleted from HA-Ca$_V$1.3 or when CaMKII V102E is coexpressed. In addition, coexpression of CaMKII greatly enhanced the coimmunoprecipitation of FLAG-Ca$_V$1.3 with HA-Ca$_V$1.3, which is also blunted by deleting the CaMKII binding domain from HA-Ca$_V$1.3 or by expressing the Ca$_V$1.3-binding deficient mutant CaMKII V102E. Representative blots are shown from three similar independent experiments.

3.2.3 Ser1486 of $Ca_V1.3$ CTD is not significantly phosphorylated by CaMKII

As I reviewed in Section 1.4.5, it was suggested that activated CaMKII can phosphorylate voltage-gated Ca^{2+} channels as a feedback mechanism. Previous studies showed that CaMKII can phosphorylate β subunits and facilitate channel function in a Ca^{2+}-dependent manner (Koval et al., 2010). In addition, it was proposed that CaMKII may also phosphorylate Ser1486 at the C-terminal domain of $Ca_V1.3$ to facilitate the channel function by shifting the current peak to a more hyperpolarized membrane potential (Gao et al., 2006). However, whether Ser1486 is bona fide CaMKII phosphorylation site has not been tested, and no study has been done to systematically examine CaMKII phosphorylation sites within $Ca_V1.3$.

We first tested whether the C-terminal domain can be significantly phosphorylated by CaMKII and whether mutating Ser1486 to alanine affects the phosphorylation. We generated GST-tagged proteins that contain wild-type or S1486A $Ca_V1.3$ C-terminal domains (both short and long splice isoforms: $Ca_V1.3_S$ and $Ca_V1.3_L$), and performed *in vitro* kinase assay with CaMKII using [γ-^{32}P]ATP. As a positive control (Grueter et al., 2008), we showed that both GST-tagged β1 and β2 subunits can be phosphorylated by purified CaMKII (Fig 3.3A). Mutating Thr498/499 in β1 and β2 respectively decreased the phosphorylation by CaMKII significantly. However, we did not detect significant phosphorylation of either the long or short form of the $Ca_V1.3$ C-terminal domain, and mutating Ser1486 to alanine had no effect. These data indicate that Ser1486 cannot be efficiently phosphorylated by CaMKII, at least *in vitro*.

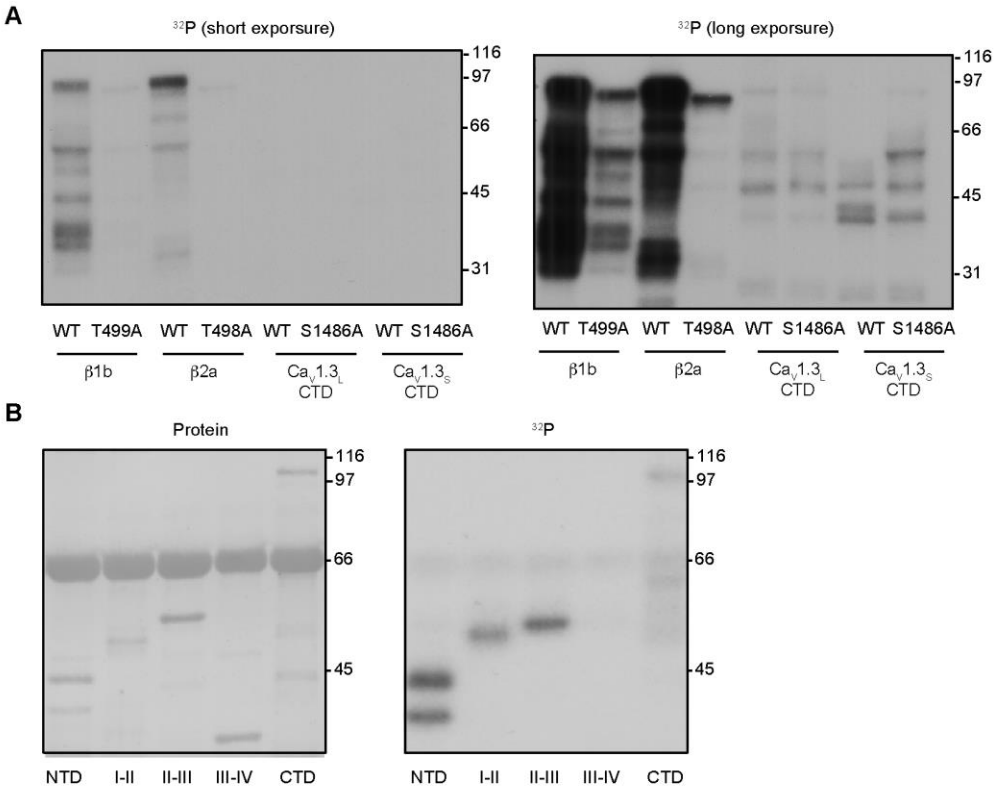

FIGURE 3.3 Multiple Ca$_V$1.3 intracellular domains, but not Ca$_V$1.3 CTD, can be efficiently phosphorylated by CaMKIIα *in vitro*. *A*, comparison of CaMKIIα phosphorylation of β1b, β2a subunits with wild-type Ca$_V$1.3 CTD or the S1486A mutant. Equal mass (2 μg) of purified GST-tagged proteins were incubated with purified mouse CaMKIIα at 30 ^{o}C for 10 minutes in the presence of [γ-^{32}P]ATP. Both β1b and β2a can be readily phosphorylated by CaMKIIα, which is blocked by mutating the previously reported phosphorylation sites (Thr499 for β1b or Thr498 for β2a) to alanines. However, neither the long or short splice isoform of the Ca$_V$1.3 CTD shows significant phosphorylation by CaMKIIα (the right panel shows long exposure for weak phosphorylations). *B*, CaMKIIα phosphorylates multiple intracellular domains of Ca$_V$1.3 *in vitro*. Purified GST-tagged Ca$_V$1.3 domains with equal mass (2 μg) were incubated with purified mouse CaMKIIα at 30 ^{o}C for 10 minutes in the presence of [γ-^{32}P]ATP. There are significant ^{32}P incorporations with Ca$_V$1.3 NTD, I-II linker and II-III linker. In addition, there is also a weak ^{32}P incorporation with Ca$_V$1.3 CTD. Representative autoradiographs are shown from two to three independent experiments.

3.2.4 CaMKII phosphorylates $Ca_V1.3$ at multiple intracellular domains

We then systematically examined whether any of the $Ca_V1.3$ intracellular domain can be phosphorylated by CaMKII. We generated GST-tagged $Ca_V1.3$ intracellular domains and performed *in vitro* kinase assay with purified mouse CaMKIIα. As shown Fig. 3.4, three intracellular domains were significantly phosphorylated by CaMKII: N-terminal domain, I-II linker and II-III linker. We also detected weak phosphorylation of the C-terminal domain in these experiments.

3.2.5 Identification of CaMKII phosphorylation sites within $Ca_V1.3$

We submitted NTD, I-II, and II-III fragments phosphorylated using nonradioactive ATP for mass spectrometry analysis to identify the phosphorylation sites. Fig 3.4B shows one example of a phospho-peptide from the $Ca_V1.3$ I-II linker. To confirm the identified phosphorylation sites, we generated phospho-null mutants of the identified sites (S97/S98/S100/S110 for NTD, S517/S519 for I-II linker, and S802 for II-III linker) and repeated the *in vitro* analysis using [γ-^{32}P]ATP. As shown in Fig. 3.5C, mutating the serines to alanines completely abolished the phosphorylation by CaMKII, confirming these are the major CaMKII phosphorylation sites in the intracellular domains, at least *in vitro*.

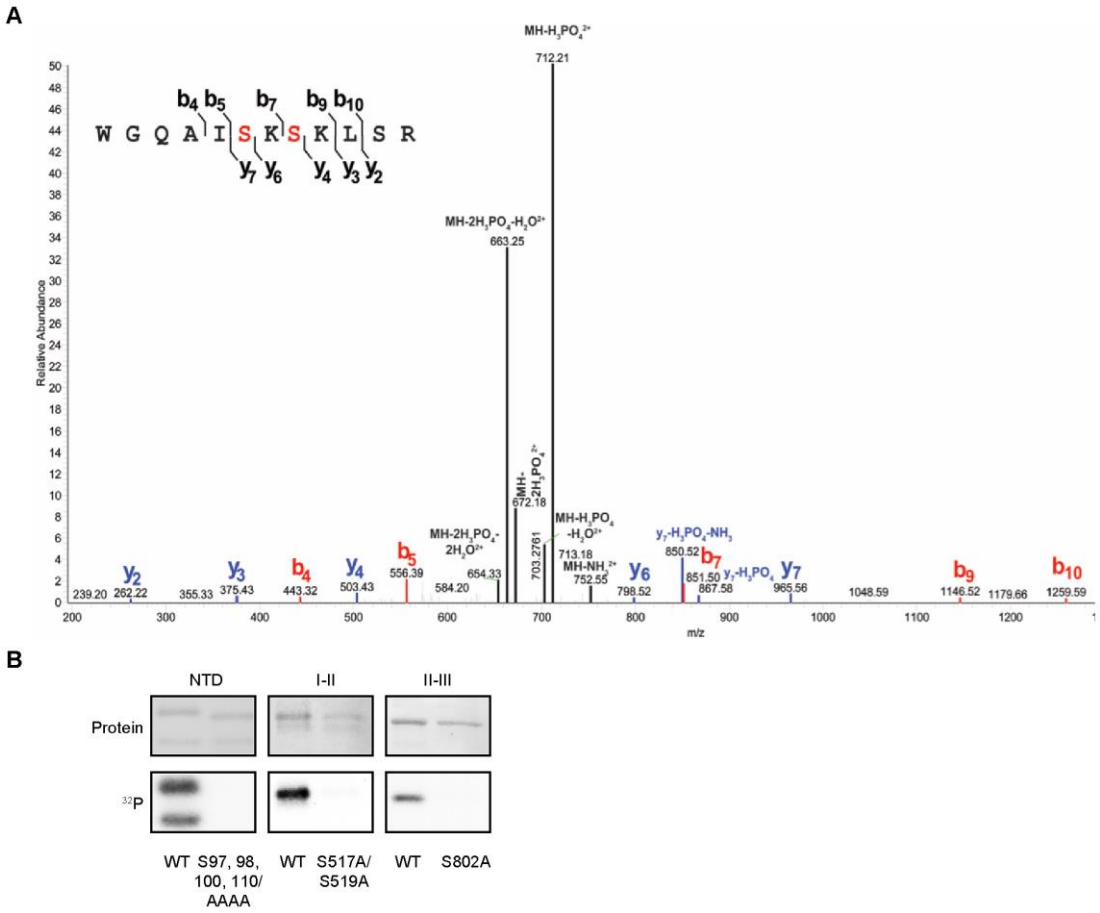

FIGURE 3.4 Identification of CaMKIIα phosphorylation sites within $Ca_V1.3$ intracellular domains by mass spectrometry and site-directed mutagenesis. *A*, a spectrum from the LC-MS/MS showing the phosphorylation of Ser517 and Ser519 of $Ca_V1.3$ intracellular I-II loop. Identified peptide breakpoints in this peptide were shown at the top left corner. Purified GST-tagged $Ca_V1.3$ intracellular domains (2 μg each) were incubated with 10 nM purified mouse CaMKIIα at 30ºC for 10 minutes with nonradioactive ATP. Samples were then resolved by SDS-PAGE and the gel was stained by colloidal blue. Bands corresponding to the full-length proteins were excised and submitted for mass spectrometry analysis. *B*, protein stains (top panels) and autoradiographs (bottom panels) showing mutation of the identified phosphorylation sites to alanine blocks CaMKII phosphorylation. Representative protein stains and autoradiographs are shown from three independent experiments. Data in panel A were annotated by Anthony J. Baucum II, Ph.D.

3.2.6 $Ca_V1.3$ NTD phosphorylation by CaMKII depends on CaMKII/RKR motif interaction

As discussed in Section 1.4.3, scaffold proteins can bring kinases to their substrates, so that the kinase can phosphorylate the substrate more efficiently. Since the phosphorylation sites in the N-terminal domain of $Ca_V1.3$ are close to the RKR motif, we tested the hypothesis that binding to the RKR motif is necessary for efficient CaMKII phosphorylation by comparing CaMKII phosphorylation of GST-tagged wild-type NTD with GST-NTD RKR/AAA mutant. As shown in Fig. 3.5, wild-type GST-NTD is significantly phosphorylated by CaMKII within 5 minutes. However, mutating the $R^{83}KR^{85}$ to alanines almost completely abolished the phosphorylation at Ser97, Ser98, Ser100 and Ser110, indicating that binding to the RKR motif is required for efficient CaMKII phosphorylation of NTD.

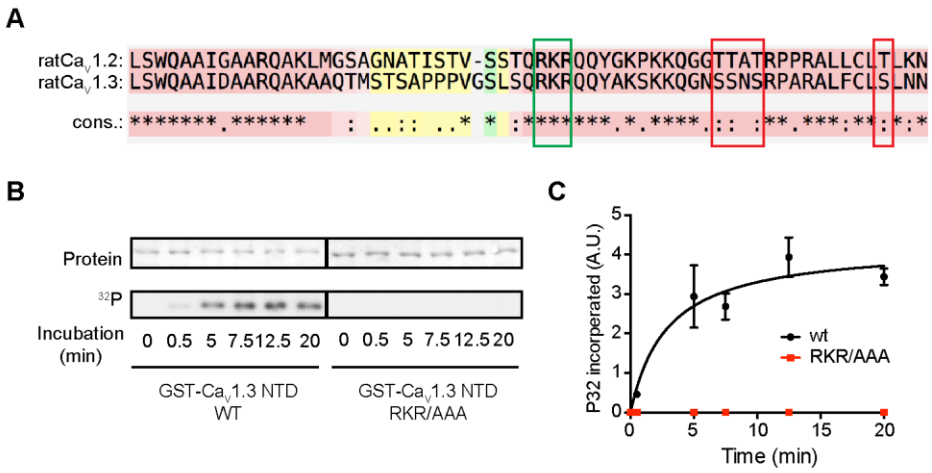

FIGURE 3.5 CaMKII/Cav1.3 NTD interaction is required for efficient Cav1.3 NTD phosphorylation by CaMKII. *A*, sequence alignment between rat Cav1.3 NTD and Cav1.2 NTD. For display purposes, only part of the NTD sequence (Cav1.3 L51-N113) was shown. The RKR motif is in green box, and the identified CaMKII phosphorylation sites are in red boxes. The binding domain is in close proximity with the phosphorylation sites. Also note that all Cav1.3 phosphorylation sites are serines while all corresponding Cav1.2 sites are threonines. *B*, Cav1.3 NTD RKR/AAA (that does not bind to CaMKII anymore) is not efficiently phosphorylated by CaMKII. Purified GST-tagged proteins were incubated with purified mouse CaMKIIα at 30°C in the presence of [γ-^{32}P]ATP and stopped by 1x Laemmli buffer at indicated time points. Protein stains (top panels) and autoradiographs (bottom panels) showing mutation of the CaMKII binding site blocks CaMKII phosphorylation of Cav1.3 NTD. *C*, quantification of the ^{32}P incorporation from the autoradiograph normalized to corresponding protein stains. Representative protein stains and autoradiographs are shown from three independent experiments.

3.3 Discussion and future directions

3.3.1 Potential mechanisms for L-type Ca^{2+} channel clustering

Recent studies using super-resolution microscopy have provided evidence that L-type Ca^{2+} channels are clustered in neurons (Moreno et al., 2016; Zhang et al., 2016). However, more work still needs to be done to fully understand the mechanisms underlying this phenomenon. Santana's group reported that clustering of $Ca_V1.3$ is Ca^{2+}-dependent and is mediated by calmodulin through the C-terminal domain, and that the average size of the cluster is about 8 channels. Since there is only one calmodulin binding site within the C-terminal domain, it is hard to explain how the two lobes of calmodulin can bring 8 channels together at once. One possibility is that the calmodulin binding site (NSCaTE) within the N-terminal domain is also involved in clustering. This way multiple Ca^{2+}/calmodulin molecules could cluster several channels together. Another possibility is that CaMKII as a dodecamer can serve as a hub to bring multiple channels together. Consistent with this idea, we showed that CaMKII could link more than one $Ca_V1.3$ L-type Ca^{2+} channels at least *in vitro*. It is possible that more than one clustering mechanism is contributing to the observed cluster size. More works need to be done to carefully examine this.

How many L-type Ca^{2+} channels can CaMKII cluster still remains unclear. One way to examine this is to directly observe the purified complex under the electron microscope (EM). The structure of CaMKII has been studied using negative staining with EM, and the recent breakthrough of solving $Ca_V1.1$ L-type Ca^{2+} channel structure is also through cryo-EM. It will be interesting to directly image the mixture of activated CaMKII and L-

type Ca^{2+} channels to determine how many channels are associated with an individual CaMKII holoenzyme.

To test whether CaMKII is involved in channel clustering in neurons, one potential future direction is to perform the super-resolution microscopy in cultured hippocampal neurons in the presence or absence of transfected CaMKII shRNA. Changing of cluster size upon CaMKII knockdown will be a direct indicator that CaMKII is required in cluster L-type Ca^{2+} channels.

3.3.2 Clustering and coupling between Ca^{2+} channels and other channels

In addition to homomeric clustering of L-type Ca^{2+} channels, it is also possible that L-type Ca^{2+} channels can be clustered and coupled to other channels to facilitate crosstalk. For example, Shapiro's group observed that $Ca_V1.2$ could be coupled to TRPV1 through scaffold protein AKAP150 (Zhang et al., 2016). Recently, a functional coupling between the NMDA receptor and L-type Ca^{2+} channel was proposed in excitation-transcription coupling (Li et al., 2016). Since activated CaMKII binds to both NMDA receptor and L-type Ca^{2+} channels, it is worth testing whether CaMKII can physically link NMDA receptor and L-type Ca^{2+} channels both in heterologous systems and in tissue samples. One potential direction would be to examine the interaction between L-type Ca^{2+} channels and NMDA receptors in wild-type and CaMKII knockout mice brain tissues.

3.3.3 Effects of CaMKII phosphorylation sites on $Ca_V1.3$ channels

We identified at least three groups of CaMKII phosphorylation sites in $Ca_V1.3$ N-terminal domain, I-II linker, and II-III linker. Although the functional effects of these sites remain

to be tested, at least one site (Ser802, corresponding to Ser793 in the Sandoval study) has been recently reported to be phosphorylated by PKG and is responsible for PKG mediated repression of the channel (Section 1.4.5 (Sandoval et al., 2017)). Therefore it is reasonable to hypothesize that at least one of the CaMKII phosphorylation sites has a repressive effect on the channel. The different phosphorylation sites may have different or even opposing effects on the channel, and further experiments need to be done to tease these possibilities apart.

We also observed that efficient CaMKII phosphorylation of $Ca_V1.3$ NTD requires the RKR motif that brings CaMKII to proximity. It is possible that there are sites within other intracellular domains that are phosphorylated by CaMKII only in the presence of certain scaffold proteins. For example, it is possible that the C-terminal domain of $Ca_V1.3$ contains CaMKII phosphorylation sites that were not detected in our screen due to the lack of densin or Shank3 in these assays. Therefore, further experiments need to be done to examine this possibility.

CHAPTER IV

A NOVEL α/β SUBUNIT INTERACTION REGULATES Ca^{2+}-DEPENDENT INACTIVATION OF L-TYPE Ca^{2+} CHANNELS

Summary

L-type Ca^{2+} channels contain three subunits: pore-form α1 subunit, β subunit, and membrane-integrated α2δ subunit. It is well established that the β subunit associates with the α interacting domain (AID) within the I-II linker of the α1 subunit. Here I present data describing a novel interaction between the α1 subunit N-terminal domain (NTD) of both $Ca_V1.2$ and $Ca_V1.3$ and the β2a subunit *in vitro*. Among the four β subunits, β2a seems to have the strongest binding toward $Ca_V1.2$-NTD. Truncation and site-directed mutagenesis showed that the NTD/β2a interaction requires the CaMKII-binding RKR motif of the $Ca_V1.2$-NTD and the N-terminus and/or the Guanylate kinase (GK) domain of the β2a subunit. Peptide competition studies suggest that β subunits can bind to the NTD and I-II linker simultaneously. Furthermore, NTD/β2a interaction is enhanced at slightly acidic pH. Lastly, mutations that disrupt NTD/β interaction specifically accelerate Ca^{2+}-dependent inactivation of $Ca_V1.2$ channels when β2a, but not β3, is coexpressed. Taken together, these data identify a novel mechanism for L-type Ca^{2+} channel regulation by the β2a subunit.

4.1 Experimental procedures

DNA constructs

Rabbit $Ca_V1.2$ cDNA (a gift from Dr. William Thiel, Genbank accession number X15539) was used to amplify a fragment encoding the $Ca_V1.2$ CTD (D1507-L2171). DNAs encoding all other $Ca_V1.2$ intracellular domains were amplified from a rat $Ca_V1.2$ cDNA construct (a gift from Dr. Gerald W. Zamponi, University of Calgary, Canada, Genbank accession number: NM_012517): NTD, M1-K124; I-II, S405-N524; II-III, Q754-I901; III-IV, V1167-Y1220. DNAs encoding rat $Ca_V1.3$ NTD B1 region M69-L93 and $Ca_V1.2$ NTD B1 region M65-K91 were also amplified. All cDNAs encoding GST-tagged proteins were inserted into pGEX-4T1 using traditional ligation or sequence and ligation independent cloning (SLIC; (Li and Elledge, 2007)).

For constructs encoding His-tagged β subunits, rat β1b , β2a, β3 and β4 complete coding sequences (accession numbers X61394, M80545, M88751, and L02315, generous gifts from Dr. Edward Perez-Reyes, University of Virginia) were inserted into the pREST A vector (Thermo Fisher Scientific, Cat. # V35120). M1-P59, V60-S120, P121-P218, S225-T410, and H411-Q604 were deleted to generate β2a-ΔNT, ΔSH3, ΔHOOK, ΔGK, and ΔCT, respectively. Site-directed mutagenesis and all deletions were done following the one-step mutagenesis protocol described by Liu et al (Liu and Naismith, 2008).

Protein purification

Expression and purification of recombinant mouse CaMKIIα has been described previously (McNeill and Colbran, 1995). pGEX-4T1 and pREST A plasmids were

transformed into BL21(DE3) bacteria cells to express GST-tagged proteins and His-tagged proteins, respectively. Cells were grown in LB media at 37°C to reach OD~0.6. IPTG (0.2 mM) was then added to induce the protein expression at room temperature for 2 hours. $Ca_V1.2$ full-length C-terminal domain fragments were expressed in Rosetta 2(DE3) BL21 cells engineered to contain rare tRNAs (EMD Millipore Cat. #71400). Expressed proteins were purified using Pierce Glutathione Agarose beads (Cat. #16101, for GST-tagged proteins) or Qiagen Ni-NTA agarose (Cat. #30210, for His-tagged proteins) following manufacturer's instructions. Eluted proteins were then dialyzed in 10 mM HEPES pH 7.5, 25 μM PMSF, 62.5 μM Benzamidine, 62.5 μM EDTA, 0.1% Triton X-100 overnight with one buffer change. For His-tagged proteins, 150 mM NaCl was also included in the dialysis buffer to reduce protein precipitation during dialysis.

CaMKII autophosphorylation and GST pulldown

For Fig. 4.1A, 1.25 μM purified mouse CaMKIIα was incubated with 50 mM HEPES, pH 7.5, 10 mM $Mg(CH_3COO)_2$, 0.5 mM $CaCl_2$, 2.5 μM calmodulin, and 40 μM ATP on ice for 90 s before addition of EDTA (20 mM final) to terminate phosphorylation by chelation of Mg^{2+} and Ca^{2+}. This would be used later as pre-autophosphorylated CaMKIIα. GST-tagged proteins (62.5 nM) were first incubated with 125 nM pre-autophosphorylated CaMKIIα and 20 μl pre-washed Glutathione Agarose Beads (Thermo Fisher Scientific, Cat. #16100, 50% v/v) in GST pulldown buffer (50 mM Tris-HCl pH 7.5; 150 mM NaCl; 1% (v/v) Triton X-100) for 1 h at 4 °C. His-tagged β2a proteins were then added and an aliquot (5%) of each incubation was saved as input. After incubating at 4°C for another 1 h, beads were separated and washed three times with GST pulldown buffer. GST

protein complexes were eluted by incubation with 40 μl of 20 mM glutathione (pH 8.0) in GST pulldown buffer at 4°C for 10 min. For Fig. 4.1B and Fig. 4.2, 250-500 nM of GST- and His-tagged proteins were incubated with 20 μl pre-washed Glutathione Agarose Beads in GST pulldown buffers for 1 h before washes and elution. For Fig 4.2D, a final concentration of 50 μM of peptide was included in the pulldown when indicated. The peptide sequences were: $Ca_V1.2$ NT B1, AGNATISTVSSTQRKRQQYGKPKKQ; AID, QQLEEDLKGYLDWITQAE. For Fig. 4.3, the pH of the GST pulldown buffer was adjusted to 6.5, 7.0, 7.5, and 8.0 by HCl or NaOH.

Electrophysiology

HEK293T cells were grown to 70–80% confluence and transfected with Gene Porter reagent (Genlantis) or Fugene 6 (Promega) according to the manufacturer's protocols. Cells were plated in 35 mm dishes and transfected with $Ca_V1.2$ subunit cDNAs: Cav1.2 wild-type or RKR/AAA mutant (1.5 μg), β2a or β1b (1 μg), and α2δ1 (1 μg). pEGFP-N1 (0.1 μg) was cotransfected, which facilitated identification of transfected cells by fluorescence. Cells were subjected to whole-cell patch clamp recordings 48 h after transfection. The external solution contained the following (in mM): 150 Tris, 1 $MgCl_2$, and 10 $CaCl_2$ or $BaCl_2$. The internal solution contained the following (in mM): 140 N-methyl-D-glucamine, 10 HEPES, 2 $MgCl_2$, 2 Mg-ATP, and 5 EGTA. The pH of both solutions was adjusted to 7.3 with methanesulfonic acid. Electrode resistances were 6-8 MΩ in the bath solution and series resistance was ~6-8 MΩ before compensated up to 70%. The holding voltage was -80mV. Data were acquired with an EPC-9 amplifier and Patchmaster software (HEKA Elektronik) and analyzed using Igor Pro software (Wavemetrics). For Fig. 4.5, cells were step-depolarized to 10 mV for 1 s and the

residual current was normalized to the peak current for fractional *I* in panel C. The difference between the fractional I_{Ba} and I_{Ca} was calculated for fractional CDI. For Fig. 4.6, currents were evoked by 5 ms pulses from -80 mV to 10 mV at 100 Hz for 1 s. Peak currents were normalized to the first peak and plotted against time. Statistical analysis was performed using SigmaPlot (Systat Software). Average data are presented as mean ± SEM. For current density plots, peak current amplitudes were normalized to whole-cell capacitance.

4.2 Results

4.2.1 A novel interaction between $Ca_V1.2$/$Ca_V1.3$ NTD and β subunits

CaMKII has been shown to bind both the β subunit (Grueter et al., 2008) and the α subunit NTD (Chapter II in this work). Therefore we hypothesized that CaMKII holoenzymes can simultaneously interact with both the α subunit NTD and the β subunit to cause conformational changes that regulate the channel function. As an initial test of this hypothesis, we performed glutathione-agarose co-sedimentation assay with GST-tagged $Ca_V1.2$ NTD and His-tagged β2a subunit in the presence or absence of pre-activated CaMKIIα. To our surprise, we found that even in the absence of autophosphorylated CaMKII, there is a direct interaction between the GST-tagged $Ca_V1.2$ NTD and His-tagged β2a subunit (Fig 4.1A). This suggests that β subunit may be able to interact with the N-terminal domain in addition to the α interacting domain (AID) in the I-II linker.

We then tested whether the β2a subunit can interact with the NTDs of both $Ca_V1.2$ and $Ca_V1.3$ L-type Ca^{2+} channels. As a positive control, we confirmed that His-tagged β2a subunit can interact with the I-II linker domains of both $Ca_V1.2$ and $Ca_V1.3$, consistent with previous reports (Pragnell et al., 1994). Moreover, His-tagged β2a interact with GST-tagged NTDs of both $Ca_V1.2$ and $Ca_V1.3$, but not GST alone (Fig. 4.1B). This indicates that the NTD/β2a interaction is a common feature of $Ca_V1.2$ and $Ca_V1.3$.

As reviewed in Section 1.2.3, there are four different β genes in the mammalian genome, with dozens of different splice isoforms, and it is well-established that β subunits differentially modulate the channel kinetics. Therefore, we investigated whether the $Ca_V1.2$-NTD can interact with representative variants of all four β subunits. As shown in Fig. 4.1C, glutathione-agarose co-sedimentation assays indicate that $Ca_V1.2$-NTD binds to β2a better than any of the other β subunits tested. Together, these data showed that there is an unexpected and selective interaction between neuronal L-type Ca^{2+} α subunit NTDs and the β2a subunit.

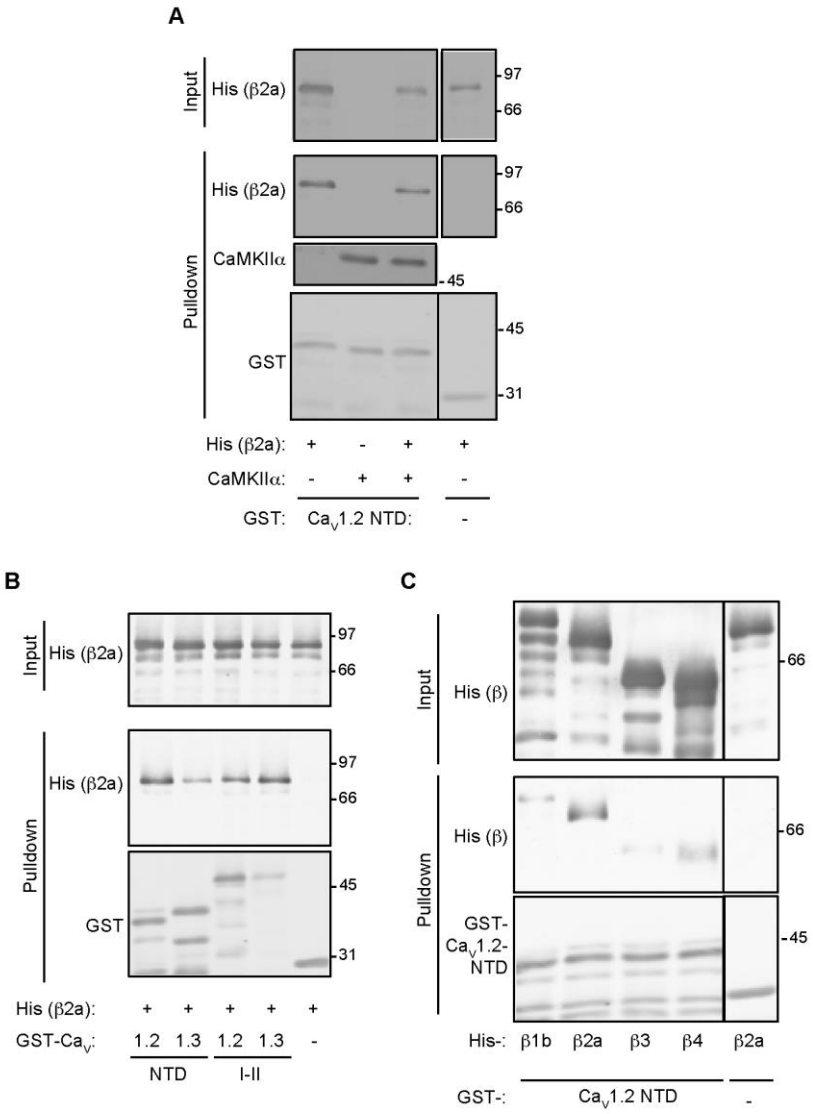

FIGURE 4.1 Ca^{2+} channel β subunits directly interact with $Ca_V1.2$ and $Ca_V1.3$ L-type Ca^{2+} channel N-terminal domains. *A*, association of β2a subunit with $Ca_V1.2$ NTD does not require the presence of activated CaMKII. Glutathione-agarose co-sedimentation assays show that His-tagged β2a associates with GST-tagged $Ca_V1.2$ NTD in the absence or presence of activated CaMKII. *B*, Glutathione-agarose co-sedimentation assays comparing β2a binding between $Ca_V1.2$/$Ca_V1.3$ NTDs and I-II linkers, which contain the canonical β subunit binding domain AID. *C*, interaction with $Ca_V1.2$ NTD is β subunit-selective. Glutathione-agarose co-sedimentation assays show that β2a has the strongest interaction with $Ca_V1.2$ NTD among all β subunits. Representative immunoblots are shown from two to three independent experiments.

4.2.2 Characterization of the molecular determinants for NTD/β interaction

The NTDs of $Ca_V1.2$/$Ca_V1.3$ contain multiple previously identified domains that are important for channel regulation, such as the NSCaTE calmodulin binding site (Dick et al., 2008; Tadross et al., 2008), a CaBP1 binding site (Oz et al., 2011), a densin binding site (in $Ca_V1.2$ only (Wang et al., 2017)), and the RKR motif for CaMKII binding (Chapter II and III from this work). As an initial step to test whether any of these binding domains overlap with the β binding site, we tested whether the NTD B1 region that contains the RKR motif for CaMKII binding is able to directly interact with the β subunit. As shown in Fig. 4.2A, the amounts of His-tagged β2a that were pulled down by NTD B1 regions from $Ca_V1.2$ or $Ca_V1.3$ NTDs were comparable to that were pulled down by the full-length $Ca_V1.2$ and $Ca_V1.3$ NTDs. This suggests that the NTD B1 regions of $Ca_V1.2$ and $Ca_V1.3$ are sufficient to bind β subunits.

We next tested whether the RKR/AAA mutation that disrupts CaMKII interaction also prevents β subunit from binding to the NTD. As shown in Fig 4.2B, in a glutathione-agarose co-sedimentation assay where we screened all $Ca_V1.2$ intracellular domains, only NTD and I-II linker significantly pulled down the His-tagged β2a subunit. Furthermore, mutating the RKR amino acids to alanines completely abolishes β2a interaction with the NTD. This suggests that the RKR motif is required for binding to the β2a subunit, in addition to CaMKII (see Chapter II).

Since the β subunit is a highly modular protein, and each module has a specialized function, we tested the role of each module(s) in binding to the NTD. We generated a series of His-tagged β2a proteins each lacking an individual module. As shown in Fig.

4.2C, β2a subunits that lack the N-terminal module or the GK module show significantly less interaction with GST-tagged $Ca_V1.2$ NTD, while deleting SH3, HOOK or C-terminal modules has little effect. This suggests that the N-terminal and/or the GK module are responsible for NTD/β interaction.

Since the GK module of β subunits contains the α binding pocket (ABP), which mediates the high affinity I-II linker AID/β interaction, we tested whether the NTD and I-II linker bind to β subunit in a competing manner, or both NTD and I-II linker can interact with β subunit simultaneously. To do this, we performed glutathione-agarose co-sedimentation assay in the presence of competing peptides. As shown in Fig. 4.2D, a100-fold molar excess of AID peptide significantly reduces the I-II/β2a interaction, but has no effect on NTD/β2a interaction. We did not observe any competing effect of the NTD B1 peptide on either NTD/β2a interaction or I-II/β2a interaction. Since the GST-NTD B1 is sufficient in mediating NTD/β2a interaction (Fig 4.2A), the lack of competing effect of NTD B1 peptide could be due to a conformational difference between the GST-tagged protein and the free peptide.

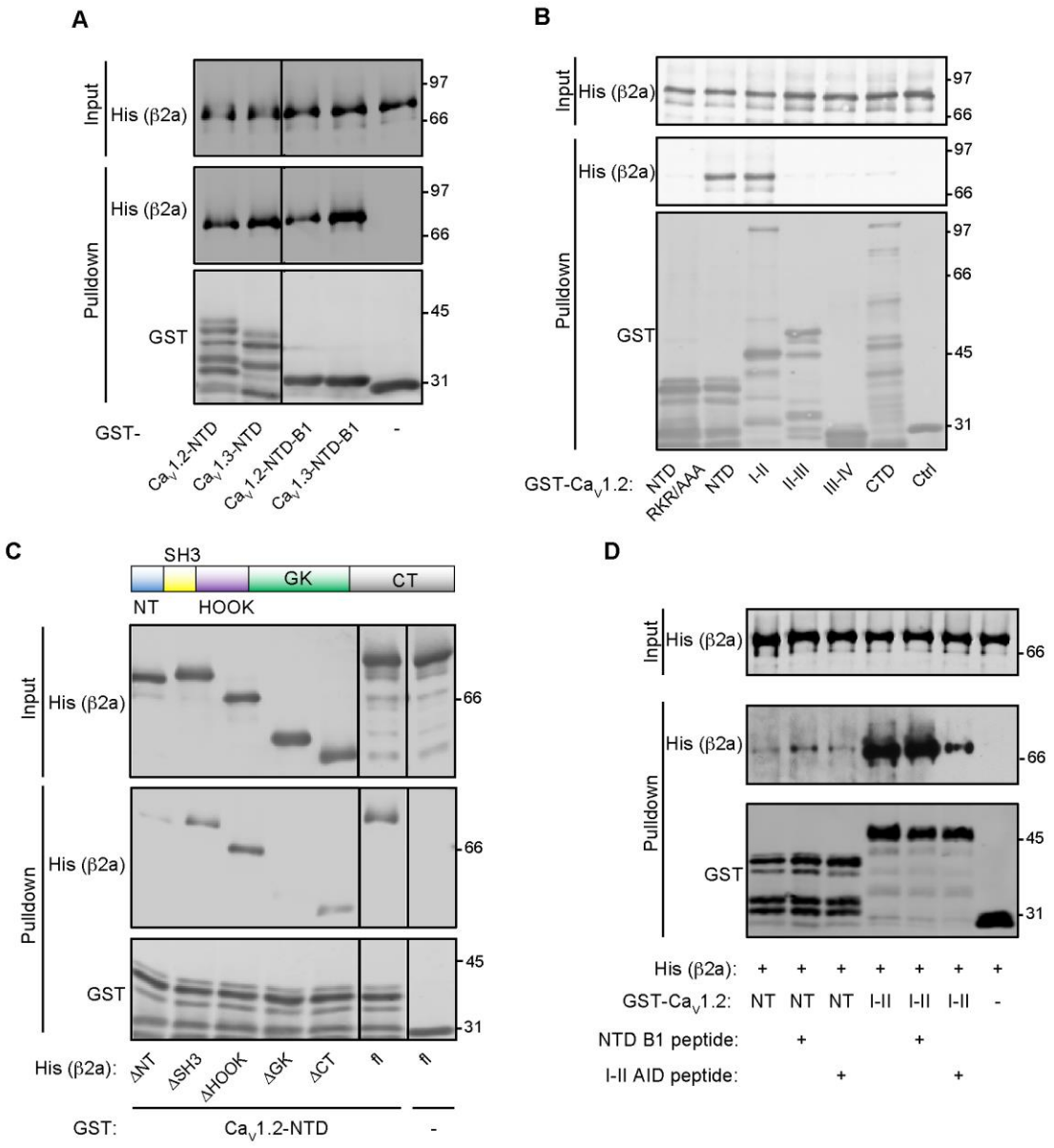

FIGURE 4.2 Characterization of the molecular determinants for β/NTD interaction. *A*, Cav1.2/Cav1.3 NTD B1 regions are sufficient in mediating β/NTD interaction. Glutathione-agarose co-sedimentation assays comparing β2a pulldown among full-length Cav1.2/Cav1.3 NTDs and NTD B1 regions. Cav1.2/Cav1.3 NTD B1 regions pull down β2a as efficient as the full-length NTDs. *B*, a systematic screen of Cav1.2 intracellular domains that directly bind β2a subunit. Glutathione-agarose co-sedimentation assays show that both NTD and I-II linker efficiently pull down β2a subunit. In addition, the RKR/AAA mutant that prevents CaMKII binding also disrupts

NTD/β2a interaction. *C*, deletion of β2a N-terminal region and GK domain affects NTD/β2a interaction. Individual domains were deleted from the full-length His-tagged β2a subunit and the resulting truncated proteins were tested for the ability to interact with $Ca_V1.2$ NTD. Deletion of SH3, HOOK or C-terminal regions has little effect on the NTD/β2a interaction, while deletion of N-terminal region or GK domain greatly affects the interaction. *D*, binding to NTD and I-II linker AID does not seem to compete with each other. Glutathione-agarose co-sedimentation assays of β2a subunit with either $Ca_V1.2$ NTD or I-II linker in the presence of NTD B1 or AID peptide. AID peptide from the I-II linker greatly reduces β2a/I-II linker interaction, but has no effect on β2a/NTD interaction. We did not observe the competition effect of NTD B1 peptide on β2a/NTD or β2a/I-II linker interaction. Representative immunoblots are shown from two to three independent experiments. Experiments in panel D were performed by Lan Hu.

4.2.3 The NTD/β interaction is pH-dependent

During our glutathione-agarose co-sedimentation assays, we noticed that the pulldown efficiency of β2a could be very variable. We reasoned that one contributing factor could be the slight pH difference resulted from different batches and volume ratios of purified proteins that have been mixed. This could also be physiologically relevant since the local pH in the cytosol can change dramatically both in physiological and pathological conditions. To test the effect of pH on NTD/β2a interaction, we repeated the glutathione-agarose co-sedimentation assays between GST-tagged $Ca_V1.2$/$Ca_V1.3$ NTDs and His-tagged β2a subunit in buffers with pH ranging from 6.5 to 8. As shown in Fig. 4.3, for both $Ca_V1.2$ and $Ca_V1.3$ NTDs, the NTD/β2a interaction is the strongest when pH is low, and weakens upon increasing pH. This suggests that the NTD/β2a interaction pH-sensitive, bringing the possibility that the cytosolic pH may modulate the channel function.

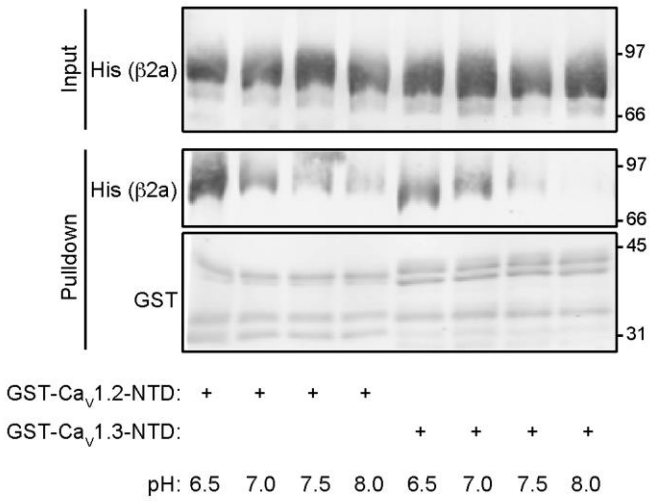

FIGURE 4.3 NTD/β2a interaction is pH-dependent. Glutathione-agarose co-sedimentation assays show that the NTD/β2a interaction is stronger when the pH is lower and weaker when the pH is higher. His-tagged β2a and GST-tagged $Ca_V1.2$ or $Ca_V1.3$ NTD proteins were incubated with glutathione-agarose beads in the presence of GST pulldown buffer with different pH adjusted by either HCl or NaOH. After one hour of incubation at 4 ^oC, the beads were then spun down and washed three times with GST pulldown buffers of corresponding pH. Protein complexes were eluted by incubation with 20 mM glutathione for 10 min at 4 ^oC. Representative immunoblots are shown from three independent experiments.

4.2.4 Effects of disrupting NTD/β interaction on voltage-dependent activation of $Ca_V1.2$ Ca^{2+} channels

We then set out to test whether disruption of the NTD/β2a interaction changes the voltage dependency of $Ca_V1.2$. We assessed the voltage-dependent activation of Ca^{2+} currents via $Ca_V1.2$ WT and RKR/AAA by 50 ms depolarizations from -80 mV to various voltages. As shown in Fig. 4.4A, WT and RKR/AAA $Ca_V1.2$ show similar voltage-dependent activation when coexpressed with β2a (V_h = -12.4 ± 0.9 mV for $Ca_V1.2$ WT, n = 10, and V_h = -17.9 ± 1.9 mV for $Ca_V1.2$ RKR/AAA, n = 9, p = 0.08. k = -6.4 ± 0.3 for $Ca_V1.2$ WT, n = 10, and k = -5.4 ± 0.4 for $Ca_V1.2$ RKR/AAA, n = 9, Student's *t*-test, p = 0.06). However, when coexpressed with β1b, there seems to be a slight positive shift in terms half-maximal voltage (V_h = -3.3 ± 1.3 mV for $Ca_V1.2$ WT, n = 6, and V_h = 2.3 ± 2.0 mV for $Ca_V1.2$ RKR/AAA, n = 7, p = 0.05. k = -7.0 ± 0.9 for $Ca_V1.2$ WT, n = 6, and k = -9.2 ± 0.6 for $Ca_V1.2$ RKR/AAA, n = 7, Student's *t*-test, p = 0.09, Fig. 4.4B). Our biochemical data suggest β2 has the strongest binding to the $Ca_V1.2$ NTD. Thus it is unclear why the RKR/AAA mutant has a significant effect on voltage-dependency when β1, but not β2, is coexpressed.

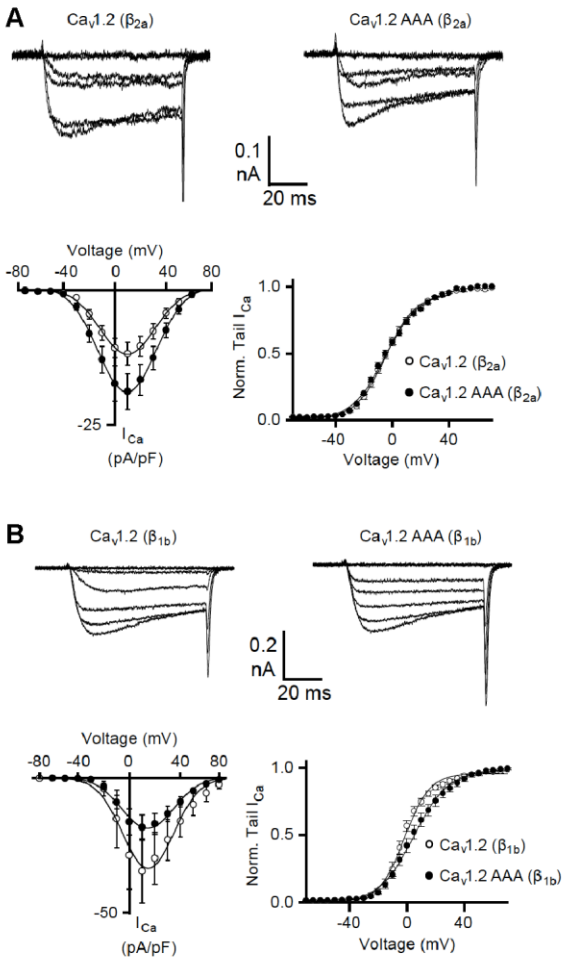

FIGURE 4.4 Effects of disrupting NTD/β interaction on voltage-dependent activation of $Ca_V1.2$ channels in HEK293T cells. *A*, I_{Ca} was evoked by 50 ms depolarizations from -80 mV to various voltages and normalized to cell capacitance. Representative current traces and plots of current density against voltage are shown for cells co-transfected with $Ca_V1.2$ wild-type or $Ca_V1.2$ RKR/AAA mutant with β2a and α2δ. *B*, the same as A, except that β1b used co-expressed instead of β2a. Experiments in this figure were performed and analyzed by Shiyi Wang from Amy Lee's lab, University of Iowa, Iowa City.

4.2.5 NTD/β2a interaction modulates Ca^{2+}-dependent inactivation of $Ca_V1.2$ Ca^{2+} channels when coexpressed with β2a

We next tested the impact of NTD/β2a interaction on the inactivation of $Ca_V1.2$ Ca^{2+} channels using a sustained depolarization protocol (holding at -80 mV, and depolarized to 10 mV for 1 s). The ratio between the residual current at 1 s to the peak current (Fractional I_{Ca}) provides one measure of inactivation. As shown in Fig. 4.5A, there is a significant decrease in the residual Ca^{2+} current for $Ca_V1.2$ RKR/AAA compared to WT (Fractional I_{Ca} = 0.44 ± 0.02, n = 10 for $Ca_V1.2$ WT; Fractional I_{Ca} = 0.28 ± 0.02, n = 9 for $Ca_V1.2$ RKR/AAA, Student's *t*-test: $p < 0.01$), but there is no change when Ba^{2+} is the charge carrier (Fractional I_{Ba} = 0.86 ± 0.02, n = 9 for $Ca_V1.2$; Fractional I_{Ba} = 0.84 ± 0.01, n = 10 for $Ca_V1.2$ RKR/AAA, Student's *t*-test: $p = 0.98$). This suggests that disrupting the NTD/β2a interaction enhances the Ca^{2+}-dependent inactivation of $Ca_V1.2$ channels. This effect is further manifested in the Fractional CDI, which is the difference between the Fractional I_{Ca} and Fractional I_{Ba} (0.42 ± 0.02 for $Ca_V1.2$ WT versus 0.56 ± 0.02 for $Ca_V1.2$ RKR/AAA, Student's *t*-test: $p < 0.01$). However, when coexpressed with β1b, $Ca_V1.2$ WT and $Ca_V1.2$ RKR/AAA show similar inactivation for both I_{Ca} and I_{Ba} (Fractional I_{Ca} = 0.10 ± 0.01, n = 3; Fractional I_{Ba} = 0.46 ± 0.14, n = 4 for $Ca_V1.2$ WT; Fractional I_{Ca} = 0.10 ± 0.02, n = 8; Fractional I_{Ba} = 0.47 ± 0.08, n = 5 for $Ca_V1.2$ RKR/AAA, $p > 0.99$ for both I_{Ca} and I_{Ba}).

We also tested the Ca^{2+}-dependent inactivation using a high frequency depolarization protocol. As shown in Fig. 4.6A, a series of repetitive depolarization of 100 Hz evoked Ca^{2+} entry with rapidly decreasing current peaks. With $Ca_V1.2$ RKR/AAA, the decay rate of the peak current is higher than $Ca_V1.2$ WT, a phenomenon that is not seen when

Ba^{2+} is the charge carrier. Thus disrupting the NTD/β2a interaction also affects Ca^{2+}-dependent inactivation upon high frequency depolarization. However, the effect of RKR/AAA on CDI is not observed with the β1b subunit. Taken together, these data suggest that the NTD/β2a interaction modulates Ca^{2+}-dependent inactivation of $Ca_V1.2$ Ca^{2+} channels in a β subunit-specific manner.

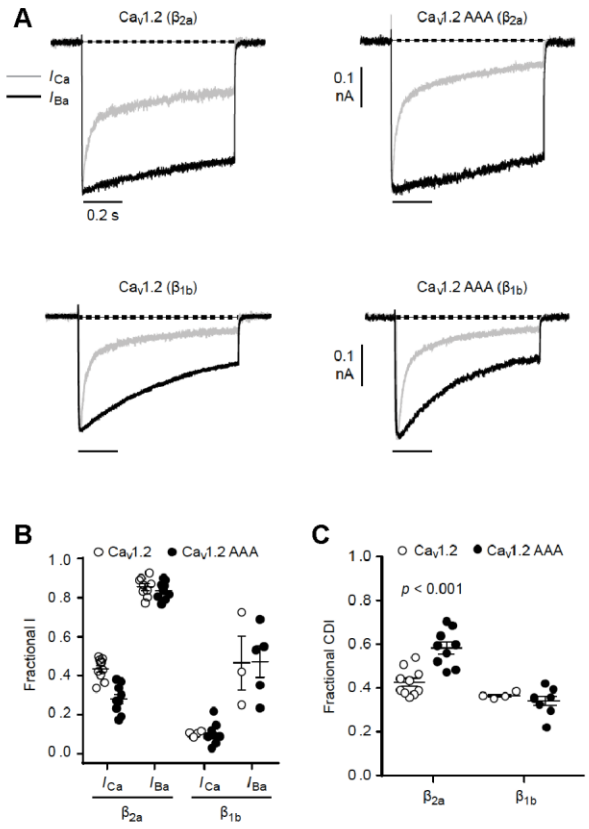

FIGURE 4.5 Disrupting NTD/β interaction enhances step depolarization-induced CDI of $Ca_V1.2$ channels when coexpressed with β2a. *A*, Comparison of $Ca_V1.2$ WT- or RKR/AAA-mediated I_{Ca} and I_{Ba} when β1b (top panel) or β2a (bottom panel) is coexpressed. Cells were held at -80 mV and depolarized to 10 mV for 1 s. I_{Ca} (gray) and I_{Ba} (black) traces were superimposed to show the Ca^{2+}-dependent inactivation. When $Ca_V1.2$ RKR/AAA is expressed, the I_{Ca} is inactivated faster than $Ca_V1.2$ WT while there is no difference of I_{Ba}. *B* and *C*, quantification and summary of CDI from $Ca_V1.2$ WT or RKR/AAA channels when coexpressed with β1b or β2a subunit. B shows the residual currents that were normalized to the peak current (Fractional I). C shows the difference between the Fractional I_{Ca} and I_{Ba}, which is the Fractional CDI. Experiments in this figure were performed and analyzed by Shiyi Wang from Amy Lee's lab, University of Iowa, Iowa City.

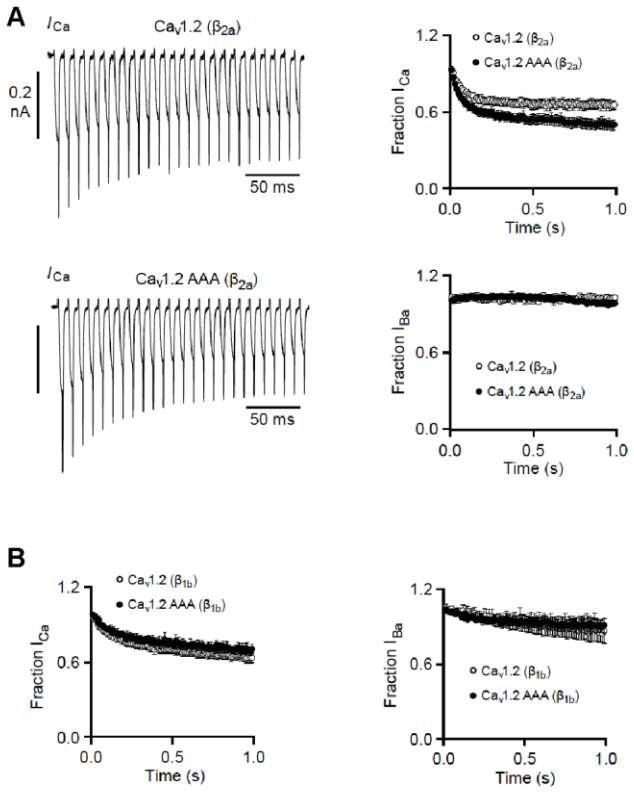

FIGURE 4.6 Disrupting NTD/β interaction enhances high frequency depolarization-induced CDI of $Ca_V1.2$ channels when coexpressed with β2a. *A*, representative traces and summary of $Ca_V1.2$ WT and $Ca_V1.2$ RKR/AAA when coexpressed with β2a. Currents were evoked by 5ms pulses from -80 to 10 mV at 100 Hz. Current amplitudes were normalized to the first in the train and plotted against time. $Ca_V1.2$ RKR/AAA shows faster inactivation compared to $Ca_V1.2$ WT only when Ca^{2+} is the charge carrier. *B*, no differences in CDI were observed between $Ca_V1.2$ WT and $Ca_V1.2$ RKR/AAA when coexpressed with β1b. The same protocol was used as panel A, except that $Ca_V1.2$ WT and $Ca_V1.2$ RKR/AAA were coexpressed with β1b instead of β2a. $Ca_V1.2$ RKR/AAA shows no difference from WT when Ca^{2+} or Ba^{2+} is the charge carrier. Experiments in this figure were performed and analyzed by Shiyi Wang from Amy Lee's lab, University of Iowa, Iowa City.

4.3 Discussion and future directions

4.3.1 Comparison of NTD/β interaction with previously identified interactions

It is well established that the ABP of the β subunit interacts with the AID in the Ca_V1 and Ca_V2 channels (Chen et al., 2004; Pragnell et al., 1994; Van Petegem et al., 2004). In addition to the AID/ABP interaction, several low affinity α/β interactions have been previously reported. The C-terminus of β4 may specifically interact with the N-terminal domain of $Ca_V2.1$, regulating channel inactivation and voltage-dependent activation (Walker et al., 1998; Walker et al., 1999). The β2 subunit was shown to interact with the IQ domain of $Ca_V1.2$, potentially competing with calmodulin in binding to the IQ domain to regulate channel gating (Zhang et al., 2005b). Both the $Ca_V2.1$-NTD/β4 and the $Ca_V1.2$-CTD/β2 interactions are weaker than the AID/ABP interaction (which has a k_D of ~6 nM). Also, AID/ABP interaction is conserved for all Ca_V1/Ca_V2 α subunits and β subunits, while the $Ca_V2.1$-NTD/β4 interaction shows α and β subunit-specificity. The new $Ca_V1.2$/1.3-NTD/β interaction described here seems to represent another subunit-selective interaction.

4.3.2 Potential mechanism of NTD/β2 regulation

Our data suggest that $Ca_V1.2$/1.3-NTD does not compete with I-II linker AID to bind to β subunits (Fig. 4.2D). Thus it is possible that the AID/ABP interaction anchors β subunits to the channel, and the $Ca_V1.2$/1.3-NTD/β interaction plays a dynamic modulatory role. In fact, it was previously observed that a particular orientation of β subunit relative to α subunit is important for channel regulation (Chen et al., 2009; Zhang et al., 2008).

Therefore, it is possible that the AID/ABP interaction poses β in an orientation that is favorable for NTD/β interaction, and the NTD/β interaction is able to regulate the channel function dynamically.

The β subunit has been shown to regulate voltage-gated inactivation of the channel (Buraei and Yang, 2013). Our findings show that NTD/β2a interaction also regulates Ca^{2+}-dependent inactivation. One immediate question is whether the NTD/β interaction is modulated by Ca^{2+}/calmodulin. The NTD/β interaction could serve as a Ca^{2+}/calmodulin sensor or an effector for Ca^{2+}-dependent inactivation. Distinguishing the two possibility will greatly help us understand the channel regulation.

Last, but not least, it is well known that the behavior of β2a is opposite from other β subunits due to the N-terminal palmitoylation (Chien et al., 1996; Qin et al., 1998). It would be interesting to examine whether other splice isoforms of β2 subunits also regulate Ca^{2+}-dependent inactivation, and if so, do they have similar or opposite effects.

4.3.3 Potential roles of CaMKII in modulating NTD/β2 regulation

We showed that the RKR motif that is required for CaMKII interaction is also required for NTD/β interaction (Fig. 4.2B). This raises the possibility that CaMKII and β subunits compete to bind to the N-terminal domain. The apparent binding affinity of CaMKII to N-NTD seems to be higher than that of β subunits. However, β subunits have the advantage of being anchored through the high affinity AID/ABP interaction at the I/II linker. Therefore, it is important to test in intact cell systems whether the competition between CaMKII and β subunits exists, and how this might contribute to the channel

regulation. Recently, Tsien's group showed that efficient nuclear CREB signaling requires a conformational change in the L-type Ca^{2+} channels (Li et al., 2016). It is unclear what mediates the conformational change and how this affects the signaling machinery such as CaMKIIα and CaMKIIγ. Our data provided at least one hypothesis: the conformational change may cause a shift in the relative position of α and β, therefore masking/revealing the RKR motif for CaMKII binding. More experiments in intact cells, such as Förster resonance energy transfer (FRET) assays, could be informative in answering these questions.

CHAPTER V

THE N-TERMINAL DOMAIN OF $Ca_V1.3$ ENCODES A NUCLEAR PROTEIN THAT REGULATES NEURONAL MORPHOLOGY AND GENE TRANSCRIPTION

Summary

$Ca_V1.3$ is one of the major L-type Ca^{2+} channel $\alpha1$ subunits in the brain. Ca^{2+} influx through $Ca_V1.3$ is involved in a variety of processes including excitation-transcription coupling in hippocampus and repetitive firing in midbrain dopaminergic neurons. However, non-channel functions of $Ca_V1.3$ have not been explored. Here I present data showing that the N-terminal domain (NTD) of $Ca_V1.3$ can be proteolyzed in a Ca^{2+}-dependent process. The protein structure and function prediction tool I-TASSER predicted that the $Ca_V1.3$ NTD is a DNA binding protein. Expression of mCherry-tagged $Ca_V1.3$ NTD both in HEK293T cells and in cultured hippocampal neurons suggests that it is predominantly localized in the nucleus. Interestingly, mutating the RKR motif to alanines within the NTD significantly affects nuclear localization. Furthermore, RNA sequencing from hippocampal neurons overexpressing the $Ca_V1.3$ NTD revealed changes in the transcription levels of ~300 genes. Lastly, overexpressing $Ca_V1.3$ NTD in hippocampal neurons results in smaller dendritic spine size with no change of spine density. Together, these data suggest an unexpected non-channel function of $Ca_V1.3$ that may have an important role in neuronal physiology and pathology.

5.1 Experimental procedures

DNA plasmids and transfection

A plasmid encoding $Ca_V1.3$ with an N-terminal HA-tag (pCGNH-$Ca_V1.3$) was made by inserting rat $Ca_V1.3$ cDNA into the pCGN vector. The DNA fragment that encodes rat $Ca_V1.3$ NTD (M1-K124) was PCR-amplified and inserted into pmCherry-C1 vector through the BglII site using SLIC cloning to generate pmCherry-NTD. The $R^{83}KR^{85}$ sequence was then mutated to alanines using site-directed mutagenesis to generate pmCherry-NTD-RKR/AAA.

The lentiviral transfer vectors were modified from FSy(0.5)GW, a generous gift from Dr. Pavel Osten, Max Planck Institute for Medical Research, Germany (Dittgen et al., 2004). Briefly, a DNA oligo that encodes V5 tag together with another oligo that encodes porcine teschovirus-1 2A sequence (P2A, (Kim et al., 2011)) were inserted upstream of the GFP coding sequence of FSy(0.5)GW to generate FSVPG (FSy(0.5)-V5-P2A-GFP). The DNA fragment encoding rat $Ca_V1.3$ NTD was then inserted into FSVPG upstream of the V5 sequence to make FSVPG-$Ca_V1.3$ NTD.

Cell culture and transfection

HEK293T cells were purchased from ATCC (Cat. # CRL-3216) and maintained in DMEM (Cat. #11995065) with 10% fatal bovine serum (Cat. #16140071), 1x Glutamax (Cat. # 35050061) and 100 U/mL Penicillin-Streptomycin (Cat. # 15140122). All media and supplements were purchased form Thermo Fisher Scientific. For Fig. 5.1, a total of 4 μg of DNA were transfected into a 35 mm dish (pCGNH-$Ca_V1.3$, 2 μg; β3, 1 μg; $\alpha2\delta$, 1 μg). Forty-eight hours of transfection, cells were either directly lysed by 2x Laemmli

buffer or treated by 40 mM KCl Tyrode's solution (105 mM NaCl, 40 mM KCl, 2 mM $CaCl_2$, 2 mM $MgCl_2$, 10 mM HEPES, and 10 mM glucose, pH 7.3 adjusted with NaOH) for 30 s before lysed by 2x Laemmli buffer. A dish of non-transfected cells was included to control for antibody specificity.

For Fig. 5.2B, a total of 3 μg of DNA (1.5 μg of GFP and 1.5 μg of mCherry or mCherry-Ca_V1.3 NTD WT or RKR/AAA) were transfected into HEK293T cells in a 35 mm dish. After 24 hours of transfection, cells were split into in a well of a 12-well plate containing a 16 mm coverslip that has been coated with poly-L-lysine and washed with Milli Q water. After 24 hours of split, the cells were fixed with ice-cold 4% PFA-4% sucrose in 0.1 M phosphate buffers for 8 minutes and washed with PBS three times. Coverslips were then mounted on a slide with ProLong Gold Antifade Mountant with DAPI (Thermo Fisher Scientific, Cat. # P36931).

For Fig. 5.2C, dissociated rat E18 hippocampal neurons were prepared as previously described (Sala et al., 2003), and transfected after 8 days *in vitro* (DIV). A total of 1 μg of DNA (0.5 μg of GFP and 0.5 μg of mCherry or mCherry-Ca_V1.3 NTD WT/AAA) was transfected into each well of a 12-well plate using Lipofectamine 2000 with a DNA:lipid ratio of 1:1. After ~72 hours of transfection, the neurons were fixed and mounted the same way as the HEK293T cells.

For Fig 5.4, hippocampal neurons were transfected at DIV 14 and fixed at DIV 19. A total of 1 μg of DNA (0.5 μg of GFP and 0.5 μg of mCherry or mCherry-Ca_V1.3 NTD) were transfected into each well of a 12-well plate using Lipofectamine 2000 with a DNA:lipid ratio of 1:1.

Confocal microscopy

For Fig. 5.2 B and C, images were collected using an Olympus FV-1000 inverted confocal microscope with a 40/1.30 numeric aperture Plan-Neofluar oil lens. The binocular lens was used to identify transfected neurons based on the GFP channel. Pinhole size was set to auto and z position was adjusted for maximum DAPI intensity, so that the plane that is being imaged runs across the middle of the nucleus.

For Fig. 5.4, images were collected using an LSM 710 META Inverted confocal microscope using 63x (1.40 Plan-apochromat oil) objectives. Cells were selected for analysis based on GFP expression. Dendritic spine measurements were performed using 10–14 images of a neuron in the z-plane using a z-step size of ~0.3 μm. Images were imported into IMARIS software (RRID:SCR_007370) for quantitative analysis. Nonprimary dendritic segments (20–50 μm long) at least 60 μm from the cell body and devoid of intersecting dendrites were selected. Dendritic spine density was analyzed as number of spines/10 μm, and the average spine density for each cell was calculated from 2–4 dendritic segments.

Virus production

To package lentiviruses that express $Ca_V1.3$ NTD or control GFP, HEK293T cells were split into two tripleflasks (Thermo Fisher Scientific, Cat. #132913) the day before transfection. A total of 360 μg of DNA (144 μg transfer vector, 72 μg pRSV-REV, 72 μg pVSVG and 72 μg pMDL) were mixed with 720 μl PEI (1mg/ml stock) in 12 ml of serum-free DMEM. After 20 minutes of incubation, the DNA/PEI complex was divided into two triple flasks. The medium was decanted 12 hours after transfection. And subsequent

medium containing the virus was collected 36 and 60 hours after transfection. Medium from the two time points was combined and filtered through a 0.45 μm filter (Nalgene #166-0045 Rapid-Flow Sterile Filter Unit). Filtered medium was then transferred into centrifuge tubes (Beckman, Cat. #326823) with 2 mL of 20% sucrose (w/v in PBS) at the bottom. Tubes were centrifuged at 112,500 xg for 2 hours at 4ºC. Viruses were resuspended in a total volume of 100 μl of cold PBS, aliquoted, and frozen at -80 ºC. Virus titer was assayed using the Lenti-X p24 Rapid Titer Kit (Clontech, Cat. # 632200) following manufacturer's instruction.

Overexpression of $Ca_V1.3$ NTD in hippocampal neurons and RNAseq

Dissociated rat hippocampal neurons were grown in laminin- and poly L lysine-treated 6 cm dishes at a density of ~20,000 cells/cm^2. Neurons of DIV 10 were infected with lentiviruses expressing either GFP or $Ca_V1.3$ NTD-P2A-GFP at a MOI (Multiplicity of infection) of 20. Four days after infection, neurons were harvested for RNA extraction using the PureLink RNA Mini Kit (Thermo Fisher Scientific, Cat. # 12183018A) following manufacturer's instruction. Two biological replicates were included for the GFP control condition, and three for the $Ca_V1.3$ NTD-P2A-GFP condition. The RNA integrity numbers (RIN) for all five replicates were between 9.7 and 10, suggesting a high quality of RNA integrity. Extracted RNAs were sequenced at the HudsonAlpha Institute for Biotechnology, Huntsville, AL. Around 28-47 million paired reads were sequenced for each of the replicates.

5.2 Results

5.2.1 $Ca_V1.3$ L-type Ca^{2+} channel N-terminal domain may undergo Ca^{2+}-dependent proteolysis

During the characterization of $Ca_V1.3$ channels with an N-terminal HA-tag in HEK293T cells (Section 2.2.5), we observed an interesting phenomenon: the HA antibody detected a small product that roughly corresponds to the size of the N-terminal domain (~15 kDa) in addition to the full-length HA-$Ca_V1.3$ channel (Fig. 5.1). Since the HA tag is located to the N terminus of the $Ca_V1.3$ channel, we hypothesized that the small product could be generated by a potential proteolytic event near the membrane proximal part of the N-terminal domain.

As reviewed in Section 1.4.7, multiple groups have previously reported Ca^{2+}-dependent proteolysis of $Ca_V1.2$ channels (Gomez-Ospina et al., 2006; Hell et al., 1996; Michailidis et al., 2014). In particular, Catterall's group showed that Ca^{2+} influx through NMDA receptors could induce $Ca_V1.2$ C-terminal proteolysis mediated by a Ca^{2+}-dependent protease calpain (Hell et al., 1996). To test whether the putative N-terminal domain proteolysis is also Ca^{2+}-dependent, we pretreated transfected HEK293T cells with 40 mM K^+ to depolarize the membrane and activate $Ca_V1.3$ channels. As shown in Fig. 5.1A and B, pretreatment with Tyrode's solution that contains 40 mM KCl seems to increase the proteolysis, suggesting the cleavage of N-terminal domain is dependent on membrane depolarization.

It is known that the resting membrane potential of HEK293T cells is higher than that of neurons. We hypothesized that the basal level of cleavage seen in Fig. 5B is due to

Ca^{2+} influx through $Ca_V1.3$ Ca^{2+} channels at the resting membrane potential. To test this, we included nimodipine in the culture medium to block $Ca_V1.3$ Ca^{2+} channels after the transfection, and found that the N-terminal cleavage of $Ca_V1.3$ Ca^{2+} channels was reduced. Again, this is consistent with depolarization-dependent proteolysis of the $Ca_V1.3$ N-terminal domain.

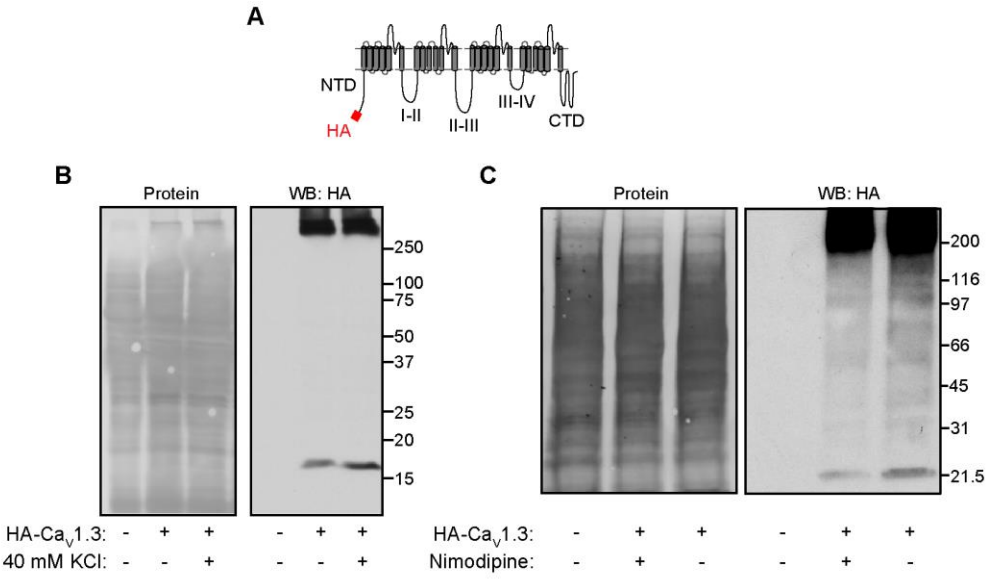

FIGURE 5.1 $Ca_V1.3$ channels undergoes N-terminal proteolysis in HEK293T cells. *A*, a schematic diagram of the N-terminal HA-tagged $Ca_V1.3$ construct. The $Ca_V1.3$ coding sequence was inserted after the HA tag (YPYDVPDYA, 9 amino acids) with a linker sequence SLGGPSR in between. The resulting HA-$Ca_V1.3$ has 137 amino acids in the intracellular N-terminal domain, with a predicted molecular weight of 15.0 kDa. *B*, cleavage of HA-$Ca_V1.3$ is enhanced by high K^+ depolarization. HEK293T cells expressing HA-$Ca_V1.3$ with $\beta3$ and $\alpha2\delta$ were lysed directly using 2x Laemmli buffer or treated with 40 mM K^+ Tyrode's solution before lysis. Protein stain (left) shows similar loading of sample. An immunoblot from a 4-20% gradient SDS-PAGE gel shows full-length of HA-$Ca_V1.3$ at around 250 kDa and the cleaved product at around 15 kDa. The cleaved product is increased when cells were first exposed to 40 mM K^+ Tyrode's solution to activate $Ca_V1.3$ L-type Ca^{2+} channels. *C*, cleavage of HA-$Ca_V1.3$ is reduced by the L-type Ca^{2+} channel blocker nimodipine (10 μM) in the culture medium. The same as B, except that nimodipine was added 12 hours after transfection where indicated to block Ca^{2+} influx via the $Ca_V1.3$ L-type Ca^{2+} channels.

5.2.2 $Ca_V1.3$ L-type Ca^{2+} channel N-terminal is a nucleus-located protein

Examination of the sequence of the $Ca_V1.3$ N-terminal domain revealed that the RKR motif resembles a nuclear localization signal (NLS). Indeed, the $R^{83}KR^{85}$ sequence is predicted to be part of a functional NLS using NucPred, an online protein nuclear localization prediction tool (Fig. 5.2A, (Brameier et al., 2007)). Furthermore, we used I-TASSER to predict the 3-D structure of the N-terminal domain of $Ca_V1.3$ (Yang et al., 2015), and found that it is predicted to be a DNA-binding protein with structural similarity to the transcription factor C/EBPβ (CCAAT/Enhancer Binding Protein β, Fig. 5.2B).

To determine the actual subcellular localization, we co-expressed mCherry-tagged $Ca_V1.3$ NTD or mCherry alone in HEK293T cells with untagged GFP to outline the cell shape. As shown in Fig. 5.2C, untagged mCherry is expressed throughout the cell, overlapping with GFP. However, mCherry-tagged $Ca_V1.3$ NTD is seen predominantly overlapping with the DAPI nuclear counter stain. Furthermore, mutating part of the putative NLS ($R^{83}KR^{85}$) to alanines completely abolished the nuclear-enrichment of mCherry-tagged $Ca_V1.3$ NTD. We also tested the subcellular localization of the mCherry-tagged $Ca_V1.3$ NTD in cultured hippocampal neurons. As shown in Fig. 5.2D, mCherry-tagged $Ca_V1.3$ NTD is enriched in the nucleus, but is excluded from the nucleus upon the RKR/AAA mutation. Together, these data suggest that the cleaved $Ca_V1.3$ NTD is a potential nuclear protein.

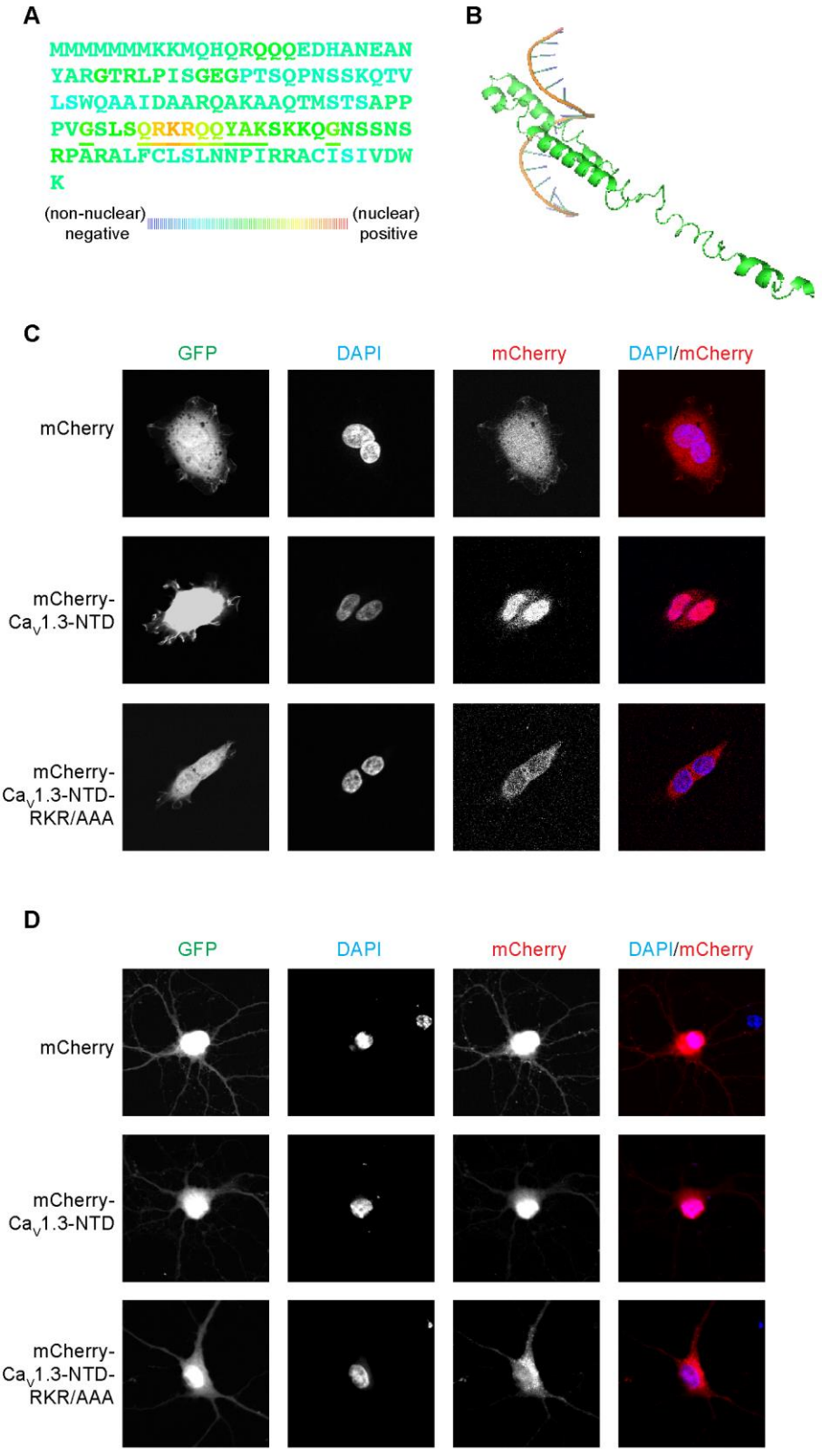
A
MMMMMMMKKMQHQRQQQEDHANEAN
YARGTRLPISGEGPTSQPNSSKQTV
LSWQAAIDAARQAKAAQTMSTSAPP
PVGSLSQRKRQQYAKSKKQGNSSNS
RPARALFCLSLNNPIRRACISIVDW
K
(non-nuclear) negative
(nuclear) positive
B
C
GFP
DAPI
mCherry
DAPI/mCherry
mCherry
mCherry-Ca$_V$1.3-NTD
mCherry-Ca$_V$1.3-NTD-RKR/AAA
D
GFP
DAPI
mCherry
DAPI/mCherry
mCherry
mCherry-Ca$_V$1.3-NTD
mCherry-Ca$_V$1.3-NTD-RKR/AAA

FIGURE 5.2 $Ca_V1.3$ NTD is predicted to be a DNA binding protein and is localized in the nucleus. *A*, sequence analysis of $Ca_V1.3$-NTD by a protein nuclear localization prediction tool NucPred (http://nucpred.bioinfo.se/nucpred/, (Brameier et al., 2007)). The putative nuclear localization signal is underscored. *B*, structure and function prediction of $Ca_V1.3$ NTD by I-TASSER (https://zhanglab.ccmb.med.umich.edu/I-TASSER/, (Yang et al., 2015)). Full length of $Ca_V1.3$ NTD was submitted to the I-TASSER server for automated protein structure prediction. The most likely "ligand" of $Ca_V1.3$ NTD is predicted to be nucleic acid, with a structural similarity with transcription factor C/EBPβ (CCAAT/Enhancer Binding Protein β). *C* and *D*, subcellular localization of mCherry-$Ca_V1.3$ NTD WT and mCherry-$Ca_V1.3$ NTD RKR/AAA in HEK293T cells (C) and in cultured hippocampal neurons (D). pEGFP-N1 is coexpressed to show the cell morphology. Untagged mCherry overlaps nicely with GFP. mCherry-$Ca_V1.3$ NTD WT is primarily located in the nucleus, while mCherry-$Ca_V1.3$ NTD RKR/AAA is predominantly in the cytosol, suggesting the RKR motif can serve as a functional nuclear localization signal (NLS). Each figure shows a 50 μm x 50 μm square in panel C and a 100 μm x 100 μm square in panel D.

5.2.3 Overexpression of $Ca_V1.3$ NTD changes the neuronal transcriptome

Since the $Ca_V1.3$ NTD is predicted to be a DNA-binding protein and can be localized in the nucleus, we asked whether overexpressing the $Ca_V1.3$ NTD affects gene transcription. We infected neurons with lentiviruses that express either GFP alone or V5-tagged $Ca_V1.3$ NTD and GFP separated by a self-cleaving P2A peptide ($Ca_V1.3$ NTD-V5-P2A-GFP) under the Synapsin promoter. Four days later, we extracted RNA for next generation sequencing.

Comparing with GFP virus-infected neurons, a total of 35 genes were up-regulated and 357 genes were down-regulated in neurons infected by $Ca_V1.3$ NTD-V5-P2A-GFP (Fig. 5.3 A and B). Pathway enrichment analysis showed that genes encoding histones and kinesin proteins were enriched among those repressed by overexpressing the $Ca_V1.3$ NTD (Fig. 5.3 C and D). Thus our data suggest that $Ca_V1.3$ NTD may selectively suppress the expression of kinesins and histones in neurons.

A

	NTD vs Ctrl
Up-regulated genes	35
Down-regulated genes	357
Total changed	392

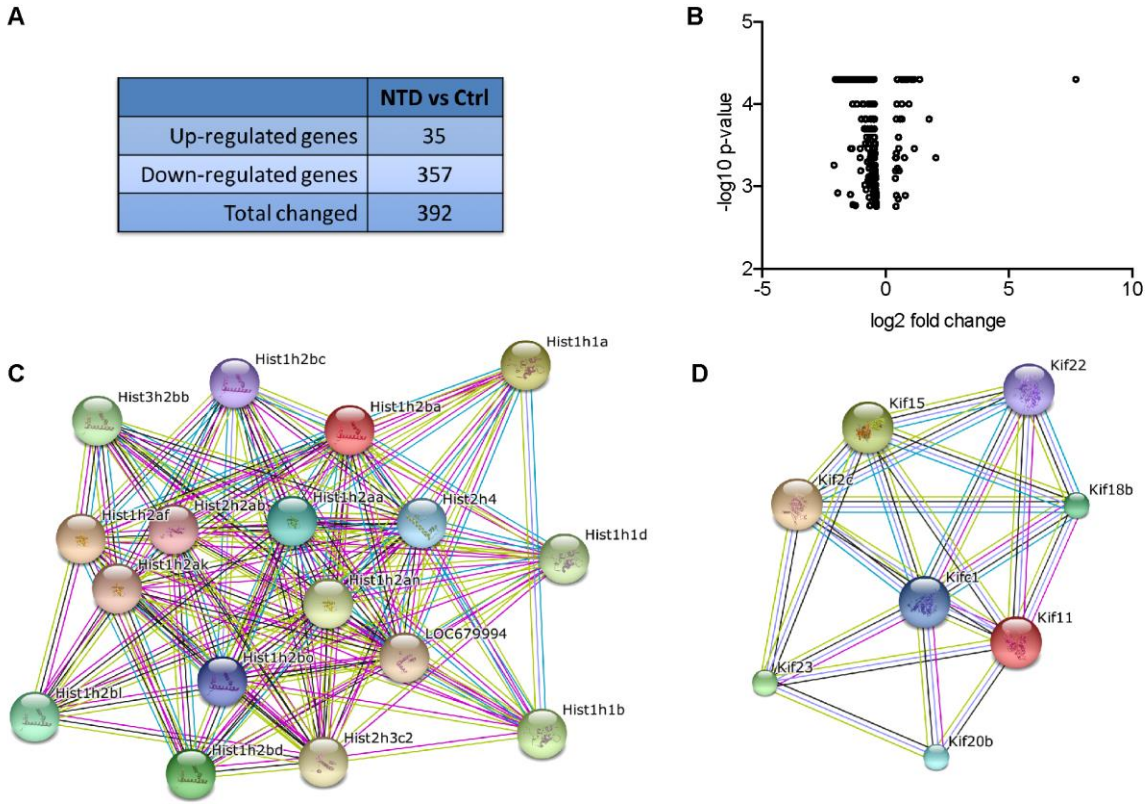

FIGURE 5.3 Overexpression of Cav1.3 NTD in cultured hippocampal neurons changes gene transcription in neurons. Neurons of DIV 10 were infected with lentiviruses expressing either GFP or Cav1.3 NTD-P2A-GFP, where P2A is a high efficient self-cleavage peptide to separate Cav1.3 NTD from GFP. Four days after infection, RNAs were extracted for next generation RNA sequencing. *A*, a summary of overall changes of mRNA levels in neurons overexpressing Cav1.3 NTD compared to GFP control. A total of 35 genes were significantly up-regulated and 357 genes were down-regulated when overexpressing Cav1.3 NTD. *B*, a volcano plot of the 392 genes that are significantly changed in mRNA levels. The dot at the top right corner represents the mRNA change from Cav1.3 (*Cacna1d*). *C* and *D*, pathway analysis of the genes that were down regulated upon overexpressing Cav1.3 NTD. The genes that were down-regulated by overexpressing Cav1.3 NTD were enriched in histones (C) and motor proteins (D).

5.2.4 Overexpression of Ca_V1.3 NTD changes neuronal morphology

Lastly, we examined whether overexpressing the Ca_V1.3 NTD affects neuronal morphology. We co-transfected neurons of DIV 14 to express mCherry or mCherry-Ca_V1.3 NTD with GFP to show the cell morphology. Five days after transfection, we imaged the dendrites and spines of transfected neurons with z stacks and reconstructed the dendrites and spines through the GFP signal using IMARIS software. As shown in Fig. 5.4A, overexpression of Ca_V1.3 NTD does not change the overall spine density of the neurons. However, as shown in Fig. 5.4B-D, the spine neck diameter, spine surface area, the spine volume are all reduced upon overexpressing Ca_V1.3 NTD.

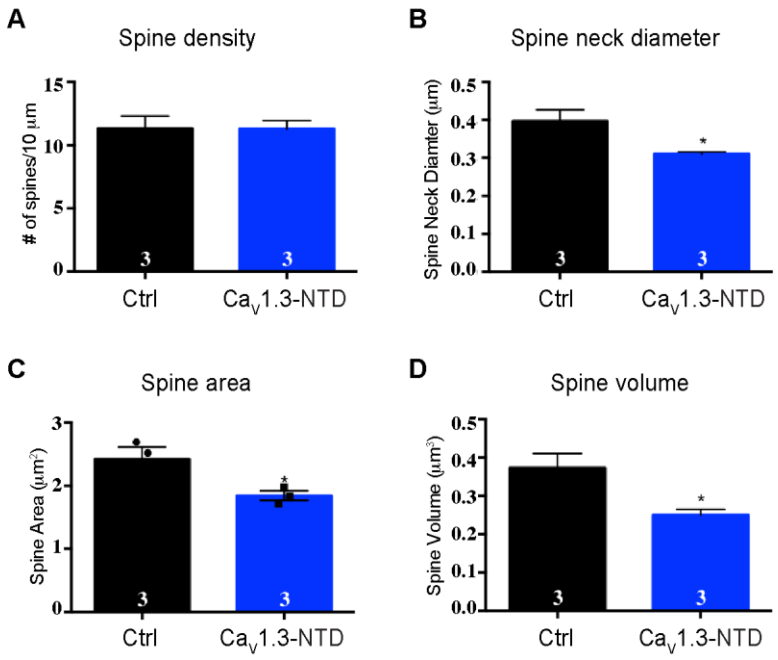

FIGURE 5.4 Overexpression of $Ca_V1.3$ NTD in cultured hippocampal neurons changes neuronal morphology. Cultured hippocampal neurons of DIV 14 were transfected with pEGFP-N1 and mCherry or mCherry-$Ca_V1.3$ NTD. Five days after transfection, neurons were fixed with 4% paraformaldehyde-4% sucrose in 0.1 M phosphate buffer, washed three times with PBS, and mounted on slides. Dendritic spine measurements were performed using 10–14 images of a cell in the z-plane using a z-step size of ~0.3 μm. *A*, overexpression of $Ca_V1.3$ NTD does not alter spine density of cultured hippocampal neurons. *B-D*, overexpression decreases the spine neck diameter (B), spine area (C), and spine volume (D) in cultured hippocampal neurons. Three neurons from two independent cultures were analyzed. *, $p<0.05$, student two-tailed *t*-test. Confocal imaging and IMARIS measurement in this figure were performed by Jason Stephenson.

5.3 Discussion and future directions

5.3.1 Calpain as a potential candidate that mediates $Ca_V1.3$ NTD proteolysis

As discussed in Section 1.4.7, calpain has been shown in many studies to cleave $Ca_V1.2$ at specific sites in a Ca^{2+}-dependent manner (De Jongh et al., 1994; Hell et al., 1996). Data described here suggest that the cleavage of $Ca_V1.3$ NTD depends on channel opening and may also be Ca^{2+}-dependent (Fig. 5.1). Thus is it tempting to hypothesize that calpain is mediating $Ca_V1.3$ NTD proteolysis. Initial predictions using available bioinformatics tools suggest that there is a potential calpain cleavage site at Leu^{109}^Ser^{110} of $Ca_V1.3$ NTD. Further mass spectrometry analysis will be needed to confirm/identify the cleavage site. It is also worth pointing out that Ser^{110} is one of the CaMKII phosphorylation sites identified in Chapter III. If Leu^{109}^Ser^{110} is indeed the cleavage site by calpain, it would be interesting to see whether CaMKII phosphorylation of Ser^{110} affects the efficiency of proteolysis.

5.3.2 $Ca_V1.3$ NTD as a nuclear protein

Nuclear proteins that exceed 40 kDa require a nuclear localization signal to be transported into the nucleus. The observed cleavage product of $Ca_V1.3$ NTD is around 17 kDa, well under the limit for diffusion into the nucleus through nuclear pores. However, this does not mean that active transport through nuclear localization signal is not important for proper signaling. Nuclear transport of Ca^{2+}/calmodulin is a good example of this. Even though Ca^{2+}/calmodulin is small enough to diffuse through the nuclear pores, efficient nuclear signaling of calmodulin still requires CaMKIIγ (or CaMKIγ for Parvalbumin-positive interneurons), which has a nuclear localization signal (Cohen

et al., 2016; Ma et al., 2014). Therefore, the RKR motif may still be important for $Ca_V1.3$ NTD translocation in neurons. This also raises the question whether CaMKII or β2a binding to the RKR motif can mask the nuclear localization signal and retain $Ca_V1.3$ NTD in the cytosol.

$Ca_V1.3$ NTD is predicted to be a DNA binding protein by I-TASSER (Fig. 5.2A). However, this still needs to be confirmed experimentally. With candidate DNA binding probes, electrophoresis mobility shift assay will be needed to directly test the protein/DNA interaction. It will be especially informative if this could be combined with the RNAseq data to identify potential $Ca_V1.3$ NTD target sequences in the promoter regions of genes affected by $Ca_V1.3$ NTD overexpression.

5.3.3 Potential links between $Ca_V1.3$ NTD proteolysis and Parkinson Disease

Recently, $Ca_V1.3$ has become one focus in Parkinson's disease research (Chan et al., 2007; Hurley et al., 2013). Deleting $Ca_V1.3$ is protective in Parkinson Disease mouse models and blocking $Ca_V1.3$ channels in adults could “rejuvenate” the dopaminergic neurons to a pacemaking form only observed in younger mice (Chan et al., 2007). Consistent with this viewpoint, post-mortem studies discovered that there is an increase in $Ca_V1.3$ expression levels in cerebral cortex of early Parkinson Disease, even before the pathology changes occur (Hurley et al., 2013). A clinical trial has recently started testing the potential beneficial effects of $Ca_V1.3$ specific antagonist Isradipine in early Parkinson Disease (Biglan et al., 2017; Parkinson Study, 2013)

It has been shown that $Ca_V1.2$ L-type Ca^{2+} channels undergo age-dependent, calpain-mediated proteolysis (Michailidis et al., 2014), suggesting there is an age-related

change in calpain cleavage in aging neurons. It is also known that $Ca_V1.3$, but not $Ca_V1.2$, is important for repetitive firing in substantia nigra pars compacta (SNc) dopaminergic neurons. Thus it is possible that $Ca_V1.3$ channels in SNc dopaminergic neurons also undergo age-dependent, calpain-mediated proteolysis. Our data suggest that at least one of the proteolysis products is a small protein from the N-terminal domain that can be localized in the nucleus and regulate gene transcription and neuronal morphology *in vitro*. Therefore it is possible that the potential beneficial effect of $Ca_V1.3$ channel blocker Isradipine is to block the excessive Ca^{2+} influx to the neurons and prevent further nuclear expression of $Ca_V1.3$ NTD. One potential experiment to directly test this idea is to overexpresses $Ca_V1.3$ NTD in the SNc by viral expression and examine whether it causes dopaminergic neuron death and/or behavior changes.

CHAPTER VI

CONCLUSIONS AND FUTURE DIRECTIONS

6.1 The $Ca_V1.3$ NTD as a multifunctional regulatory domain

Studies of L-type Ca^{2+} channel regulation by intracellular domains have mostly focused on the C-terminus. Data described in this dissertation highlight the importance of the $Ca_V1.3$ N-terminal domain in regulating channel function and signaling in multiple ways (Fig. 6.1): 1) the RKR motif in the NTD recruits activated CaMKII to the channel to mediate nuclear CREB signaling; 2) the dodecameric CaMKII may cluster multiple Ca^{2+} channels together via the NTD interaction to facilitate compartmentalized signaling within a nanodomain; 3) the RKR motif is required for efficient phosphorylation of the $Ca_V1.3$ NTD; 4) the RKR motif is required for a novel NTD/β interaction that regulates Ca^{2+}-dependent inactivation of the channel; 5) the $Ca_V1.3$ NTD may undergo proteolysis, and the RKR motif is part of a nuclear localization signal; the cleaved $Ca_V1.3$ NTD is localized in the nucleus and regulates neuronal morphology and gene transcription.

I hope the findings in this thesis can serve as a starting point to fully understand the multifunctional roles of NTD in regulating L-type Ca^{2+} channel. In particular, the following immediate directions may help to yield a better understanding of NTD regulation of the channel.

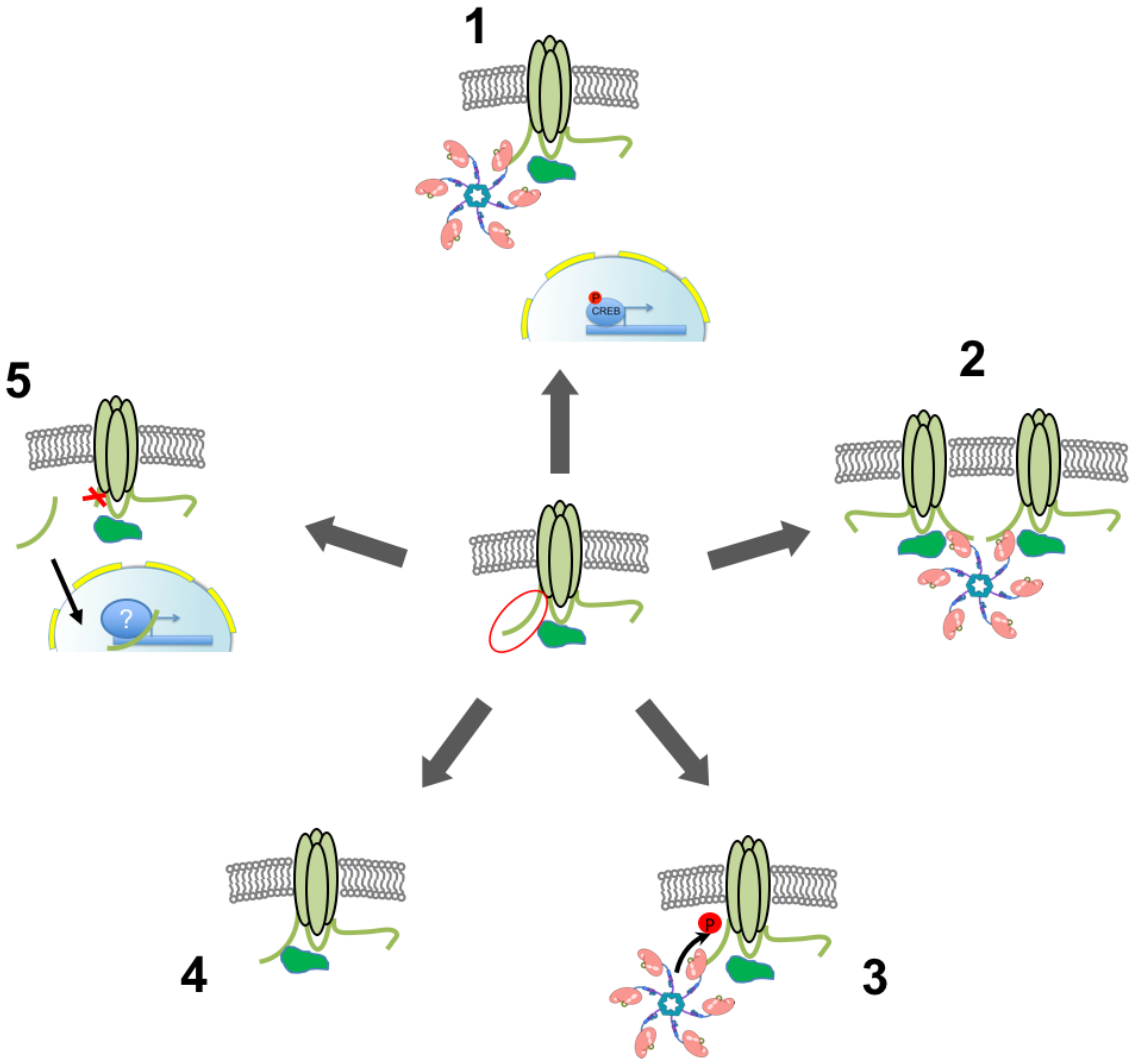

FIGURE 6.1 Multifunctional regulation of $Ca_V1.3$ by the NTD. 1) the NTD recruits CaMKII to the channel to mediate nuclear CREB signaling; 2) the dodecameric CaMKII may cluster multiple Ca^{2+} channels together via the NTD; 3) recruitment of CaMKII via the RKR motif is required for efficient phosphorylation of $Ca_V1.3$ intracellular domains; 4) the RKR motif is required for a novel NTD/β interaction that regulates Ca^{2+}-dependent inactivation of the channel; 5) the $Ca_V1.3$ NTD may undergo proteolysis, and can be localized in the nucleus to regulate neuronal morphology and gene transcription.

6.2 Understanding events within the Ca^{2+} channel nanodomain

In our study, we showed that the CaMKII/NTD interaction is important for excitation-transcription coupling. However, the functional consequences of this recruitment are unclear. The current model suggests that recruitment of CaMKII to the channel domain may help to facilitate CaMKIIα phosphorylation of CaMKIIγ in a trans-holoenzyme way. If this is the case, multiple docking sites are needed. β1/β2, densin, Shank3 may provide additional docking sites for CaMKIIα and/or CaMKIIγ. Whether these proteins exhibit any selectivity between CaMKIIα and CaMKIIγ remains untested. In addition, calcineurin should also be recruited to both Ca_V1.3 and Ca_V1.2 channels to dephosphorylate CaMKIIγ to expose the nuclear localization signal. Confirming the docking sites for calcineurin is also critical. We performed our experiments in the presence of β3, which does not interact with CaMKII. It will be interesting to compare the excitation-transcription coupling efficiency between β1/β2- and β3- associated L-type Ca^{2+} channels.

In addition, according to the CaMKIIγ shuttling model, one holoenzyme of CaMKIIγ can transport up to 12 Ca^{2+}/calmodulin molecules. It is unclear whether calcineurin dephosphorylation of CaMKIIγ requires that all CaMKIIγ subunits are Ca^{2+}/calmodulin-bound. If calcineurin dephosphorylates CaMKIIγ when only one or few CaMKIIγ subunits are Ca^{2+}/calmodulin-bound, shuttling of CaMKIIγ to the nucleus might be uneconomical to neurons. Another possibility is that recruitment of calcineurin to the channel and/or calcineurin dephosphorylation is slower than CaMKIIγ Thr287

phosphorylation and calmodulin trapping. Therefore, by the time CaMKIIγ embarks, CaMKIIγ is fully loaded with Ca^{2+}/calmodulin.

6.3 Visualizing channel clustering

More experiments need to be done to examine the channel clustering by CaMKII *in vitro* and its physiological significance. Ca^{2+} channels tagged with different fluorescent proteins can be transfected into neurons to visualized channel clusters in the absence or presence of CaMKII knockdown. Förster resonance energy transfer (FRET) studies can also be used to examine the effect of CaMKII on channel clustering. Since CaMKII interacts with NTDs of both $Ca_V1.2$ and $Ca_V1.3$, it is therefore possible that $Ca_V1.2$ and $Ca_V1.3$ exist in the same cluster. With different scaffold proteins of their own, the coexistence of $Ca_V1.2$ and $Ca_V1.3$ in a cluster may further facilitate the downstream signaling pathway by maximizing the potential routes. It is also important to examine the stoichiometry between the channel and CaMKII. One way to do this is to use cryo-electron microscope (cryo-EM) to directly visualize the channel/kinase complexes. Furthermore, high spatial and temporal resolution of Ca^{2+} imaging may be needed to directly examine the impact of channel clustering on Ca^{2+} nanodomain. The excitation-transcription coupling could be used as indirect readout for the signaling within L-type Ca^{2+} channel nanodomain.

6.4 Potential interplays among the RKR motif-binding proteins

Chapter II and IV showed that the RKR motif within the NTD binds CaMKII and β2a subunits, respectively. Chapter V showed that the RKR residues might be part of a nuclear localization signal. It is therefore important to test whether any of these interactions is competing with each other.

One possible competition may occur between CaMKII and the Ca^{2+} channel β2a subunit. CaMKII is highly abundant in the forebrain. However, β subunits are pre-anchored to the channel through the I-II linker. Therefore, it is possible that the NTD/CaMKII and the NTD/β interactions are dynamically regulated. Recent work from Tsien's lab showed that voltage-dependent conformational changes are important for excitation-transcription coupling. Based on our data, one hypothesis is that the β subunit may bind to the NTD at the inactive state of the channel. Activation of the channel may displace the β subunit from binding to the NTD, exposing the RKR motif to allow for CaMKII recruitment. This is consistent with the findings that voltage-dependent conformational changes are required for CaMKII recruitment. One interesting experiment is to coexpress the channel with an NTD-binding deficient β subunit to allow for constitutive exposure of the RKR motif. If the competition hypothesis is correct, recruitment of CaMKII and the subsequent CREB signaling will no longer rely on the voltage-dependent conformational changes.

6.5 *In vivo* studies of channel regulation and CREB signaling

To test the importance of the RKR motif in regulating channel functions *in vivo*, it will be desirable to generate a mouse model where the RKR motif can be mutated/removed conditionally. We can then investigate the role of the RKR motif in learning and memory.

Lastly, neurons experience and convey various patterns of stimulations to the nucleus via multiple pathways. The subsequent transcription responses could/should be very different. Using CREB phosphorylation as a readout is a powerful approach to understand the mechanism, but may be oversimplified in the context of the learning and memory behavior. Therefore, it is important to link a stimulus to a specific pattern of transcription responses and eventually to morphological and functional/behavioral changes. It will be interesting to use a series of reporters (such as *c-fos*-driven GFP) to label and isolate active neurons in a specific learning paradigm, and use RNA sequencing to identify the specific subset of genes that are affected by mutating the RKR motif.

6.6 Closing remarks

Findings presented in this dissertation highlighted the importance of the L-type Ca^{2+} channel N-terminal domain in regulating channel functions *in vitro*. Surprisingly, the RKR motif is responsible for multiple protein interactions and for potential channel clustering as well as efficient phosphorylation. These findings may provide a framework

for future studies on how L-type Ca^{2+} channels are regulated and how they mediate synaptic plasticity in mammals.

REFERENCES

Abiria, S.A., and Colbran, R.J. (2010). CaMKII associates with CaV1.2 L-type calcium channels via selected beta subunits to enhance regulatory phosphorylation. J Neurochem *112*, 150-161.

Ahlijanian, M.K., Westenbroek, R.E., and Catterall, W.A. (1990). Subunit structure and localization of dihydropyridine-sensitive calcium channels in mammalian brain, spinal cord, and retina. Neuron *4*, 819-832.

Alexander, G.E., and Crutcher, M.D. (1990). Functional architecture of basal ganglia circuits: neural substrates of parallel processing. Trends in neurosciences *13*, 266-271.

Altier, C., Dubel, S.J., Barrere, C., Jarvis, S.E., Stotz, S.C., Spaetgens, R.L., Scott, J.D., Cornet, V., De Waard, M., Zamponi, G.W.*, et al.* (2002). Trafficking of L-type calcium channels mediated by the postsynaptic scaffolding protein AKAP79. J Biol Chem *277*, 33598-33603.

Bacskai, B.J., Hochner, B., Mahaut-Smith, M., Adams, S.R., Kaang, B.K., Kandel, E.R., and Tsien, R.Y. (1993). Spatially resolved dynamics of cAMP and protein kinase A subunits in Aplysia sensory neurons. Science *260*, 222-226.

Bading, H., Ginty, D.D., and Greenberg, M.E. (1993). Regulation of gene expression in hippocampal neurons by distinct calcium signaling pathways. Science *260*, 181-186.

Barria, A., Derkach, V., and Soderling, T. (1997a). Identification of the Ca2+/calmodulin-dependent protein kinase II regulatory phosphorylation site in the alpha-amino-3-hydroxyl-5-methyl-4-isoxazole-propionate-type glutamate receptor. J Biol Chem *272*, 32727-32730.

Barria, A., and Malinow, R. (2005). NMDA receptor subunit composition controls synaptic plasticity by regulating binding to CaMKII. In Neuron (United States), pp. 289-301.

Barria, A., Muller, D., Derkach, V., Griffith, L.C., and Soderling, T.R. (1997b). Regulatory phosphorylation of AMPA-type glutamate receptors by CaM-KII during long-term potentiation. Science *276*, 2042-2045.

Baucum, A.J., 2nd, Jalan-Sakrikar, N., Jiao, Y., Gustin, R.M., Carmody, L.C., Tabb, D.L., Ham, A.J., and Colbran, R.J. (2010). Identification and validation of novel spinophilin-associated proteins in rodent striatum using an enhanced ex vivo shotgun proteomics approach. Molecular & cellular proteomics : MCP *9*, 1243-1259.

Baucum, A.J., 2nd, Shonesy, B.C., Rose, K.L., and Colbran, R.J. (2015). Quantitative proteomics analysis of CaMKII phosphorylation and the CaMKII interactome in the mouse forebrain. ACS chemical neuroscience *6*, 615-631.

Bayer, K.U., De Koninck, P., Leonard, A.S., Hell, J.W., and Schulman, H. (2001). Interaction with the NMDA receptor locks CaMKII in an active conformation. Nature *411*, 801-805.

Bayer, K.U., LeBel, E., McDonald, G.L., O'Leary, H., Schulman, H., and De Koninck, P. (2006). Transition from reversible to persistent binding of CaMKII to postsynaptic sites and NR2B. J Neurosci *26*, 1164-1174.

Ben-Ari, Y. (2002). Excitatory actions of gaba during development: the nature of the nurture. In Nat Rev Neurosci (England), pp. 728-739.

Ben-Johny, M., and Yue, D.T. (2014). Calmodulin regulation (calmodulation) of voltage-gated calcium channels. In The Journal of general physiology (United States), pp. 679-692.

Benke, T.A., Luthi, A., Isaac, J.T., and Collingridge, G.L. (1998). Modulation of AMPA receptor unitary conductance by synaptic activity. Nature *393*, 793-797.

Berridge, M.J. (1998). Neuronal calcium signaling. Neuron *21*, 13-26.

Bers, D.M. (2002). Cardiac excitation-contraction coupling. In Nature (England), pp. 198-205.

Biglan, K.M., Oakes, D., Lang, A.E., Hauser, R.A., Hodgeman, K., Greco, B., Lowell, J., Rockhill, R., Shoulson, I., Venuto, C.*, et al.* (2017). A novel design of a Phase III trial of isradipine in early Parkinson disease (STEADY-PD III). In Ann Clin Transl Neurol (United States), pp. 360-368.

Bingol, B., Wang, C.F., Arnott, D., Cheng, D., Peng, J., and Sheng, M. (2010). Autophosphorylated CaMKIIalpha acts as a scaffold to recruit proteasomes to dendritic spines. Cell *140*, 567-578.

Bito, H., Deisseroth, K., and Tsien, R.W. (1996). CREB phosphorylation and dephosphorylation: a Ca(2+)- and stimulus duration-dependent switch for hippocampal gene expression. Cell *87*, 1203-1214.

Bourtchuladze, R., Frenguelli, B., Blendy, J., Cioffi, D., Schutz, G., and Silva, A.J. (1994). Deficient long-term memory in mice with a targeted mutation of the cAMP-responsive element-binding protein. In Cell (United States), pp. 59-68.

Brameier, M., Krings, A., and MacCallum, R.M. (2007). NucPred--predicting nuclear localization of proteins. In Bioinformatics (England), pp. 1159-1160.

Branch, S.Y., Sharma, R., and Beckstead, M.J. (2014). Aging decreases L-type calcium channel currents and pacemaker firing fidelity in substantia nigra dopamine neurons. J Neurosci *34*, 9310-9318.

Brandt, A., Striessnig, J., and Moser, T. (2003). CaV1.3 channels are essential for development and presynaptic activity of cochlear inner hair cells. In J Neurosci (United States), pp. 10832-10840.

Braun, M., Ramracheya, R., Bengtsson, M., Zhang, Q., Karanauskaite, J., Partridge, C., Johnson, P.R., and Rorsman, P. (2008). Voltage-gated ion channels in human pancreatic beta-cells: electrophysiological characterization and role in insulin secretion. In Diabetes (United States), pp. 1618-1628.

Budde, T., Meuth, S., and Pape, H.C. (2002). Calcium-dependent inactivation of neuronal calcium channels. Nature Reviews Neuroscience *3*, 873-883.

Bunemann, M., Gerhardstein, B.L., Gao, T., and Hosey, M.M. (1999). Functional regulation of L-type calcium channels via protein kinase A-mediated phosphorylation of the beta(2) subunit. J Biol Chem *274*, 33851-33854.

Buraei, Z., and Yang, J. (2010). The beta subunit of voltage-gated Ca2+ channels. Physiological reviews *90*, 1461-1506.

Buraei, Z., and Yang, J. (2013). Structure and function of the beta subunit of voltage-gated Ca(2)(+) channels. Biochim Biophys Acta *1828*, 1530-1540.

Burgdorf, C.E., Schierberl, K.C., Lee, A.S., Fischer, D.K., Van Kempen, T.A., Mudragel, V., Huganir, R.L., Milner, T.A., Glass, M.J., and Rajadhyaksha, A.M. (2017). Extinction of contextual cocaine memories requires Ca_v1.2 within D1R-expressing cells and recruits hippocampal Ca_v1.2-dependent signaling mechanisms. The Journal of Neuroscience.

Calin-Jageman, I., Yu, K., Hall, R.A., Mei, L., and Lee, A. (2007). Erbin enhances voltage-dependent facilitation of Ca(v)1.3 Ca2+ channels through relief of an autoinhibitory domain in the Ca(v)1.3 alpha1 subunit. J Neurosci *27*, 1374-1385.

Carrion, A.M., Link, W.A., Ledo, F., Mellstrom, B., and Naranjo, J.R. (1999). DREAM is a Ca2+-regulated transcriptional repressor. Nature *398*, 80-84.

Catterall, W.A. (2000). Structure and regulation of voltage-gated Ca2+ channels. Annual review of cell and developmental biology *16*, 521-555.

Catterall, W.A. (2011). Voltage-gated calcium channels. Cold Spring Harbor perspectives in biology *3*, a003947.

Chan, C.S., Guzman, J.N., Ilijic, E., Mercer, J.N., Rick, C., Tkatch, T., Meredith, G.E., and Surmeier, D.J. (2007). 'Rejuvenation' protects neurons in mouse models of Parkinson's disease. Nature *447*, 1081-1086.

Chang, B.H., Mukherji, S., and Soderling, T.R. (1998). Characterization of a calmodulin kinase II inhibitor protein in brain. Proc Natl Acad Sci U S A *95*, 10890-10895.

Chao, L.H., Stratton, M.M., Lee, I.H., Rosenberg, O.S., Levitz, J., Mandell, D.J., Kortemme, T., Groves, J.T., Schulman, H., and Kuriyan, J. (2011). A mechanism for tunable autoinhibition in the structure of a human Ca2+/calmodulin- dependent kinase II holoenzyme. Cell *146*, 732-745.

Chen, Y.H., He, L.L., Buchanan, D.R., Zhang, Y., Fitzmaurice, A., and Yang, J. (2009). Functional dissection of the intramolecular Src homology 3-guanylate kinase domain coupling in voltage-gated Ca2+ channel beta-subunits. FEBS Lett *583*, 1969-1975.

Chen, Y.H., Li, M.H., Zhang, Y., He, L.L., Yamada, Y., Fitzmaurice, A., Shen, Y., Zhang, H., Tong, L., and Yang, J. (2004). Structural basis of the alpha1-beta subunit interaction of voltage-gated Ca2+ channels. Nature *429*, 675-680.

Chien, A.J., Carr, K.M., Shirokov, R.E., Rios, E., and Hosey, M.M. (1996). Identification of palmitoylation sites within the L-type calcium channel beta2a subunit and effects on channel function. J Biol Chem *271*, 26465-26468.

Chrivia, J.C., Kwok, R.P., Lamb, N., Hagiwara, M., Montminy, M.R., and Goodman, R.H. (1993). Phosphorylated CREB binds specifically to the nuclear protein CBP. Nature *365*, 855-859.

Clapham, D.E. (2003). TRP channels as cellular sensors. In Nature (England), pp. 517-524.

Clapham, D.E. (2007). Calcium signaling. In Cell (United States), pp. 1047-1058.

Cohen, S.M., Ma, H., Kuchibhotla, K.V., Watson, B.O., Buzsaki, G., Froemke, R.C., and Tsien, R.W. (2016). Excitation-Transcription Coupling in Parvalbumin-Positive Interneurons Employs a Novel CaM Kinase-Dependent Pathway Distinct from Excitatory Neurons. Neuron *90*, 292-307.

Colbran, R.J., and Brown, A.M. (2004). Calcium/calmodulin-dependent protein kinase II and synaptic plasticity. Curr Opin Neurobiol *14*, 318-327.

Colbran, R.J., and Soderling, T.R. (1990). Calcium/calmodulin-independent autophosphorylation sites of calcium/calmodulin-dependent protein kinase II. Studies on the effect of phosphorylation of threonine 305/306 and serine 314 on calmodulin binding using synthetic peptides. J Biol Chem *265*, 11213-11219.

Collingridge, G.L., Kehl, S.J., and McLennan, H. (1983). Excitatory amino acids in synaptic transmission in the Schaffer collateral-commissural pathway of the rat hippocampus. The Journal of physiology *334*, 33-46.

Coste, B., Mathur, J., Schmidt, M., Earley, T.J., Ranade, S., Petrus, M.J., Dubin, A.E., and Patapoutian, A. (2010). Piezo1 and Piezo2 are essential components of distinct mechanically activated cation channels. In Science (United States), pp. 55-60.

Cui, G., Jun, S.B., Jin, X., Pham, M.D., Vogel, S.S., Lovinger, D.M., and Costa, R.M. (2013). Concurrent activation of striatal direct and indirect pathways during action initiation. In Nature (England), pp. 238-242.

Da Silva, W.C., Cardoso, G., Bonini, J.S., Benetti, F., and Izquierdo, I. (2013). Memory reconsolidation and its maintenance depend on L-voltage-dependent calcium channels and CaMKII functions regulating protein turnover in the hippocampus. In Proc Natl Acad Sci U S A (United States), pp. 6566-6570.

Dash, P.K., Hochner, B., and Kandel, E.R. (1990). Injection of the cAMP-responsive element into the nucleus of Aplysia sensory neurons blocks long-term facilitation. Nature *345*, 718-721.

Davis, H.P., and Squire, L.R. (1984). Protein synthesis and memory: a review. Psychol Bull *96*, 518-559.

Dayan, E., and Cohen, L.G. (2011). Neuroplasticity subserving motor skill learning. In Neuron (United States), pp. 443-454.

De Jongh, K.S., Colvin, A.A., Wang, K.K., and Catterall, W.A. (1994). Differential proteolysis of the full-length form of the L-type calcium channel alpha 1 subunit by calpain. J Neurochem *63*, 1558-1564.

De Jongh, K.S., Murphy, B.J., Colvin, A.A., Hell, J.W., Takahashi, M., and Catterall, W.A. (1996). Specific phosphorylation of a site in the full-length form of the alpha 1 subunit of the cardiac L-type calcium channel by adenosine 3',5'-cyclic monophosphate-dependent protein kinase. In Biochemistry (United States), pp. 10392-10402.

De Rubeis, S., He, X., Goldberg, A.P., Poultney, C.S., Samocha, K., Cicek, A.E., Kou, Y., Liu, L., Fromer, M., Walker, S.*, et al.* (2014). Synaptic, transcriptional and chromatin genes disrupted in autism. Nature *515*, 209-215.

Deisseroth, K., Bito, H., and Tsien, R.W. (1996). Signaling from synapse to nucleus: postsynaptic CREB phosphorylation during multiple forms of hippocampal synaptic plasticity. Neuron *16*, 89-101.

Deisseroth, K., Heist, E.K., and Tsien, R.W. (1998). Translocation of calmodulin to the nucleus supports CREB phosphorylation in hippocampal neurons. Nature *392*, 198-202.

Deisseroth, K., Mermelstein, P.G., Xia, H., and Tsien, R.W. (2003). Signaling from synapse to nucleus: the logic behind the mechanisms. Curr Opin Neurobiol *13*, 354-365.

Dick, I.E., Tadross, M.R., Liang, H., Tay, L.H., Yang, W., and Yue, D.T. (2008). A modular switch for spatial Ca2+ selectivity in the calmodulin regulation of CaV channels. Nature *451*, 830-834.

Diering, G.H., Heo, S., Hussain, N.K., Liu, B., and Huganir, R.L. (2016). Extensive phosphorylation of AMPA receptors in neurons. In Proc Natl Acad Sci U S A (United States), pp. E4920-4927.

Dittgen, T., Nimmerjahn, A., Komai, S., Licznerski, P., Waters, J., Margrie, T.W., Helmchen, F., Denk, W., Brecht, M., and Osten, P. (2004). Lentivirus-based genetic manipulations of cortical neurons and their optical and electrophysiological monitoring in vivo. Proc Natl Acad Sci U S A *101*, 18206-18211.

Dittmer, P.J., Dell'Acqua, M.L., and Sather, W.A. (2014). Ca2+/calcineurin-dependent inactivation of neuronal L-type Ca2+ channels requires priming by AKAP-anchored protein kinase A. Cell reports *7*, 1410-1416.

Dixon, R.E., Moreno, C.M., Yuan, C., Opitz-Araya, X., Binder, M.D., Navedo, M.F., and Santana, L.F. (2015). Graded Ca(2)(+)/calmodulin-dependent coupling of voltage-gated CaV1.2 channels. eLife *4*.

Dixon, R.E., Yuan, C., Cheng, E.P., Navedo, M.F., and Santana, L.F. (2012). Ca2+ signaling amplification by oligomerization of L-type Cav1.2 channels. In Proc Natl Acad Sci U S A (United States), pp. 1749-1754.

Dolmetsch, R.E., Pajvani, U., Fife, K., Spotts, J.M., and Greenberg, M.E. (2001). Signaling to the nucleus by an L-type calcium channel-calmodulin complex through the MAP kinase pathway. Science *294*, 333-339.

Elgersma, Y., Fedorov, N.B., Ikonen, S., Choi, E.S., Elgersma, M., Carvalho, O.M., Giese, K.P., and Silva, A.J. (2002). Inhibitory autophosphorylation of CaMKII controls PSD association, plasticity, and learning. In Neuron (United States), pp. 493-505.

Erondu, N.E., and Kennedy, M.B. (1985). Regional distribution of type II Ca2+/calmodulin-dependent protein kinase in rat brain. J Neurosci *5*, 3270-3277.

Ertel, E.A., Campbell, K.P., Harpold, M.M., Hofmann, F., Mori, Y., Perez-Reyes, E., Schwartz, A., Snutch, T.P., Tanabe, T., Birnbaumer, L.*, et al.* (2000). Nomenclature of voltage-gated calcium channels. Neuron *25*, 533-535.

Fallon, J.L., Baker, M.R., Xiong, L., Loy, R.E., Yang, G., Dirksen, R.T., Hamilton, S.L., and Quiocho, F.A. (2009). Crystal structure of dimeric cardiac L-type calcium channel regulatory domains bridged by Ca2+* calmodulins. Proc Natl Acad Sci U S A *106*, 5135-5140.

Flavell, S.W., and Greenberg, M.E. (2008). Signaling mechanisms linking neuronal activity to gene expression and plasticity of the nervous system. Annual review of neuroscience *31*, 563-590.

Flexner, J.B., Flexner, L.B., and Stellar, E. (1963). Memory in mice as affected by intracerebral puromycin. Science *141*, 57-59.

Fuller, M.D., Emrick, M.A., Sadilek, M., Scheuer, T., and Catterall, W.A. (2010). Molecular mechanism of calcium channel regulation in the fight-or-flight response. In Sci Signal (United States), p. ra70.

Gao, L., Blair, L.A., Salinas, G.D., Needleman, L.A., and Marshall, J. (2006). Insulin-like growth factor-1 modulation of CaV1.3 calcium channels depends on Ca2+ release from IP3-sensitive stores and calcium/calmodulin kinase II phosphorylation of the alpha1 subunit EF hand. J Neurosci *26*, 6259-6268.

Gao, T., Yatani, A., Dell'Acqua, M.L., Sako, H., Green, S.A., Dascal, N., Scott, J.D., and Hosey, M.M. (1997). cAMP-dependent regulation of cardiac L-type Ca2+ channels requires membrane targeting of PKA and phosphorylation of channel subunits. Neuron *19*, 185-196.

Giese, K.P., Fedorov, N.B., Filipkowski, R.K., and Silva, A.J. (1998). Autophosphorylation at Thr286 of the alpha calcium-calmodulin kinase II in LTP and learning. Science *279*, 870-873.

Giordano, T.P., Tropea, T.F., Satpute, S.S., Sinnegger-Brauns, M.J., Striessnig, J., Kosofsky, B.E., and Rajadhyaksha, A.M. (2010). Molecular switch from L-type Ca v 1.3 to Ca v 1.2 Ca2+ channel signaling underlies long-term psychostimulant-induced behavioral and molecular plasticity. In J Neurosci (United States), pp. 17051-17062.

Gomez-Ospina, N., Tsuruta, F., Barreto-Chang, O., Hu, L., and Dolmetsch, R. (2006). The C terminus of the L-type voltage-gated calcium channel Ca(V)1.2 encodes a transcription factor. Cell *127*, 591-606.

Gonzalez, G.A., Yamamoto, K.K., Fischer, W.H., Karr, D., Menzel, P., Biggs, W., 3rd, Vale, W.W., and Montminy, M.R. (1989). A cluster of phosphorylation sites on the cyclic AMP-regulated nuclear factor CREB predicted by its sequence. Nature *337*, 749-752.

Graef, I.A., Mermelstein, P.G., Stankunas, K., Neilson, J.R., Deisseroth, K., Tsien, R.W., and Crabtree, G.R. (1999). L-type calcium channels and GSK-3 regulate the activity of NF-ATc4 in hippocampal neurons. Nature *401*, 703-708.

Granger, A.J., Shi, Y., Lu, W., Cerpas, M., and Nicoll, R.A. (2013). LTP requires a reserve pool of glutamate receptors independent of subunit type. In Nature (England), pp. 495-500.

Grover, L.M., and Teyler, T.J. (1990). Two components of long-term potentiation induced by different patterns of afferent activation. Nature *347*, 477-479.

Grueter, C.E., Abiria, S.A., Wu, Y., Anderson, M.E., and Colbran, R.J. (2008). Differential regulated interactions of calcium/calmodulin-dependent protein kinase II with isoforms of voltage-gated calcium channel beta subunits. Biochemistry *47*, 1760-1767.

Guzman, J.N., Sanchez-Padilla, J., Chan, C.S., and Surmeier, D.J. (2009). Robust pacemaking in substantia nigra dopaminergic neurons. In J Neurosci (United States), pp. 11011-11019.

Haeseleer, F., Imanishi, Y., Maeda, T., Possin, D.E., Maeda, A., Lee, A., Rieke, F., and Palczewski, K. (2004). Essential role of Ca2+-binding protein 4, a Cav1.4 channel regulator, in photoreceptor synaptic function. Nat Neurosci *7*, 1079-1087.

Haeseleer, F., Sokal, I., Verlinde, C.L., Erdjument-Bromage, H., Tempst, P., Pronin, A.N., Benovic, J.L., Fariss, R.N., and Palczewski, K. (2000). Five members of a novel Ca(2+)-binding protein (CABP) subfamily with similarity to calmodulin. J Biol Chem *275*, 1247-1260.

Hall, D.D., Davare, M.A., Shi, M., Allen, M.L., Weisenhaus, M., McKnight, G.S., and Hell, J.W. (2007). Critical role of cAMP-dependent protein kinase anchoring to the L-type calcium channel Cav1.2 via A-kinase anchor protein 150 in neurons. Biochemistry *46*, 1635-1646.

Halt, A.R., Dallapiazza, R.F., Zhou, Y., Stein, I.S., Qian, H., Juntti, S., Wojcik, S., Brose, N., Silva, A.J., and Hell, J.W. (2012). CaMKII binding to GluN2B is critical during memory consolidation. The EMBO journal *31*, 1203-1216.

Hanson, P.I., Meyer, T., Stryer, L., and Schulman, H. (1994). Dual role of calmodulin in autophosphorylation of multifunctional CaM kinase may underlie decoding of calcium signals. Neuron *12*, 943-956.

Hanson, P.I., and Schulman, H. (1992). Inhibitory autophosphorylation of multifunctional Ca2+/calmodulin-dependent protein kinase analyzed by site-directed mutagenesis. J Biol Chem *267*, 17216-17224.

Hardingham, G.E., Arnold, F.J., and Bading, H. (2001). Nuclear calcium signaling controls CREB-mediated gene expression triggered by synaptic activity. In Nat Neurosci (United States), pp. 261-267.

Hardingham, G.E., Chawla, S., Cruzalegui, F.H., and Bading, H. (1999). Control of recruitment and transcription-activating function of CBP determines gene regulation by NMDA receptors and L-type calcium channels. In Neuron (United States), pp. 789-798.

He, L.L., Zhang, Y., Chen, Y.H., Yamada, Y., and Yang, J. (2007). Functional modularity of the beta-subunit of voltage-gated Ca2+ channels. In Biophys J (United States), pp. 834-845.

He, M., Bodi, I., Mikala, G., and Schwartz, A. (1997). Motif III S5 of L-type calcium channels is involved in the dihydropyridine binding site. A combined radioligand binding and electrophysiological study. J Biol Chem *272*, 2629-2633.

Heikkila, E., Ristola, M., Endlich, K., Lehtonen, S., Lassila, M., Havana, M., Endlich, N., Holthofer, H., and Addnet, C. (2007). Densin and beta-catenin form a complex and co-localize in cultured podocyte cell junctions. Mol Cell Biochem *305*, 9-18.

Hell, J.W., Westenbroek, R.E., Breeze, L.J., Wang, K.K., Chavkin, C., and Catterall, W.A. (1996). N-methyl-D-aspartate receptor-induced proteolytic conversion of postsynaptic class C L-type calcium channels in hippocampal neurons. Proc Natl Acad Sci U S A *93*, 3362-3367.

Herlitze, S., Garcia, D.E., Mackie, K., Hille, B., Scheuer, T., and Catterall, W.A. (1996). Modulation of Ca2+ channels by G-protein beta gamma subunits. Nature *380*, 258-262.

Herring, B.E., and Nicoll, R.A. (2016). Long-Term Potentiation: From CaMKII to AMPA Receptor Trafficking. Annual review of physiology *78*, 351-365.

Hetzenauer, A., Sinnegger-Brauns, M.J., Striessnig, J., and Singewald, N. (2006). Brain activation pattern induced by stimulation of L-type Ca2+-channels: contribution of Ca(V)1.3 and Ca(V)1.2 isoforms. In Neuroscience (United States), pp. 1005-1015.

Hofmann, F., Biel, M., and Flockerzi, V. (1994). Molecular basis for Ca2+ channel diversity. Annual review of neuroscience *17*, 399-418.

Hollmann, M., Hartley, M., and Heinemann, S. (1991). Ca2+ permeability of KA-AMPA--gated glutamate receptor channels depends on subunit composition. Science *252*, 851-853.

Hosokawa, T., Mitsushima, D., Kaneko, R., and Hayashi, Y. (2015). Stoichiometry and phosphoisotypes of hippocampal AMPA-type glutamate receptor phosphorylation. Neuron *85*, 60-67.

Huang, H., Tan, B.Z., Shen, Y., Tao, J., Jiang, F., Sung, Y.Y., Ng, C.K., Raida, M., Kohr, G., Higuchi, M.*, et al.* (2012). RNA editing of the IQ domain in Ca(v)1.3 channels modulates their Ca(2)(+)-dependent inactivation. Neuron *73*, 304-316.

Hudmon, A., and Schulman, H. (2002). Neuronal Ca2+/calmodulin-dependent protein kinase II: the role of structure and autoregulation in cellular function. Annual review of biochemistry *71*, 473-510.

Hudmon, A., Schulman, H., Kim, J., Maltez, J.M., Tsien, R.W., and Pitt, G.S. (2005). CaMKII tethers to L-type Ca2+ channels, establishing a local and dedicated integrator of Ca2+ signals for facilitation. The Journal of cell biology *171*, 537-547.

Huganir, R.L., and Nicoll, R.A. (2013). AMPARs and synaptic plasticity: the last 25 years. In Neuron (United States), pp. 704-717.

Hulme, J.T., Lin, T.W., Westenbroek, R.E., Scheuer, T., and Catterall, W.A. (2003). Beta-adrenergic regulation requires direct anchoring of PKA to cardiac CaV1.2 channels via a leucine zipper interaction with A kinase-anchoring protein 15. In Proc Natl Acad Sci U S A (United States), pp. 13093-13098.

Hurley, M.J., Brandon, B., Gentleman, S.M., and Dexter, D.T. (2013). Parkinson's disease is associated with altered expression of CaV1 channels and calcium-binding proteins. In Brain (England), pp. 2077-2097.

Ikeda, S.R. (1996). Voltage-dependent modulation of N-type calcium channels by G-protein beta gamma subunits. Nature *380*, 255-258.

Iossifov, I., O'Roak, B.J., Sanders, S.J., Ronemus, M., Krumm, N., Levy, D., Stessman, H.A., Witherspoon, K.T., Vives, L., Patterson, K.E.*, et al.* (2014). The contribution of de novo coding mutations to autism spectrum disorder. In Nature (England), pp. 216-221.

Izawa, I., Nishizawa, M., Ohtakara, K., and Inagaki, M. (2002). Densin-180 interacts with delta-catenin/neural plakophilin-related armadillo repeat protein at synapses. In J Biol Chem (United States), pp. 5345-5350.

Jenkins, M.A., Christel, C.J., Jiao, Y., Abiria, S., Kim, K.Y., Usachev, Y.M., Obermair, G.J., Colbran, R.J., and Lee, A. (2010). Ca2+-dependent facilitation of Cav1.3 Ca2+ channels by densin and Ca2+/calmodulin-dependent protein kinase II. J Neurosci *30*, 5125-5135.

Jiao, Y., Jalan-Sakrikar, N., Robison, A.J., Baucum, A.J., 2nd, Bass, M.A., and Colbran, R.J. (2011). Characterization of a central Ca2+/calmodulin-dependent protein kinase IIalpha/beta binding domain in densin that selectively modulates glutamate receptor subunit phosphorylation. J Biol Chem *286*, 24806-24818.

Jin, D.Z., Guo, M.L., Xue, B., Fibuch, E.E., Choe, E.S., Mao, L.M., and Wang, J.Q. (2013a). Phosphorylation and feedback regulation of metabotropic glutamate receptor 1 by calcium/calmodulin-dependent protein kinase II. J Neurosci *33*, 3402-3412.

Jin, D.Z., Guo, M.L., Xue, B., Mao, L.M., and Wang, J.Q. (2013b). Differential regulation of CaMKIIalpha interactions with mGluR5 and NMDA receptors by Ca(2+) in neurons. J Neurochem *127*, 620-631.

Johny, M.B., Yang, P.S., Bazzazi, H., and Yue, D.T. (2013). Dynamic switching of calmodulin interactions underlies Ca(2+) regulation of CaV1.3 channels. Nat Commun *4*, 1717.

Jones, B.W., Brunet, S., Gilbert, M.L., Nichols, C.B., Su, T., Westenbroek, R.E., Scott, J.D., Catterall, W.A., and McKnight, G.S. (2012). Cardiomyocytes from AKAP7 knockout

mice respond normally to adrenergic stimulation. In Proc Natl Acad Sci U S A (United States), pp. 17099-17104.

Kalkhoven, E. (2004). CBP and p300: HATs for different occasions. In Biochem Pharmacol (England), pp. 1145-1155.

Kandel, E.R., Schwartz, J.H., Jessell, T.M., Siegelbaum, S.A., and Hudspeth, A.J. (2000). Principles of neural science, Vol 4 (McGraw-hill New York).

Keegan, L.P., Gallo, A., and O'Connell, M.A. (2001). The many roles of an RNA editor. In Nature reviews Genetics (England), pp. 869-878.

Kim, J.H., Lee, S.R., Li, L.H., Park, H.J., Park, J.H., Lee, K.Y., Kim, M.K., Shin, B.A., and Choi, S.Y. (2011). High cleavage efficiency of a 2A peptide derived from porcine teschovirus-1 in human cell lines, zebrafish and mice. PloS one *6*, e18556.

Kim, K., Lakhanpal, G., Lu, H.E., Khan, M., Suzuki, A., Hayashi, M.K., Narayanan, R., Luyben, T.T., Matsuda, T., Nagai, T.*, et al.* (2015). A Temporary Gating of Actin Remodeling during Synaptic Plasticity Consists of the Interplay between the Kinase and Structural Functions of CaMKII. Neuron *87*, 813-826.

Koval, O.M., Guan, X., Wu, Y., Joiner, M.L., Gao, Z., Chen, B., Grumbach, I.M., Luczak, E.D., Colbran, R.J., Song, L.S.*, et al.* (2010). CaV1.2 beta-subunit coordinates CaMKII-triggered cardiomyocyte death and afterdepolarizations. Proc Natl Acad Sci U S A *107*, 4996-5000.

Lacerda, A.E., Rampe, D., and Brown, A.M. (1988). Effects of protein kinase C activators on cardiac Ca2+ channels. Nature *335*, 249-251.

Lee, T.S., Karl, R., Moosmang, S., Lenhardt, P., Klugbauer, N., Hofmann, F., Kleppisch, T., and Welling, A. (2006). Calmodulin kinase II is involved in voltage-dependent facilitation of the L-type Cav1.2 calcium channel: Identification of the phosphorylation sites. J Biol Chem *281*, 25560-25567.

Li, B., Tadross, M.R., and Tsien, R.W. (2016). Sequential ionic and conformational signaling by calcium channels drives neuronal gene expression. Science *351*, 863-867.

Li, M.Z., and Elledge, S.J. (2007). Harnessing homologous recombination in vitro to generate recombinant DNA via SLIC. Nature methods *4*, 251-256.

Liang, Y., and Tavalin, S.J. (2007). Auxiliary beta subunits differentially determine pka utilization of distinct regulatory sites on Cav1.3 L type Ca2+ channels. In Channels (Austin) (United States), pp. 102-112.

Lisman, J., Yasuda, R., and Raghavachari, S. (2012). Mechanisms of CaMKII action in long-term potentiation. Nat Rev Neurosci *13*, 169-182.

Liu, H., and Naismith, J.H. (2008). An efficient one-step site-directed deletion, insertion, single and multiple-site plasmid mutagenesis protocol. BMC biotechnology *8*, 91.

Liu, X., Kerov, V., Haeseleer, F., Majumder, A., Artemyev, N., Baker, S.A., and Lee, A. (2013). Dysregulation of Ca(v)1.4 channels disrupts the maturation of photoreceptor synaptic ribbons in congenital stationary night blindness type 2. In Channels (Austin) (United States), pp. 514-523.

Ludwig, A., Flockerzi, V., and Hofmann, F. (1997). Regional expression and cellular localization of the alpha1 and beta subunit of high voltage-activated calcium channels in rat brain. J Neurosci *17*, 1339-1349.

Ma, H., Cohen, S., Li, B., and Tsien, R.W. (2013). Exploring the dominant role of Cav1 channels in signalling to the nucleus. Bioscience reports *33*, 97-101.

Ma, H., Groth, R.D., Cohen, S.M., Emery, J.F., Li, B., Hoedt, E., Zhang, G., Neubert, T.A., and Tsien, R.W. (2014). gammaCaMKII Shuttles Ca(2+)/CaM to the Nucleus to Trigger CREB Phosphorylation and Gene Expression. Cell *159*, 281-294.

Malenka, R.C., and Nicoll, R.A. (1999). Long-term potentiation--a decade of progress? In Science (United States), pp. 1870-1874.

Mathur, B.N., and Lovinger, D.M. (2012). Endocannabinoid-dopamine interactions in striatal synaptic plasticity. Frontiers in pharmacology *3*, 66.

Mayer, M.L., Westbrook, G.L., and Guthrie, P.B. (1984). Voltage-dependent block by Mg2+ of NMDA responses in spinal cord neurones. Nature *309*, 261-263.

McHugh, D., Sharp, E.M., Scheuer, T., and Catterall, W.A. (2000). Inhibition of cardiac L-type calcium channels by protein kinase C phosphorylation of two sites in the N-terminal domain. In Proc Natl Acad Sci U S A (United States), pp. 12334-12338.

McNeill, R.B., and Colbran, R.J. (1995). Interaction of autophosphorylated Ca2+/calmodulin-dependent protein kinase II with neuronal cytoskeletal proteins. Characterization of binding to a 190-kDa postsynaptic density protein. J Biol Chem *270*, 10043-10049.

Michailidis, I.E., Abele-Henckels, K., Zhang, W.K., Lin, B., Yu, Y., Geyman, L.S., Ehlers, M.D., Pnevmatikakis, E.A., and Yang, J. (2014). Age-related homeostatic midchannel proteolysis of neuronal L-type voltage-gated Ca(2)(+) channels. Neuron *82*, 1045-1057.

Michel, J.J., and Scott, J.D. (2002). AKAP mediated signal transduction. In Annual review of pharmacology and toxicology (United States), pp. 235-257.

Monteiro, P., and Feng, G. (2017). SHANK proteins: roles at the synapse and in autism spectrum disorder. In Nat Rev Neurosci (England), pp. 147-157.

Moreno, C.M., Dixon, R.E., Tajada, S., Yuan, C., Opitz-Araya, X., Binder, M.D., and Santana, L.F. (2016). Ca(2+) entry into neurons is facilitated by cooperative gating of clustered CaV1.3 channels. eLife *5*.

Morgan, S.L., and Teyler, T.J. (1999). VDCCs and NMDARs underlie two forms of LTP in CA1 hippocampus in vivo. J Neurophysiol *82*, 736-740.

Morris, R.G. (2013). NMDA receptors and memory encoding. In Neuropharmacology (England), pp. 32-40.

Mukherji, S., and Soderling, T.R. (1994). Regulation of Ca2+/calmodulin-dependent protein kinase II by inter- and intrasubunit-catalyzed autophosphorylations. J Biol Chem *269*, 13744-13747.

Murakoshi, H., Shin, M.E., Parra-Bueno, P., Szatmari, E.M., Shibata, A.C., and Yasuda, R. (2017). Kinetics of Endogenous CaMKII Required for Synaptic Plasticity Revealed by Optogenetic Kinase Inhibitor. In Neuron (United States), pp. 37-47 e35.

Murphy, J.G., Sanderson, J.L., Gorski, J.A., Scott, J.D., Catterall, W.A., Sather, W.A., and Dell'Acqua, M.L. (2014). AKAP-anchored PKA maintains neuronal L-type calcium channel activity and NFAT transcriptional signaling. Cell reports *7*, 1577-1588.

Naisbitt, S., Kim, E., Tu, J.C., Xiao, B., Sala, C., Valtschanoff, J., Weinberg, R.J., Worley, P.F., and Sheng, M. (1999). Shank, a novel family of postsynaptic density proteins that binds to the NMDA receptor/PSD-95/GKAP complex and cortactin. In Neuron (United States), pp. 569-582.

Nowak, L., Bregestovski, P., Ascher, P., Herbet, A., and Prochiantz, A. (1984). Magnesium gates glutamate-activated channels in mouse central neurones. Nature *307*, 462-465.

Nowycky, M.C., Fox, A.P., and Tsien, R.W. (1985). Three types of neuronal calcium channel with different calcium agonist sensitivity. Nature *316*, 440-443.

Obermair, G.J., Schlick, B., Di Biase, V., Subramanyam, P., Gebhart, M., Baumgartner, S., and Flucher, B.E. (2010). Reciprocal interactions regulate targeting of calcium channel beta subunits and membrane expression of alpha1 subunits in cultured hippocampal neurons. J Biol Chem *285*, 5776-5791.

Ohtakara, K., Nishizawa, M., Izawa, I., Hata, Y., Matsushima, S., Taki, W., Inada, H., Takai, Y., and Inagaki, M. (2002). Densin-180, a synaptic protein, links to PSD-95 through its direct interaction with MAGUIN-1. In Genes Cells (England), pp. 1149-1160.

Oliveria, S.F., Dell'Acqua, M.L., and Sather, W.A. (2007). AKAP79/150 anchoring of calcineurin controls neuronal L-type Ca2+ channel activity and nuclear signaling. Neuron *55*, 261-275.

Olson, P.A., Tkatch, T., Hernandez-Lopez, S., Ulrich, S., Ilijic, E., Mugnaini, E., Zhang, H., Bezprozvanny, I., and Surmeier, D.J. (2005). G-protein-coupled receptor modulation of striatal CaV1.3 L-type Ca2+ channels is dependent on a Shank-binding domain. J Neurosci *25*, 1050-1062.

Omkumar, R.V., Kiely, M.J., Rosenstein, A.J., Min, K.T., and Kennedy, M.B. (1996). Identification of a phosphorylation site for calcium/calmodulindependent protein kinase II in the NR2B subunit of the N-methyl-D-aspartate receptor. J Biol Chem *271*, 31670-31678.

Oz, S., Tsemakhovich, V., Christel, C.J., Lee, A., and Dascal, N. (2011). CaBP1 regulates voltage-dependent inactivation and activation of Ca(V)1.2 (L-type) calcium channels. J Biol Chem *286*, 13945-13953.

Paoletti, P., Bellone, C., and Zhou, Q. (2013). NMDA receptor subunit diversity: impact on receptor properties, synaptic plasticity and disease. In Nat Rev Neurosci (England), pp. 383-400.

Parkinson Study, G. (2013). Phase II safety, tolerability, and dose selection study of isradipine as a potential disease-modifying intervention in early Parkinson's disease (STEADY-PD). Mov Disord *28*, 1823-1831.

Perfitt, T.L., Wang, X., Nakagawa, T., and Colbran, R.J. (2017). Direct interaction between postsynaptic proteins Shank3 and CaMKII. Neuroscience Meeting Planner

Washington, DC: Society for Neuroscience, *Program No. 658.12 / D37*.

Peterson, B.Z., DeMaria, C.D., Adelman, J.P., and Yue, D.T. (1999). Calmodulin is the Ca2+ sensor for Ca2+ -dependent inactivation of L-type calcium channels. Neuron *22*, 549-558.

Pinggera, A., Lieb, A., Benedetti, B., Lampert, M., Monteleone, S., Liedl, K.R., Tuluc, P., and Striessnig, J. (2014). CACNA1D De Novo Mutations in Autism Spectrum Disorders Activate Cav1.3 L-Type Calcium Channels. Biological psychiatry.

Pinggera, A., and Striessnig, J. (2016). Cav 1.3 (CACNA1D) L-type Ca2+ channel dysfunction in CNS disorders. The Journal of physiology *594*, 5839-5849.

Platzer, J., Engel, J., Schrott-Fischer, A., Stephan, K., Bova, S., Chen, H., Zheng, H., and Striessnig, J. (2000). Congenital deafness and sinoatrial node dysfunction in mice lacking class D L-type Ca2+ channels. Cell *102*, 89-97.

Pragnell, M., De Waard, M., Mori, Y., Tanabe, T., Snutch, T.P., and Campbell, K.P. (1994). Calcium channel beta-subunit binds to a conserved motif in the I-II cytoplasmic linker of the alpha 1-subunit. Nature *368*, 67-70.

Putzier, I., Kullmann, P.H., Horn, J.P., and Levitan, E.S. (2009). Cav1.3 channel voltage dependence, not Ca2+ selectivity, drives pacemaker activity and amplifies bursts in nigral dopamine neurons. In J Neurosci (United States), pp. 15414-15419.

Qian, H., Patriarchi, T., Price, J.L., Matt, L., Lee, B., Nieves-Cintron, M., Buonarati, O.R., Chowdhury, D., Nanou, E., Nystoriak, M.A.*, et al.* (2017). Phosphorylation of Ser1928 mediates the enhanced activity of the L-type Ca2+ channel Cav1.2 by the beta2-adrenergic receptor in neurons. In Sci Signal (United States).

Qin, N., Platano, D., Olcese, R., Costantin, J.L., Stefani, E., and Birnbaumer, L. (1998). Unique regulatory properties of the type 2a Ca2+ channel beta subunit caused by palmitoylation. Proc Natl Acad Sci U S A *95*, 4690-4695.

Randall, A., and Tsien, R.W. (1995). Pharmacological dissection of multiple types of Ca2+ channel currents in rat cerebellar granule neurons. J Neurosci *15*, 2995-3012.

Rellos, P., Pike, A.C., Niesen, F.H., Salah, E., Lee, W.H., von Delft, F., and Knapp, S. (2010). Structure of the CaMKIIdelta/calmodulin complex reveals the molecular mechanism of CaMKII kinase activation. PLoS biology *8*, e1000426.

Reuter, H. (1967). The dependence of slow inward current in Purkinje fibres on the extracellular calcium-concentration. The Journal of physiology *192*, 479-492.

Reuter, H., and Scholz, H. (1977). The regulation of the calcium conductance of cardiac muscle by adrenaline. The Journal of physiology *264*, 49-62.

Rich, M.T., Abbott, T.B., Chung, L., Gulcicek, E.E., Stone, K.L., Colangelo, C.M., Lam, T.T., Nairn, A.C., Taylor, J.R., and Torregrossa, M.M. (2016). Phosphoproteomic Analysis Reveals a Novel Mechanism of CaMKIIα Regulation Inversely Induced by Cocaine Memory Extinction versus Reconsolidation. The Journal of Neuroscience *36*, 7613-7627.

Rivera, C., Voipio, J., Payne, J.A., Ruusuvuori, E., Lahtinen, H., Lamsa, K., Pirvola, U., Saarma, M., and Kaila, K. (1999). The K+/Cl- co-transporter KCC2 renders GABA hyperpolarizing during neuronal maturation. Nature *397*, 251-255.

Robison, A.J., Bass, M.A., Jiao, Y., MacMillan, L.B., Carmody, L.C., Bartlett, R.K., and Colbran, R.J. (2005). Multivalent interactions of calcium/calmodulin-dependent protein kinase II with the postsynaptic density proteins NR2B, densin-180, and alpha-actinin-2. J Biol Chem *280*, 35329-35336.

Robitaille, R., Adler, E.M., and Charlton, M.P. (1990). Strategic location of calcium channels at transmitter release sites of frog neuromuscular synapses. In Neuron (United States), pp. 773-779.

Roche, K.W., O'Brien, R.J., Mammen, A.L., Bernhardt, J., and Huganir, R.L. (1996). Characterization of multiple phosphorylation sites on the AMPA receptor GluR1 subunit. In Neuron (United States), pp. 1179-1188.

Sala, C., Futai, K., Yamamoto, K., Worley, P.F., Hayashi, Y., and Sheng, M. (2003). Inhibition of dendritic spine morphogenesis and synaptic transmission by activity-inducible protein Homer1a. J Neurosci *23*, 6327-6337.

Sandoval, A., Duran, P., Gandini, M.A., Andrade, A., Almanza, A., Kaja, S., and Felix, R. (2017). Regulation of L-type CaV1.3 channel activity and insulin secretion by the cGMP-PKG signaling pathway. In Cell Calcium (Netherlands), pp. 1-9.

Schmid, A., Renaud, J.F., and Lazdunski, M. (1985). Short term and long term effects of beta-adrenergic effectors and cyclic AMP on nitrendipine-sensitive voltage-dependent Ca2+ channels of skeletal muscle. J Biol Chem *260*, 13041-13046.

Scott, J.D., Dessauer, C.W., and Tasken, K. (2013). Creating order from chaos: cellular regulation by kinase anchoring. Annual review of pharmacology and toxicology *53*, 187-210.

Sculptoreanu, A., Rotman, E., Takahashi, M., Scheuer, T., and Catterall, W.A. (1993a). Voltage-dependent potentiation of the activity of cardiac L-type calcium channel alpha 1 subunits due to phosphorylation by cAMP-dependent protein kinase. Proc Natl Acad Sci U S A *90*, 10135-10139.

Sculptoreanu, A., Scheuer, T., and Catterall, W.A. (1993b). Voltage-dependent potentiation of L-type Ca2+ channels due to phosphorylation by cAMP-dependent protein kinase. Nature *364*, 240-243.

Shen, K., and Meyer, T. (1999). Dynamic control of CaMKII translocation and localization in hippocampal neurons by NMDA receptor stimulation. Science *284*, 162-166.

Shen, K., Teruel, M.N., Connor, J.H., Shenolikar, S., and Meyer, T. (2000). Molecular memory by reversible translocation of calcium/calmodulin-dependent protein kinase II. Nat Neurosci *3*, 881-886.

Shonesy, B.C., Jalan-Sakrikar, N., Cavener, V.S., and Colbran, R.J. (2014). CaMKII: a molecular substrate for synaptic plasticity and memory. In Prog Mol Biol Transl Sci (Netherlands), pp. 61-87.

Shonesy, B.C., Wang, X., Rose, K.L., Ramikie, T.S., Cavener, V.S., Rentz, T., Baucum, A.J., 2nd, Jalan-Sakrikar, N., Mackie, K., Winder, D.G.*, et al.* (2013). CaMKII regulates diacylglycerol lipase-alpha and striatal endocannabinoid signaling. Nat Neurosci *16*, 456-463.

Silva, A.J., Kogan, J.H., Frankland, P.W., and Kida, S. (1998). CREB and memory. Annual review of neuroscience *21*, 127-148.

Simms, B.A., Souza, I.A., Rehak, R., and Zamponi, G.W. (2014). The Cav1.2 N terminus contains a CaM kinase site that modulates channel trafficking and function. Pflugers Archiv : European journal of physiology.

Singh, A., Gebhart, M., Fritsch, R., Sinnegger-Brauns, M.J., Poggiani, C., Hoda, J.C., Engel, J., Romanin, C., Striessnig, J., and Koschak, A. (2008). Modulation of voltage- and Ca2+-dependent gating of CaV1.3 L-type calcium channels by alternative splicing of a C-terminal regulatory domain. J Biol Chem *283*, 20733-20744.

Stanika, R., Campiglio, M., Pinggera, A., Lee, A., Striessnig, J., Flucher, B.E., and Obermair, G.J. (2016). Splice variants of the CaV1.3 L-type calcium channel regulate dendritic spine morphology. Scientific reports *6*, 34528.

Stanika, R.I., Flucher, B.E., and Obermair, G.J. (2015). Regulation of Postsynaptic Stability by the L-type Calcium Channel CaV1.3 and its Interaction with PDZ Proteins. In Curr Mol Pharmacol (United Arab Emirates), pp. 95-101.

Stea, A., Soong, T.W., and Snutch, T.P. (1995). Determinants of PKC-dependent modulation of a family of neuronal calcium channels. In Neuron (United States), pp. 929-940.

Stephenson, J.R., Wang, X., Perfitt, T.L., Parrish, W.P., Shonesy, B.C., Marks, C.R., Mortlock, D.P., Nakagawa, T., Sutcliffe, J.S., and Colbran, R.J. (2017). A Novel Human CAMK2A Mutation Disrupts Dendritic Morphology and Synaptic Transmission, and Causes ASD-Related Behaviors. In J Neurosci (United States), pp. 2216-2233.

Strack, S., and Colbran, R.J. (1998). Autophosphorylation-dependent targeting of calcium/ calmodulin-dependent protein kinase II by the NR2B subunit of the N-methyl-D-aspartate receptor. J Biol Chem *273*, 20689-20692.

Strack, S., McNeill, R.B., and Colbran, R.J. (2000a). Mechanism and regulation of calcium/calmodulin-dependent protein kinase II targeting to the NR2B subunit of the N-methyl-D-aspartate receptor. J Biol Chem *275*, 23798-23806.

Strack, S., Robison, A.J., Bass, M.A., and Colbran, R.J. (2000b). Association of calcium/calmodulin-dependent kinase II with developmentally regulated splice variants of the postsynaptic density protein densin-180. J Biol Chem *275*, 25061-25064.

Strom, T.M., Nyakatura, G., Apfelstedt-Sylla, E., Hellebrand, H., Lorenz, B., Weber, B.H., Wutz, K., Gutwillinger, N., Ruther, K., Drescher, B.*, et al.* (1998). An L-type calcium-channel gene mutated in incomplete X-linked congenital stationary night blindness. Nature genetics *19*, 260-263.

Surmeier, D.J., Ding, J., Day, M., Wang, Z., and Shen, W. (2007). D1 and D2 dopamine-receptor modulation of striatal glutamatergic signaling in striatal medium spiny neurons. Trends in neurosciences *30*, 228-235.

Tadross, M.R., Dick, I.E., and Yue, D.T. (2008). Mechanism of local and global Ca2+ sensing by calmodulin in complex with a Ca2+ channel. Cell *133*, 1228-1240.

Takada, M., Kang, Y., and Imanishi, M. (2001). Immunohistochemical localization of voltage-gated calcium channels in substantia nigra dopamine neurons. In The European journal of neuroscience (France), pp. 757-762.

Tavalin, S.J., and Colbran, R.J. (2017). CaMKII-mediated phosphorylation of GluN2B regulates recombinant NMDA receptor currents in a chloride-dependent manner. In Molecular and cellular neurosciences (United States), pp. 45-52.

Teyler, T.J., and DiScenna, P. (1987). Long-term potentiation. Annual review of neuroscience *10*, 131-161.

Traynelis, S.F., Wollmuth, L.P., McBain, C.J., Menniti, F.S., Vance, K.M., Ogden, K.K., Hansen, K.B., Yuan, H., Myers, S.J., and Dingledine, R. (2010). Glutamate receptor ion channels: structure, regulation, and function. Pharmacol Rev *62*, 405-496.

Tsien, R.W., and Tsien, R.Y. (1990). Calcium channels, stores, and oscillations. Annu Rev Cell Biol *6*, 715-760.

Tu, J.C., Xiao, B., Naisbitt, S., Yuan, J.P., Petralia, R.S., Brakeman, P., Doan, A., Aakalu, V.K., Lanahan, A.A., Sheng, M.*, et al.* (1999). Coupling of mGluR/Homer and PSD-95 complexes by the Shank family of postsynaptic density proteins. In Neuron (United States), pp. 583-592.

Van Petegem, F., Clark, K.A., Chatelain, F.C., and Minor, D.L., Jr. (2004). Structure of a complex between a voltage-gated calcium channel beta-subunit and an alpha-subunit domain. Nature *429*, 671-675.

Walker, D., Bichet, D., Campbell, K.P., and De Waard, M. (1998). A beta 4 isoform-specific interaction site in the carboxyl-terminal region of the voltage-dependent Ca2+ channel alpha 1A subunit. J Biol Chem *273*, 2361-2367.

Walker, D., Bichet, D., Geib, S., Mori, E., Cornet, V., Snutch, T.P., Mori, Y., and De Waard, M. (1999). A new beta subtype-specific interaction in alpha1A subunit controls P/Q-type Ca2+ channel activation. J Biol Chem *274*, 12383-12390.

Wang, S., Stanika, R.I., Wang, X., Hagen, J., Kennedy, M.B., Obermair, G.J., Colbran, R.J., and Lee, A. (2017). Densin-180 Controls the Trafficking and Signaling of L-Type Voltage-Gated Cav1.2 Ca2+ Channels at Excitatory Synapses. In J Neurosci (United States), pp. 4679-4691.

Wang, Z., Kai, L., Day, M., Ronesi, J., Yin, H.H., Ding, J., Tkatch, T., Lovinger, D.M., and Surmeier, D.J. (2006). Dopaminergic control of corticostriatal long-term synaptic depression in medium spiny neurons is mediated by cholinergic interneurons. Neuron *50*, 443-452.

Westenbroek, R.E., Ahlijanian, M.K., and Catterall, W.A. (1990). Clustering of L-type Ca2+ channels at the base of major dendrites in hippocampal pyramidal neurons. Nature *347*, 281-284.

Wheeler, D., Barrett, C., Groth, R., Safa, P., and Tsien, R. (2008). CaMKII locally encodes L-type channel activity to signal to nuclear CREB in excitation-transcription coupling. The Journal of cell biology *183*, 849-863.

Wheeler, D.G., Groth, R.D., Ma, H., Barrett, C.F., Owen, S.F., Safa, P., and Tsien, R.W. (2012). Ca(V)1 and Ca(V)2 Channels Engage Distinct Modes of Ca(2+) Signaling to Control CREB-Dependent Gene Expression. Cell *149*, 1112-1124.

Wu, J., Yan, Z., Li, Z., Qian, X., Lu, S., Dong, M., Zhou, Q., and Yan, N. (2016). Structure of the voltage-gated calcium channel Cav1.1 at 3.6 Å resolution. Nature *advance online publication*.

Wu, J., Yan, Z., Li, Z., Yan, C., Lu, S., Dong, M., and Yan, N. (2015). Structure of the voltage-gated calcium channel Cav1.1 complex. Science *350*, aad2395.

Wu, X., and McMurray, C.T. (2001). Calmodulin kinase II attenuation of gene transcription by preventing cAMP response element-binding protein (CREB) dimerization and binding of the CREB-binding protein. In J Biol Chem (United States), pp. 1735-1741.

Xu, W., and Lipscombe, D. (2001). Neuronal Ca(V)1.3alpha(1) L-type channels activate at relatively hyperpolarized membrane potentials and are incompletely inhibited by dihydropyridines. J Neurosci *21*, 5944-5951.

Yang, J., Yan, R., Roy, A., Xu, D., Poisson, J., and Zhang, Y. (2015). The I-TASSER Suite: protein structure and function prediction. In Nature methods (United States), pp. 7-8.

Yang, P.S., Johny, M.B., and Yue, D.T. (2014). Allostery in Ca(2)(+) channel modulation by calcium-binding proteins. In Nat Chem Biol (United States), pp. 231-238.

Yue, D.T., Backx, P.H., and Imredy, J.P. (1990). Calcium-sensitive inactivation in the gating of single calcium channels. Science *250*, 1735-1738.

Zhang, H., Fu, Y., Altier, C., Platzer, J., Surmeier, D.J., and Bezprozvanny, I. (2006). Ca1.2 and CaV1.3 neuronal L-type calcium channels: differential targeting and signaling to pCREB. The European journal of neuroscience *23*, 2297-2310.

Zhang, H., Maximov, A., Fu, Y., Xu, F., Tang, T.S., Tkatch, T., Surmeier, D.J., and Bezprozvanny, I. (2005a). Association of CaV1.3 L-type calcium channels with Shank. J Neurosci *25*, 1037-1049.

Zhang, J., Carver, C.M., Choveau, F.S., and Shapiro, M.S. (2016). Clustering and Functional Coupling of Diverse Ion Channels and Signaling Proteins Revealed by Super-resolution STORM Microscopy in Neurons. In Neuron (United States), pp. 461-478.

Zhang, R., Dzhura, I., Grueter, C.E., Thiel, W., Colbran, R.J., and Anderson, M.E. (2005b). A dynamic alpha-beta inter-subunit agonist signaling complex is a novel feedback mechanism for regulating L-type Ca2+ channel opening. FASEB journal : official publication of the Federation of American Societies for Experimental Biology *19*, 1573-1575.

Zhang, Y., Chen, Y.H., Bangaru, S.D., He, L., Abele, K., Tanabe, S., Kozasa, T., and Yang, J. (2008). Origin of the voltage dependence of G-protein regulation of P/Q-type Ca2+ channels. J Neurosci *28*, 14176-14188.

Zhou, H., Kim, S.A., Kirk, E.A., Tippens, A.L., Sun, H., Haeseleer, F., and Lee, A. (2004). Ca2+-binding protein-1 facilitates and forms a postsynaptic complex with Cav1.2 (L-type) Ca2+ channels. J Neurosci *24*, 4698-4708.

Zhou, H., Yu, K., McCoy, K.L., and Lee, A. (2005). Molecular mechanism for divergent regulation of Cav1.2 Ca2+ channels by calmodulin and Ca2+-binding protein-1. J Biol Chem *280*, 29612-29619.

Zuhlke, R.D., Pitt, G.S., Deisseroth, K., Tsien, R.W., and Reuter, H. (1999). Calmodulin supports both inactivation and facilitation of L-type calcium channels. Nature *399*, 159-162.

APPENDIX A

EFFECTS OF CAMKAPS ON CAMKII AUTOPHOSPHORYLATION

To understand how different CaMKAPs affect CaMKII autophosphorylation, we performed *in vitro* autophosphorylation assay with purified mouse CaMKIIα in the absence or presence of various CaMKII binding peptides: Ca$_V$1.3 NTD B1 (M69-K93), Ca$_V$1.3 CTD G1639-K1660, β2 H485-E505, GluN2B A1290-L1310. A final concentration of 500 nM CaMKIIα was incubated with or without 1 μM of indicated peptides at 30 ^{o}C for 2 min before being stopped by 1X Laemmli buffer. Samples were then resolved on a Phos-tag gel and blotted for CaMKII to reveal different phosphorylation species. As shown in Fig. 7.1, in a control condition where there is no Ca^{2+} in the autophosphorylation assay, we observed one single band at the lower part of the gel, suggesting the electrophoresis mobility of nonphosphorylated CaMKII. Upon addition of Ca^{2+}/calmodulin, there is a dramatic shift of CaMKII. In addition, we observed at least two major bands with roughly the same amount, indicating that there are at least two different phosphorylation species of CaMKII. Incubation of CaMKII with the CDT peptide, which we did not observe CaMKII binding on our hands, has no effect on CaMKII electrophoresis mobility pattern. However, incubation of CaMKII with the NTD B1 peptide that contains the RKR motif seems to enhance the intensity of the upper band of CaMKII, suggesting NTD B1 peptide may promote autophosphorylation of another site. In contrast, incubation of either Ca^{2+} channel β2 peptide or GluN2B binding peptide completely removes the upper band while retaining the lower band that is higher

than nonphosphorylated CaMKII, indicating that incubation of CaMKII with Ca^{2+} channel β2 peptide or GluN2B binding peptide represses a second CaMKII autophosphorylation site. We hypothesize that the lower band of the doublet represents Thr286 phosphorylated CaMKII, and the upper band represents a double phosphorylation species that contains Thr286 and another unknown site. However, specific CaMKII mutations need to be done to confirm the identity of these sites.

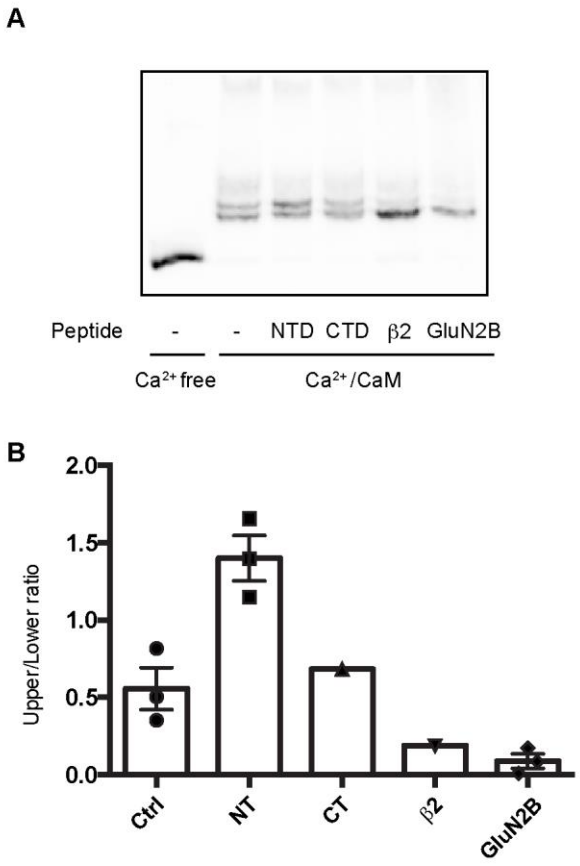

FIGURE 7.1 Effects of different CaMKAPs on CaMKII autophosphorylation. *A*, a Phos-tag gel blot showing CaMKII autophosphorylation in the absence of presence of different binding peptides. Purified mouse CaMKIIa (500 nM) was incubated with 50 mM HEPES, 10 mM $Mg(AC)_2$, 1.5 mM $CaCl_2$ (absent in the Ca^{2+}-free condition), 10 μM calmodulin, 0.5 mM ATP, 1 mM DTT at 30 °C for 2 min in the absence or presence of indicated peptides (1 μM). Samples were stopped by 1x Laemmli buffer and resolved on a Phos-tag gel followed by immunoblot with CaMKIIα antibody. *B*, quantification of three independent experiments shown in A.

APPENDIX B

EFFECTS OF RKR/AAA MUTATION ON $Ca_V1.3$ CHANNEL KINETICS

After we discovered the novel NTD/β interaction, we also tested the effects of RKR/AAA mutation on $Ca_V1.3$ channel kinetics. This is done by repeating experiments in Fig. 2.7A and D, except that β1b, β2a were cotransfected instead of β3. We observed a significant effect of RKR/AAA mutation on Ca^{2+}-dependent inactivation (CDI) when β1b or β2a, but not β3, were coexpressed (Fig. 7.2). However, the effect on CDI is opposite that observed in $Ca_V1.2$ channels. One caveat is that in Fig. 4.5, we quantified the residual current at the end of 1 second depolarization; while here cells were depolarized by a shorter period (50 ms) and we quantified the residual current at 30 ms. It is possible that RKR/AAA has opposite effect on fast and slow decays. It is also possible that $Ca_V1.2$ and $Ca_V1.3$ have intrinsic differences in terms of Ca^{2+}-dependent inactivation by the β subunits.

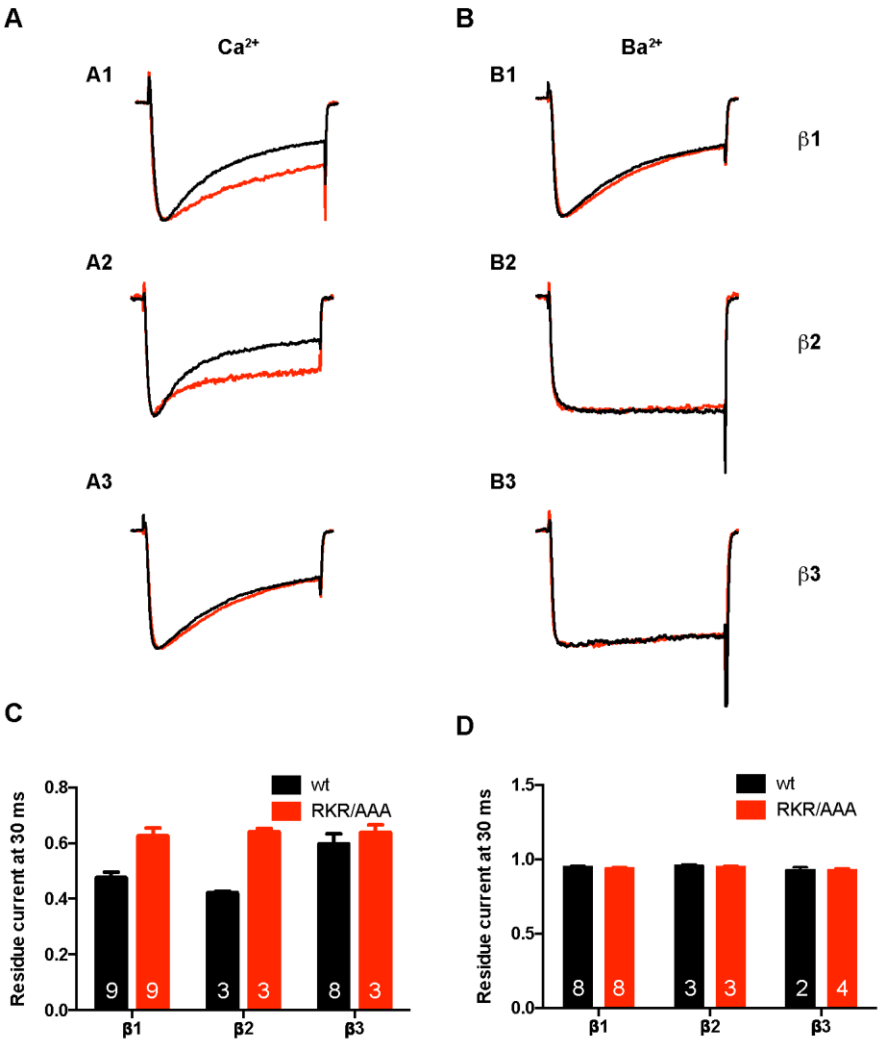

FIGURE 7.2 Effects of the RKR/AAA mutation on Cav1.3 kinetics. *A* and *B*, representative Ca^{2+} (A) and Ba^{2+} (B) traces from Cav1.3 WT (black) and Cav1.3 RKR/AAA (red) that were coexpressed with β1b, β2a, β3, respectively. *C* and *D*, summary of different groups shown in (A) and (B). Cav1.3 RKR/AAA shows less Ca^{2+}-dependent inactivation when β1b or β2a, but not β3, is coexpressed.

APPENDIX C

GENES THAT ARE DIFFERENTIALLY REGULATED BY $Ca_V1.3$ NTD OVEREXPRESSION

Table C1. Genes that are up-regulated by $Ca_V1.3$ NTD overexpression

(A total of 36, including Cacna1d1)

Gene	Fold change(log_2)	P value	Q value
Cacna1d	7.71704	5.00E-05	0.00231125
Acta2	2.04376	0.00045	0.0161593
Cnn1	1.7707	0.00015	0.00621762
Dio2	1.38875	5.00E-05	0.00231125
Hiat1	1.17078	0.00035	0.0130491
Slco1c1	1.14241	5.00E-05	0.00231125
Myl9	1.05864	5.00E-05	0.00231125
Aspa	0.951466	0.0001	0.00431823
Lmod1	0.885934	5.00E-05	0.00231125
Slc13a5	0.805401	0.0013	0.0390046
Tagln	0.789464	5.00E-05	0.00231125
Pmp2	0.771183	0.00045	0.0161593
Glul	0.744166	5.00E-05	0.00231125
Sema3d	0.742487	5.00E-05	0.00231125
Myh11	0.7046	5.00E-05	0.00231125
Ssc5d	0.68988	5.00E-05	0.00231125
Lyn	0.667891	0.00015	0.00621762
Chst9	0.659009	0.0001	0.00431823
Sspn	0.652061	5.00E-05	0.00231125
Npas4	0.585134	0.00015	0.00621762
S100a4	0.552059	0.00065	0.0218679
Postn	0.540735	0.00035	0.0130491
FAM187A	0.526762	0.00025	0.00981415
Slc13a3	0.509547	0.0014	0.041458
Csrp1	0.492357	5.00E-05	0.00231125
Hnrpd	0.487108	0.0006	0.0205506
Scd1	0.476869	5.00E-05	0.00231125
Aldoc	0.466076	0.0001	0.00431823
Hadh	0.443467	0.0013	0.0390046
Hspb1	0.441274	0.0004	0.0146569

Tmem100	0.433994	0.00015	0.00621762
Synm	0.433833	0.00045	0.0161593
Gipr	0.429297	0.00175	0.0497082
Fgfrl1	0.414849	0.00045	0.0161593
Dbi	0.414106	0.00065	0.0218679
Adamts1	0.403923	0.0008	0.0260412

Table C2. Genes that are down-regulated by $Ca_V1.3$ NTD overexpression

(A total of 357)

Gene	Fold change(log_2)	P value	Q value
Xpot	-0.372072	0.0013	0.0390046
Plec	-0.373574	0.00175	0.0497082
Rps8	-0.374504	0.0016	0.0462955
Rpl35	-0.377807	0.00135	0.0402569
Slc6a9	-0.379578	0.00165	0.0474605
Lamc1	-0.380667	0.0012	0.0366817
Tcf12	-0.392322	0.00095	0.0300355
Olig1	-0.394575	0.0013	0.0390046
Cnn3	-0.396365	0.0016	0.0462955
Ctsl1	-0.398166	0.00075	0.0246726
Rps28	-0.399488	0.0011	0.034083
Lbh	-0.39985	0.0008	0.0260412
Aox1	-0.400853	0.00095	0.0300355
Rnf185	-0.403618	0.0012	0.0366817
Rps5	-0.403874	0.0008	0.0260412
Dkc1	-0.404823	0.0012	0.0366817
Litaf	-0.407922	0.00145	0.0426058
Rpl18a	-0.408834	0.00065	0.0218679
Shroom3	-0.410595	0.0014	0.041458
Hmgn2	-0.410889	0.00065	0.0218679
Riok3	-0.414761	0.0003	0.011525
Cxcr4	-0.41599	0.0015	0.0438483
Rpl12	-0.41713	0.0004	0.0146569
Rplp1	-0.417874	0.0007	0.0233201
Myc	-0.419692	0.0012	0.0366817
Smc2	-0.42092	0.00055	0.0191261
Slc7a1	-0.426632	0.0003	0.011525
RGD1564664	-0.437178	0.00105	0.0327719
Nrp2	-0.438131	0.00035	0.0130491
Hbegf	-0.439724	0.00045	0.0161593
Efs	-0.441263	0.0003	0.011525
Gas5	-0.442023	0.00035	0.0130491
Sox11	-0.442246	0.0006	0.0205506
Lpar1	-0.44292	0.0008	0.0260412
Sema5b	-0.44322	0.00105	0.0327719
Plin2	-0.445632	0.00025	0.00981415
Usp3	-0.448388	0.00065	0.0218679
Eprs	-0.449725	0.00015	0.00621762
Dut	-0.451913	0.0013	0.0390046

Stbd1	-0.453398	0.00095	0.0300355
Ftl1	-0.45583	0.0001	0.00431823
Adamtsl3	-0.456023	0.00015	0.00621762
Txnrd1	-0.45738	0.0002	0.00807432
Chac1	-0.457637	0.00065	0.0218679
Cryab	-0.462966	0.0009	0.0287478
Srebf1	-0.464126	0.0004	0.0146569
Sqstm1	-0.46481	0.0003	0.011525
Col11a1	-0.465712	5.00E-05	0.00231125
Rps12	-0.466867	0.0001	0.00431823
Lyar	-0.469009	0.00105	0.0327719
Myt1	-0.469602	0.00025	0.00981415
Il1rap	-0.469694	0.00045	0.0161593
Podxl	-0.472296	0.00075	0.0246726
Smoc1	-0.472755	0.00105	0.0327719
Cntf	-0.479959	0.0006	0.0205506
Arl6ip6	-0.479986	0.00115	0.0354391
Zbed3	-0.480819	0.00105	0.0327719
Spon1	-0.482606	0.0001	0.00431823
Hist2h2ab	-0.485441	0.0006	0.0205506
LOC100909675	-0.488039	0.00125	0.0378036
Chst7	-0.49229	0.00055	0.0191261
Irf9	-0.493668	5.00E-05	0.00231125
Hspb8	-0.496024	5.00E-05	0.00231125
Gbp2	-0.497657	5.00E-05	0.00231125
Phlda1	-0.499258	0.00015	0.00621762
Lonp1	-0.505923	5.00E-05	0.00231125
Thbs1	-0.506042	0.00015	0.00621762
Slc7a5	-0.506314	5.00E-05	0.00231125
Sdc1	-0.507813	0.00125	0.0378036
Itga7	-0.508386	0.00045	0.0161593
Atf3	-0.509828	5.00E-05	0.00231125
Zc3hav1	-0.510458	0.00035	0.0130491
Casp4	-0.51348	5.00E-05	0.00231125
Tgif1	-0.514284	0.0001	0.00431823
Fam129a	-0.520437	5.00E-05	0.00231125
Stc2	-0.52147	0.0009	0.0287478
Mad2l1	-0.528367	0.00095	0.0300355
PVR	-0.529341	0.00045	0.0161593
E2f1	-0.530025	0.00085	0.0272784
Rfc3	-0.530291	0.0004	0.0146569
Timp3	-0.530299	0.0001	0.00431823
Rrm1	-0.530486	5.00E-05	0.00231125

Tnfrsf12a	-0.530788	0.0001	0.00431823
Smc4	-0.535907	5.00E-05	0.00231125
Car13	-0.535908	0.0015	0.0438483
S1pr3	-0.537316	5.00E-05	0.00231125
Repin1	-0.541636	0.0001	0.00431823
Fth1	-0.541665	0.0007	0.0233201
Fen1	-0.544723	0.0002	0.00807432
Mknk1	-0.545357	5.00E-05	0.00231125
Plekha4	-0.546183	0.00075	0.0246726
LOC690349	-0.546417	0.00055	0.0191261
Ier3	-0.547202	0.0002	0.00807432
Ntn1	-0.548066	0.0006	0.0205506
Ddr2	-0.554643	5.00E-05	0.00231125
Ets1	-0.566829	5.00E-05	0.00231125
Gstp1	-0.569539	5.00E-05	0.00231125
Hk2	-0.570383	0.0002	0.00807432
Atf5	-0.57144	5.00E-05	0.00231125
Atad2	-0.572149	5.00E-05	0.00231125
Ajuba	-0.572682	0.00015	0.00621762
Adamts5	-0.575945	0.0004	0.0146569
Cdkn2b	-0.576018	0.00015	0.00621762
Bcar3	-0.581471	5.00E-05	0.00231125
Nt5dc2	-0.583539	0.0001	0.00431823
Fzd10	-0.586346	0.00085	0.0272784
Shmt1	-0.589158	0.0004	0.0146569
Ascl1	-0.594421	0.0001	0.00431823
Sall3	-0.595695	5.00E-05	0.00231125
Irf7	-0.595915	0.0005	0.0176391
Pdzrn4	-0.603011	0.00015	0.00621762
Rbms1	-0.603257	5.00E-05	0.00231125
Nes	-0.603339	5.00E-05	0.00231125
Ninj1	-0.606055	5.00E-05	0.00231125
Slc3a2	-0.609046	5.00E-05	0.00231125
Akna	-0.611217	5.00E-05	0.00231125
Hist1h4b	-0.611503	5.00E-05	0.00231125
Srxn1	-0.612496	5.00E-05	0.00231125
Gsta1	-0.613765	5.00E-05	0.00231125
Ppp1r14b	-0.61606	5.00E-05	0.00231125
Rsad2	-0.617433	5.00E-05	0.00231125
Usp1	-0.619181	5.00E-05	0.00231125
Kank1	-0.619393	0.00045	0.0161593
Mt2A	-0.619544	5.00E-05	0.00231125
Rbl1	-0.620435	0.0017	0.0486117

Ccnd1	-0.627608	5.00E-05	0.00231125
Hist2h4	-0.631414	5.00E-05	0.00231125
Nxt1	-0.632103	0.0002	0.00807432
Ppp1r15a	-0.632691	5.00E-05	0.00231125
Sh3bp4	-0.632704	5.00E-05	0.00231125
Ifi44	-0.633845	5.00E-05	0.00231125
Olig2	-0.633922	5.00E-05	0.00231125
Sesn2	-0.636849	5.00E-05	0.00231125
LOC498265	-0.637615	0.0017	0.0486117
C2	-0.640349	0.0003	0.011525
Wdhd1	-0.64121	5.00E-05	0.00231125
Ptx3	-0.642136	0.00025	0.00981415
H2afx	-0.643045	5.00E-05	0.00231125
Mdc1	-0.645118	5.00E-05	0.00231125
Bmp7	-0.645587	0.00085	0.0272784
Rpa2	-0.646743	5.00E-05	0.00231125
Dll1	-0.648305	0.0001	0.00431823
Acot2	-0.659656	5.00E-05	0.00231125
Rtkn2	-0.659947	0.0008	0.0260412
Tex30	-0.662805	0.00135	0.0402569
Rlbp1	-0.663145	0.0006	0.0205506
Dhfr	-0.664575	0.00095	0.0300355
Galnt3	-0.664939	5.00E-05	0.00231125
Ezh2	-0.66662	5.00E-05	0.00231125
Syde1	-0.671138	5.00E-05	0.00231125
Traf4	-0.673707	5.00E-05	0.00231125
Pola2	-0.675992	0.00075	0.0246726
Pappa	-0.676248	5.00E-05	0.00231125
Lig1	-0.680747	5.00E-05	0.00231125
Ampd3	-0.682482	5.00E-05	0.00231125
Abcc4	-0.685353	5.00E-05	0.00231125
Tnc	-0.687546	5.00E-05	0.00231125
Cbr3	-0.687621	5.00E-05	0.00231125
Dhx58	-0.688367	0.0001	0.00431823
Sema3b	-0.6891	0.0003	0.011525
Crlf1	-0.695003	5.00E-05	0.00231125
Adm	-0.695962	5.00E-05	0.00231125
Tmpo	-0.696611	5.00E-05	0.00231125
Eif4ebp1	-0.699859	5.00E-05	0.00231125
Clspn	-0.701575	0.00035	0.0130491
Txnip	-0.701606	5.00E-05	0.00231125
Dctpp1	-0.70417	0.00085	0.0272784
Slc2a1	-0.705853	5.00E-05	0.00231125

Wdr62	-0.707907	0.0005	0.0176391
Nqo1	-0.711192	5.00E-05	0.00231125
Gadd45a	-0.714565	5.00E-05	0.00231125
Oas1b	-0.718291	0.0002	0.00807432
Prim2	-0.723516	5.00E-05	0.00231125
Cenpw	-0.726938	0.0005	0.0176391
Ckap2	-0.729229	5.00E-05	0.00231125
Unc5b	-0.730523	5.00E-05	0.00231125
Kntc1	-0.733997	5.00E-05	0.00231125
Loxl4	-0.734058	5.00E-05	0.00231125
Chst3	-0.736422	5.00E-05	0.00231125
Lgals3	-0.738132	5.00E-05	0.00231125
Hmmr	-0.742708	5.00E-05	0.00231125
Kif23	-0.75061	5.00E-05	0.00231125
Spag5	-0.756008	5.00E-05	0.00231125
Fn1	-0.762015	5.00E-05	0.00231125
Rhbdf2	-0.765344	0.00025	0.00981415
Fbxl7	-0.766726	5.00E-05	0.00231125
Ephx2	-0.770084	5.00E-05	0.00231125
Ifi27	-0.777001	5.00E-05	0.00231125
Pmepa1	-0.777639	0.00015	0.00621762
Wdr16	-0.77945	5.00E-05	0.00231125
Mcm2	-0.782945	5.00E-05	0.00231125
Cenpq	-0.787347	0.0011	0.034083
Lmnb1	-0.787857	5.00E-05	0.00231125
Bub1	-0.78846	5.00E-05	0.00231125
Rassf4	-0.793246	5.00E-05	0.00231125
Dbf4	-0.793434	5.00E-05	0.00231125
Map3k1	-0.79812	5.00E-05	0.00231125
Slc1a5	-0.798669	5.00E-05	0.00231125
Lgals9	-0.799263	5.00E-05	0.00231125
Fbxo5	-0.808504	0.0003	0.011525
Osgin1	-0.812542	5.00E-05	0.00231125
Hist1h2bk	-0.812704	5.00E-05	0.00231125
Cenpi	-0.813988	5.00E-05	0.00231125
Cdkn2c	-0.815701	0.0002	0.00807432
Usp18	-0.831137	5.00E-05	0.00231125
Fam83d	-0.833084	0.00015	0.00621762
Tcf19	-0.836748	0.00095	0.0300355
Hist2h3c2	-0.838898	5.00E-05	0.00231125
Mis18bp1	-0.841125	5.00E-05	0.00231125
Gmnn	-0.844898	5.00E-05	0.00231125
Mcm7	-0.852378	5.00E-05	0.00231125

Cdc6	-0.854304	0.0002	0.00807432
Hist1h1d	-0.854408	5.00E-05	0.00231125
Tsku	-0.870791	5.00E-05	0.00231125
Serpine1	-0.875833	5.00E-05	0.00231125
Trip13	-0.890312	0.0001	0.00431823
Arhgap11a	-0.890848	5.00E-05	0.00231125
Prkg2	-0.893061	5.00E-05	0.00231125
Spta1	-0.893588	5.00E-05	0.00231125
Brca1	-0.900591	5.00E-05	0.00231125
Casc5	-0.909771	5.00E-05	0.00231125
Sgcg	-0.911438	5.00E-05	0.00231125
Pold1	-0.911771	5.00E-05	0.00231125
Fancd2	-0.920849	5.00E-05	0.00231125
Pole	-0.924398	5.00E-05	0.00231125
Slc7a11	-0.926811	5.00E-05	0.00231125
Bcas1	-0.927406	5.00E-05	0.00231125
Nsl1	-0.932276	0.0001	0.00431823
Pla2g7	-0.937594	5.00E-05	0.00231125
Casp12	-0.940875	5.00E-05	0.00231125
Mcm6	-0.941261	5.00E-05	0.00231125
Plk4	-0.943196	5.00E-05	0.00231125
Sox8	-0.951408	5.00E-05	0.00231125
Aurkb	-0.952281	5.00E-05	0.00231125
Car8	-0.953092	5.00E-05	0.00231125
Calcrl	-0.953472	5.00E-05	0.00231125
Cdt1	-0.958855	5.00E-05	0.00231125
Ung	-0.959905	5.00E-05	0.00231125
Pcdh15	-0.960747	5.00E-05	0.00231125
Kif20b	-0.962466	5.00E-05	0.00231125
Cdk2	-0.965704	5.00E-05	0.00231125
Cfb	-0.973961	0.00015	0.00621762
Spc25	-0.980335	5.00E-05	0.00231125
Hmox1	-0.982027	5.00E-05	0.00231125
Ccnf	-0.986076	5.00E-05	0.00231125
Tbxas1	-0.993547	5.00E-05	0.00231125
Foxm1	-1.00346	5.00E-05	0.00231125
Cenpu	-1.0082	0.00065	0.0218679
Bmp2	-1.02411	0.00035	0.0130491
Pole2	-1.02505	0.00045	0.0161593
Nkx2-2	-1.04073	5.00E-05	0.00231125
Cdc45	-1.04473	5.00E-05	0.00231125
Phf19	-1.05417	5.00E-05	0.00231125
Kif15	-1.05458	5.00E-05	0.00231125

Cspg4	-1.05633	5.00E-05	0.00231125
Abcb1a	-1.06505	5.00E-05	0.00231125
Gins1	-1.08415	5.00E-05	0.00231125
Trib3	-1.09781	5.00E-05	0.00231125
Cep55	-1.10088	5.00E-05	0.00231125
Aspm	-1.10153	5.00E-05	0.00231125
Cks2	-1.10218	5.00E-05	0.00231125
Ccnb1	-1.11039	5.00E-05	0.00231125
Hmgb2	-1.11117	5.00E-05	0.00231125
Cdca8	-1.11898	5.00E-05	0.00231125
Nuf2	-1.12501	5.00E-05	0.00231125
Tacc3	-1.12601	5.00E-05	0.00231125
Timeless	-1.12828	5.00E-05	0.00231125
Tk1	-1.12887	5.00E-05	0.00231125
Rad51	-1.13286	5.00E-05	0.00231125
Prc1	-1.13622	5.00E-05	0.00231125
Pttg1	-1.15513	0.0001	0.00431823
Fibin	-1.15571	5.00E-05	0.00231125
Sox10	-1.15688	5.00E-05	0.00231125
Birc5	-1.15816	5.00E-05	0.00231125
Ube2t	-1.16416	0.0001	0.00431823
Ercc6l	-1.16468	5.00E-05	0.00231125
Dlgap5	-1.16653	5.00E-05	0.00231125
Hist1h2bl	-1.16742	5.00E-05	0.00231125
Bmp6	-1.18036	5.00E-05	0.00231125
Mastl	-1.18548	5.00E-05	0.00231125
Pllp	-1.18911	5.00E-05	0.00231125
Uhrf1	-1.19456	5.00E-05	0.00231125
Mcm3	-1.19765	5.00E-05	0.00231125
Orc1	-1.22275	0.0017	0.0486117
Mt1a	-1.2287	5.00E-05	0.00231125
Slc35d3	-1.23054	5.00E-05	0.00231125
Bard1	-1.23148	5.00E-05	0.00231125
Cdca7	-1.23335	5.00E-05	0.00231125
Hjurp	-1.24001	5.00E-05	0.00231125
Melk	-1.2577	5.00E-05	0.00231125
Iqgap3	-1.2665	5.00E-05	0.00231125
Fam64a	-1.27131	5.00E-05	0.00231125
Hist1h2bo	-1.27847	5.00E-05	0.00231125
Plk1	-1.28483	5.00E-05	0.00231125
Tpx2	-1.28659	5.00E-05	0.00231125
Mki67	-1.29847	5.00E-05	0.00231125
Hist1h2ak	-1.301	5.00E-05	0.00231125

Ifi27l2b	-1.30621	5.00E-05	0.00231125
Gcnt1	-1.30786	5.00E-05	0.00231125
Matn4	-1.32029	0.00165	0.0474605
E2f7	-1.32505	0.0001	0.00431823
Depdc1b	-1.33125	0.0001	0.00431823
Hist1h2aa	-1.33993	5.00E-05	0.00231125
Hist1h2ail	-1.35521	5.00E-05	0.00231125
Ube2c	-1.35593	5.00E-05	0.00231125
Dll3	-1.35914	0.00035	0.0130491
Hist1h1a	-1.36001	5.00E-05	0.00231125
Ect2	-1.36064	5.00E-05	0.00231125
Racgap1	-1.36768	5.00E-05	0.00231125
Kif22	-1.36869	5.00E-05	0.00231125
Sapcd2	-1.39348	5.00E-05	0.00231125
Mcm5	-1.39432	5.00E-05	0.00231125
Fam111a	-1.40025	5.00E-05	0.00231125
Ccnb2	-1.40302	0.00035	0.0130491
Hist3h2bb	-1.41063	5.00E-05	0.00231125
P2ry2	-1.42096	0.00125	0.0378036
Cdc20	-1.42129	5.00E-05	0.00231125
Hist1h2bd	-1.42168	5.00E-05	0.00231125
Hist1h2af	-1.42561	5.00E-05	0.00231125
Espl1	-1.42706	5.00E-05	0.00231125
Kif11	-1.42967	5.00E-05	0.00231125
RGD1309870	-1.44112	5.00E-05	0.00231125
Hist1h2an	-1.456	5.00E-05	0.00231125
Cenpf	-1.46749	5.00E-05	0.00231125
Knstrn	-1.47066	5.00E-05	0.00231125
Nusap1	-1.47258	5.00E-05	0.00231125
Cenpt	-1.47293	5.00E-05	0.00231125
Ndc80	-1.47299	5.00E-05	0.00231125
Mybl2	-1.47405	5.00E-05	0.00231125
Kifc1	-1.50257	5.00E-05	0.00231125
Rrm2	-1.51027	5.00E-05	0.00231125
Ccna2	-1.52735	5.00E-05	0.00231125
Kif2c	-1.52903	5.00E-05	0.00231125
Top2a	-1.53599	5.00E-05	0.00231125
Cdk1	-1.54077	5.00E-05	0.00231125
Mms22l	-1.56517	5.00E-05	0.00231125
Cdca2	-1.57014	5.00E-05	0.00231125
Fbn2	-1.58614	5.00E-05	0.00231125
Exo1	-1.59638	5.00E-05	0.00231125
Pbk	-1.60373	5.00E-05	0.00231125

Fam89a	-1.62619	5.00E-05	0.00231125
Cdca3	-1.67027	5.00E-05	0.00231125
Asf1b	-1.67552	5.00E-05	0.00231125
Hist1h2ba	-1.6804	5.00E-05	0.00231125
Kif18b	-1.68312	5.00E-05	0.00231125
Mcm10	-1.69012	5.00E-05	0.00231125
Sfrp2	-1.70812	5.00E-05	0.00231125
Gal3st1	-1.74665	5.00E-05	0.00231125
Pdgfra	-1.75674	5.00E-05	0.00231125
Hist1h1b	-1.78801	5.00E-05	0.00231125
Cenpa	-1.84257	5.00E-05	0.00231125
Ttk	-1.84839	5.00E-05	0.00231125
Cyp4b1	-1.87099	5.00E-05	0.00231125
Eme1	-1.93552	0.0012	0.0366817
Tmem255b	-1.96431	5.00E-05	0.00231125
Troap	-2.03015	5.00E-05	0.00231125
Mxd3	-2.08668	0.00055	0.0191261